

**The application of *in situ* AFM to the study  
of molecular and macromolecular  
crystallization**

Trevor R. Keel BSc (Hons) MRSC

Thesis submitted to the university of Nottingham for the degree of  
Doctor of Philosophy, June 2004

## Contents

Abstract	5
List of Abbreviations	7
<b>Chapter 1: Introduction</b>	<b>9</b>
1.1 Crystallization	9
1.2 The growth of crystals from solution	10
1.2.1 Supersaturation	10
1.2.2 Nucleation	13
1.2.3 Crystal growth	13
1.2.4 Crystal growth mechanisms	14
1.2.4.1 <i>Continuous growth</i>	16
1.2.4.2 <i>Surface nucleation</i>	16
1.2.4.3 <i>Spiral growth</i>	16
1.2.4.4 <i>Other step sources</i>	18
1.3 The physical appearance of crystalline solids	20
1.3.1 Crystal morphology	20
1.3.2 Polymorphism	21
1.4 Experimental techniques used to study nucleation and growth	21
Processes	
1.4.1 Nucleation	22
1.4.2 Crystal growth	22
1.4.2.1 <i>Optical microscopy</i>	24
1.4.2.2 <i>Interferometry</i>	24
1.4.2.3 <i>Electron microscopy</i>	25
1.5 Atomic Force Microscopy	27
1.5.1 AFM imaging modes	28
1.5.1.1 <i>Contact mode</i>	30
1.5.1.2 <i>Tapping mode</i>	31
1.5.1.3 <i>Non-contact mode</i>	31

1.5.2	Force-distance measurements	31
1.5.3	The role of AFM in the study of crystallization phenomena	32
1.5.3.1	<i>Macromolecular crystallization</i>	34
1.5.3.2	<i>Pharmaceutical crystallization</i>	35
1.6	Project aims	35
<b>Chapter 2: Crystallization, habit modification and microscopical analysis of a pharmaceutical excipient, adipic acid.</b>		<b>38</b>
2.1	Introduction	39
2.1.1	Crystallization and the pharmaceutical industry	39
2.1.2	Crystal morphology and structure of pharmaceutical materials	39
2.1.2.1	<i>Supersaturation</i>	40
2.1.2.2	<i>Crystallizing solvent</i>	42
2.1.2.3	<i>Impurities and additives</i>	42
2.1.3	Adipic acid	44
2.1.3.1	<i>Crystal structure and morphology</i>	44
2.1.3.2	<i>Polymorph formation</i>	44
2.1.3.3	<i>Habit modification</i>	46
2.1.4	Chapter aims	47
2.2	Materials and methods	48
2.2.1	Preparation of adipic acid crystals	48
2.2.2	Preparation of imaging solutions	49
2.2.3	AFM analysis	50
2.2.4	SEM analysis	51
2.3	Results and discussion	52
2.3.1	Seed crystal optimization	52
2.3.2	Surface restructuring on the (100) face of un-doped adipic acid crystals	54
2.3.3	Growth and dissolution of adipic acid crystals	59
2.3.4	Crystallization of adipic acid in the presence of octanoic acid	64
2.4	Conclusions	70
<b>Chapter 3: The surface characterization of a model protein crystal</b>		<b>73</b>

3.1	Introduction	74
3.1.1	Macromolecular crystal growth – A brief history	74
3.1.2	Lysozyme	78
3.1.3	The study of tetragonal lysozyme crystal growth	78
3.1.4	Chapter aims	81
3.2	Materials and methods	82
3.2.1	Substrate preparation	82
3.2.2	Seed crystal growth	82
3.2.3	Preparation of imaging solutions	83
3.2.4	AFM analysis	83
3.3	Results and discussion	86
3.3.1	Seed crystal immobilization	86
3.3.1.1	<i>Plain glass coverslides</i>	87
3.3.1.2	<i>Nickel-coated TEM grids</i>	87
3.3.1.3	<i>Poly-L-Lysine-coated glass coverslides</i>	87
3.3.2	Mechanisms of growth on the (110) face of tetragonal lysozyme crystals	90
3.3.2.1	<i>High supersaturation (<math>\sigma &gt; 1.0</math>)</i>	90
3.3.2.2	<i>Medium supersaturation (<math>0.99 &gt; \sigma &gt; 0.8</math>)</i>	97
3.3.2.3	<i>Low supersaturation (<math>\sigma &lt; 0.79</math>)</i>	99
3.3.3	Molecular resolution features on the crystal surfaces	101
3.3.3.1	<i>Step edge heights</i>	102
3.3.3.2	<i>Molecular resolution imaging</i>	104
3.4	Conclusions	111
<b>Chapter 4: Polymorphism in lysozyme crystallization – An AFM study</b>		<b>113</b>
4.1	Introduction	114
4.1.1	Polymorphism	114
4.1.2	Lysozyme polymorphs	114
4.1.3	Monoclinic lysozyme	115
4.1.4	Chapter aims	116

4.2	Materials and methods	118
4.2.1	Seed crystal growth and immobilization	118
4.2.2	Preparation of imaging solutions	118
4.2.3	AFM analysis	119
4.3	Results and discussion	120
4.4	Conclusions	128
<b>Chapter 5: An AFM analysis of a poorly diffracting protein crystal – Response Regulator 02 receiver domain (RR02rec)</b>		<b>129</b>
5.1	Introduction	130
5.1.1	X-ray diffraction	130
5.1.1.1	<i>Diffraction limit (resolution)</i>	133
5.1.1.2	<i>Mosaicity</i>	133
5.1.2	Variables affecting macromolecular crystal quality	134
5.1.3	Response regulator proteins in <i>S. pneumoniae</i>	135
5.1.4	Chapter aims	139
5.2	Materials and methods	140
5.2.1	Cloning, over-expression and purification of RR02rec	140
5.2.2	Crystallization	141
5.2.2.1	<i>Vapour diffusion methods</i>	141
5.2.2.2	<i>Crystallization screens and optimization</i>	144
5.2.3	Seed crystal growth for AFM experiments	144
5.2.4	Imaging conditions	145
5.2.5	AFM analysis	145
5.3	Results	147
5.4	Discussion	153
5.5	Conclusions	158
<b>Chapter 6: General conclusions</b>		<b>160</b>
	References	165
	Acknowledgements	182
	Publications and presentations	183

## Abstract

The crystallization of molecules from solution encompasses a number of key areas in science and technology, ranging from the purification and separation of industrial chemicals through to the arrangement of fragile biomacromolecules in ordered arrays suitable for structural analysis. However, as there are only a small number of techniques suitable for the study of such assemblies, many fundamental aspects governing the crystallization of molecules from solution are still poorly understood. In the studies presented here we have attempted to improve the understanding of this subject by investigating the crystallization of a series of molecules of both pharmaceutical and biological importance, using *in situ* Atomic Force Microscopy (AFM). A particular aim of the PhD was to develop the experimental protocols necessary to investigate macromolecular crystals known to exhibit poor diffraction properties, and subsequently to relate AFM data to these properties.

The first study carried out concerned the crystallization and habit modification of a pharmaceutical excipient molecule, adipic acid. By using AFM we were able, for the first time, to directly observe the behavior of the dominant (100) face in both an air and liquid environment. A number of important observations were made including solute reorganization in air, etch pit formation and growth inhibition by the structurally related habit modifier, octanoic acid.

We subsequently investigated various aspects of the crystallization of the model protein, lysozyme. The rate and mechanisms of growth of the (110) surface of the tetragonal crystal were observed using *in situ* AFM at a range of supersaturations ( $\sigma$ ), a study that uncovered a previously unreported mechanistic event. The (110) and (101) faces were then both investigated at higher resolution, revealing molecular resolution features corresponding directly to basic crystallographic data.

The polymorphic characteristics displayed by many macromolecular crystals were then investigated in a short study concerning the growth and structure of the monoclinic form of the lysozyme crystal. The dominant (101) face of the crystal was investigated at both high and low protein/precipitant concentrations, allowing us to unambiguously distinguish between two crystalline forms of the same macromolecule.

Finally, by utilizing the experimental techniques developed throughout the previous studies, we investigated a poorly diffracting crystal constructed from a protein found in *Streptococcus pneumoniae*, Response Regulator 02 receiver domain (RR02rec). By studying the surface of crystalline RR02rec with *in situ* AFM, we were able to uncover various features of the crystal lattice that may have contributed to the poor diffraction properties displayed by the crystal during previous X-ray studies.

Besides revealing a range of new molecular scale details concerning the structure and growth of each of these crystal systems, these studies culminated in a successful attempt to relate direct microscopical observations of growth dynamics of a protein crystal system (RR02rec) to the limited results obtained from previous crystallographic studies performed on this protein. As an approach this offers considerable promise in identifying problems with certain crystals and, in conjunction with future advances in AFM technology, may offer information that could lead to the acceleration and enhancement of X-ray diffraction analyses.

## List of Abbreviations

2D	Two-Dimensional
2D-FFT	Two-Dimensional Fast Fourier Transformation
3D	Three-Dimensional
AFM	Atomic Force Microscopy
ATP	Adenosine Triphosphate
B+S	Birth and Spread model
$c$	Solution concentration
$c_0$	Equilibrium concentration of the solution, i.e., the solubility
CLSM	Confocal Laser Scanning Microscopy
CMTC	Cadmium Mercury Thiocyanate
CMV	Cucumber Mosaic Virus
Cryo-TEM	Cryogenic Transmission Electron Microscopy
$d$	Interplanar distance
DLS	Dynamic Light Scattering
DNA	Deoxyribonucleic Acid
$E_{att}$	Attachment Energy
<i>E. coli</i>	<i>Escherichia coli</i>
EM	Electron Microscopy
HEPES	4-(2-hydroxyethyl)-1-piperazineethanesulfonic acid
HEWL	Hen Egg White Lysozyme
(hkl)	Miller indices of a crystal face
[hkl]	A specific crystallographic direction
<hkl>	A crystallographically equivalent, non-specific direction
HPK	Histidine Protein Kinase
HPLC	High Performance Liquid Chromatography
IPA	Isopropyl Alcohol
IPTG	Isopropylthiogalactoside
L/W	Length/Width ratio
$n$	A whole number of wavelengths
NC-AFM	Non-Contact Atomic Force Microscopy

NMBA	4-Nitro-4'-Methyl Benzylidene Aniline
pI	Isoelectric Point
PBC	Periodic Bond Chain theory
PCR	Polymerase Chain Reaction
PDB	Protein Data Bank
PEG	Polyethylene Glycol
PLL	Poly-L-Lysine
PSD	Power Spectral Density
RH	Relative Humidity
RR	Response Regulator
RR02rec	Response Regulator 02 Receiver Domain
<i>S. pneumoniae</i>	<i>Streptococcus pneumoniae</i>
SDS-PAGE	Sodium Dodecyl Sulfate Polyacrylamide Gel Electrophoresis
SEM	Scanning Electron Microscopy
SPM	Scanning Probe Microscopy
STM	Scanning Tunneling Microscopy
STMV	Satellite Tobacco Mosaic Virus
tRNA	Transfer Ribonucleic Acid
TEM	Transmission Electron Microscopy
TCSTS	Two-Component Signal Transduction System
TLK	Terrace-Ledge-Kink
TM-AFM	Tapping Mode Atomic Force Microscopy
Tris	Tris(hydroxymethyl)aminomethane
TYMV	Turnip Yellow Mosaic Virus
$\theta$	Glancing angle of the incident beam
$\lambda$	Wavelength
$\sigma$	Supersaturation

## **Chapter**

# **1**

## **Introduction**

### **1.1 Crystallization**

Solids can be defined by the way their constituent atoms, ions or molecules are packed. If the packing of a specific material is regular, forming an infinite three-dimensional array exhibiting long-range order, it is said to be crystalline (Davey and Garside, 2000).

Crystallization plays a part in almost every area of science and technology. However, in this thesis we restrict ourselves to crystals formed of pharmaceutical materials and of biological macromolecules.

In these two areas, crystallization plays quite different roles on vastly different scales. The majority of pharmaceutically relevant materials are small organic molecules that are prepared in the crystalline state and subsequently ground into powders for use in dosage formulations – indeed, approximately 90% of all pharmaceutical products, such as tablets, aerosols, capsules, suspensions, and suppositories contain a drug in crystalline form (Shekunov and York, 2000).

A good knowledge of the fundamental aspects of crystallization is particularly important in the pharmaceutical industry for a number of reasons. Firstly, crystallization is generally carried out on a large scale, so the system must be well understood to ensure a good yield of (often valuable) material. Secondly, to avoid the classic formulation problems associated with crystallization (such as poor filtering and washing characteristics, bioinequivalence and tableting failure to name but a few), it is

vitality important that the crystalline product exhibits ‘manufacturing-friendly’ characteristics and uniformity from batch-to-batch – ie, the particles exhibit similar sizes and morphologies, the same crystal structure and a similar degree of perfection (Shekunov and York, 2000).

The requirements of crystals formed from biological macromolecules are somewhat different. For the past 70 years, they have primarily been associated with the elucidation of structural information. As such, biological crystal growers are generally concerned with the formation of a comparatively small quantity of highly-ordered crystals for use in X-ray diffraction experiments, often from minute quantities of the solute of interest. Indeed, the morphology and other physical characteristics that are often so important in crystalline pharmaceutical materials generally matter little to structural biologists.

Whilst both types of crystal discussed throughout this thesis have quite different requirements, the fundamental physical chemistry that governs the crystallization of pharmaceutical materials and biological macromolecules is the same, as both are grown from *solution*. As such, the introduction to this thesis concentrates on the theoretical principles of crystallization from solution, and methods that can be employed to study the nucleation and growth of such crystals.

## 1.2 The growth of crystals from solution

### 1.2.1 Supersaturation

To grow crystals of any compound from solution, the solute molecules must be brought into a thermodynamically unstable state. To achieve this, the solubility limit of that compound must be exceeded. A solution whose solute concentration exceeds its solubility is known as a *supersaturated solution*, and represents a chemical system not at equilibrium. This situation is best described using a phase (or solubility) diagram, a schematic example of which is presented in figure 1.1.

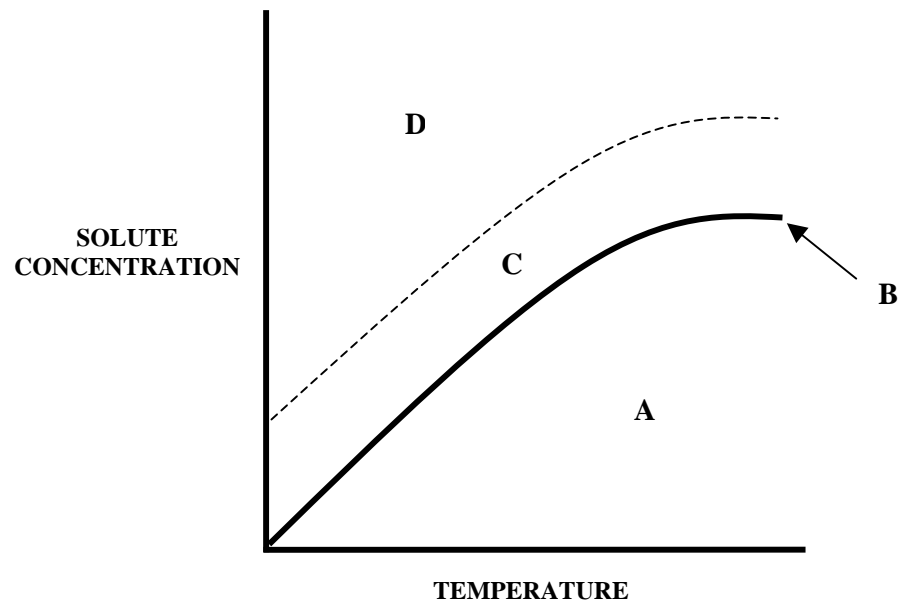


**Figure 1.1.** A typical solubility diagram for crystallization from solution, plotting the solute concentration versus the system temperature. The solid line labeled **B** represents the saturation limit of the material in the solvent. Anywhere below this limit (region **A**), the system is undersaturated and no crystal will form or grow from these conditions. Above the saturation limit (**C & D**), the system is supersaturated. In region **D**, the solution is relatively heavily supersaturated, so both spontaneous nucleation and crystal growth may occur. However, in region **C** the system is closer to the saturation limit meaning nucleation cannot occur, but growth of existing nuclei may. This region is more commonly known as the metastable zone.

When a solution resides in the supersaturated region, a thermodynamic driving force exists that is able to promote the exclusion of solute molecules from solution with the subsequent net accumulation of the solid state. If properly controlled, this can eventually lead to the formation of crystalline solids of that solute (McPherson, 1999).

Formally, the supersaturation,  $\sigma$ , can be defined in thermodynamic terms as the dimensionless difference in chemical potential between a molecule in an equilibrium state and a molecule in its supersaturated state. However, the most common approximation is:

$$\sigma = \ln (c/c_0) \qquad \text{equation 1.1}$$

Where  $c_0$  is the solubility of the solute at defined conditions and  $c$  is the concentration of the solute.

Supersaturation may be created in a solution by a range of methods, all of which involve the controlled manipulation of the solute concentration, the solute solubility, or a combination of the two. Selecting the method most appropriate for the solute of interest is of utmost importance, and is discussed further at numerous points throughout this thesis.

The reason that the supersaturated state can physically exist is due to the presence of a specific energy barrier called the activation free energy of germination. This barrier originates from the inevitable energetic requirement of forming the solid state from solution - without it, molecules would immediately precipitate out of solution the instant the solubility limit was exceeded. Indeed, at low levels of supersaturation, the amplitude of the energy fluctuations in solution may not be large enough to exceed this energy barrier – thus, such solutions are often unable to promote the initial formation of nuclei, but can support crystal growth. This region is known as the metastable zone (see figure 1.1).

However, when the system is sufficiently supersaturated the energy barrier will be surmounted and solute molecules will begin to coalesce into aggregates, which, if of sufficient dimensions, create nuclei. This represents the first step of crystal growth and is known as nucleation. The number of molecules necessary to create an effective nucleation cluster is inversely proportional to the supersaturation – thus, as the supersaturation is increased the probability of nucleation also increases.

### 1.2.2 Nucleation

Nucleation is a vital step in the crystallization process, and is of immense practical importance in pharmaceutical and biological systems. The process of nucleation can be split into three main categories – homogenous, heterogeneous (which are both examples of primary nucleation) and secondary nucleation. These are discussed at length for both crystals of pharmaceutical and biological importance elsewhere (McPherson, 1999; Rodriguez-Hornedo and Murphy, 1999; Bergfors, 2003) so only a brief overview will be given here.

Nucleation is said to be homogenous when it occurs in the bulk of the solution. This is believed to be a rare occurrence as most crystallizing systems contain random impurities that may induce nucleation. Indeed, the presence of foreign bodies or ‘catalytic’ substrates can induce nucleation at supersaturations lower than those required for homogenous nucleation. A substrate allows adsorption of crystallizing material and lowers the value of the activation free energy of germination. The extent of this reduction depends on the degree to which the catalyzing body mimics the structure of the solute. This type of nucleation is referred to as heterogeneous (Davey and Garside, 2000).

Naturally, the best match between a substrate and crystallizing solute exists when the substrate is a ‘seed’ crystal of that solute (or a closely structurally related molecule). Nucleation that occurs on, or is promoted by, a seed crystal of the crystallizing solute is known as secondary nucleation. The advantage of applying secondary nucleation (or seeding) to a system is that it completely removes the need for that system to undergo nucleation at all.

### 1.2.3 Crystal growth

Once the nucleation step has been overcome nuclei grow, eventually developing into macroscopic crystals. This stage of the crystallization process is known as crystal growth.

For crystal growth to proceed, the surface of the crystal must first be able to ‘capture’ growth units arriving from solution and subsequently integrate them into the crystal lattice. Whilst this process is dependent on a number of factors, the most important is the availability of so-called ‘kinked’ sites on the developing crystal surface.

This situation is best described by the Terrace-Ledge-Kink (TLK) model of crystal growth, a simplified schematic of which is contained in figure 1.2. The growth unit is first transported from the bulk solution to the developing crystal surface. At this point, the solute molecule will be in one of three situations (i) it will be able to integrate into the crystal lattice directly because it has landed at a site with an available kink position (growth unit **A** in figure 1.2), (ii) it will first adsorb to the crystal surface terrace, and migrate to a step and finally adhere at a kink position (growth unit **B** in figure 1.2), or (iii) it will desorb from the surface and return to the fluid phase (growth unit **C** in figure 1.2).

Kink positions are crucial to the crystal growth process, as they offer energetically preferred binding conditions to a growth unit. Indeed, lattice integration from a kink site offers interactions in three dimensions to the arriving growth unit – from the ledge beneath it, the step behind it and its neighbouring solute molecule that had previously been integrated into the lattice. Energetically, this is preferred to the two interactions offered by the step position, and one by the ledge position.

#### 1.2.4 Crystal growth mechanisms

As previously discussed, the presence of steps and kink sites on growing crystals surfaces are vitally important in the crystal growth process. However, it is equally important from a crystal growth point of view to understand how these steps actually come into existence

The possible pathways by which a molecule passes from solution to become integrated into the crystal lattice are known as *growth mechanisms*. Three growth mechanisms are known to dominant almost all forms of crystal growth – continuous growth, surface nucleation and spiral growth (Davey and Garside, 2000). However, there are also a small number of lesser-observed mechanisms by which growth steps may be formed. These are all summarized below.

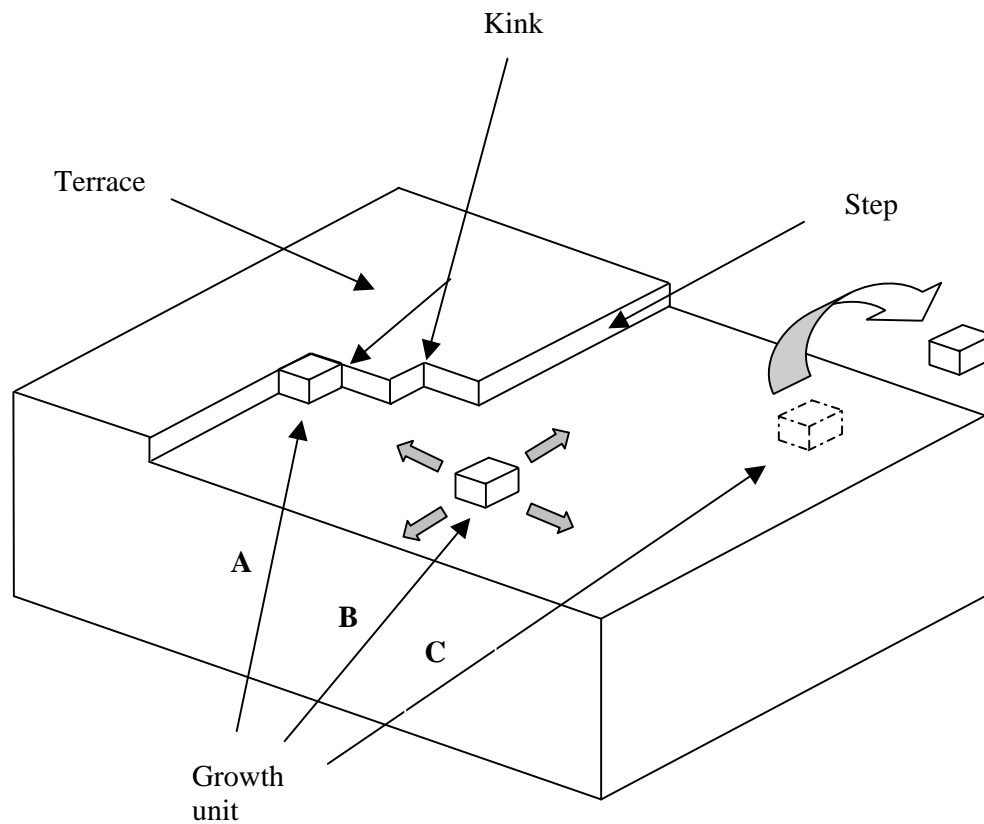


**Figure 1.2.** A schematic illustration of the Terrace-Ledge-Kink (TLK) model. In this model, growth units adsorb to the crystal terrace and either attach to a kink position directly after adsorption to the crystal surface (growth unit **A**), adsorb onto a terrace and migrate across to a step, where it locates a kink site and subsequently becomes incorporated into the crystal lattice (growth unit **B**) or desorb from the surface (growth unit **C**). The repeated addition of such growth units to kink sites results in the progression of the step across the terrace.

#### 1.2.4.1 Continuous growth

Continuous growth (or normal growth as it is sometimes termed) occurs when the energy required to form a step on the crystal surface is low and so the surface of the crystal will contain many kink and step sites. Indeed, on a molecular level such surfaces will be extremely rough, thus providing all arriving growth units with a lattice integration point (Davey and Garside, 2000). This process is rare for conventional systems and is restricted primarily to crystals grown from a melt or from the vapour phase (Chernov, 1984).

#### 1.2.4.2 Surface nucleation

The general way in which a perfect solution grown crystal develops is via a method of surface nucleation called two-dimensional nucleation (Burton *et al.*, 1951). The process is often termed the ‘Birth and Spread’ (B+S) model, and is illustrated schematically in figure 1.3.

This mechanism occurs when, unlike continuous growth, some of the growth units arriving at the surface do not immediately find a growth site – such units either return to the fluid phase, or join other adsorbed molecules on the crystal surface to form the characteristic two-dimensional (2D) islands seen in figure 1.3. New adsorbed growth units may continue to add to the kinks formed at this growth step, until a complete monomolecular layer has expanded laterally across and covered the entire crystal surface.

As growth proceeds, the supersaturation of the solution slowly diminishes due to the ‘loss’ of solute molecules to the expanding crystalline surface. Theoretically, growth on a perfect crystal surface will come to a halt when the level of supersaturation becomes too low to support the formation of new 2D nuclei. However, because the vast majority of crystals are not perfect, another growth mechanism, namely spiral growth, can become prominent.

#### 1.2.4.3 Spiral growth

Spiral growth is able to occur because of a defect that is commonly found in growing crystals – the screw dislocation. A screw dislocation is formed when one

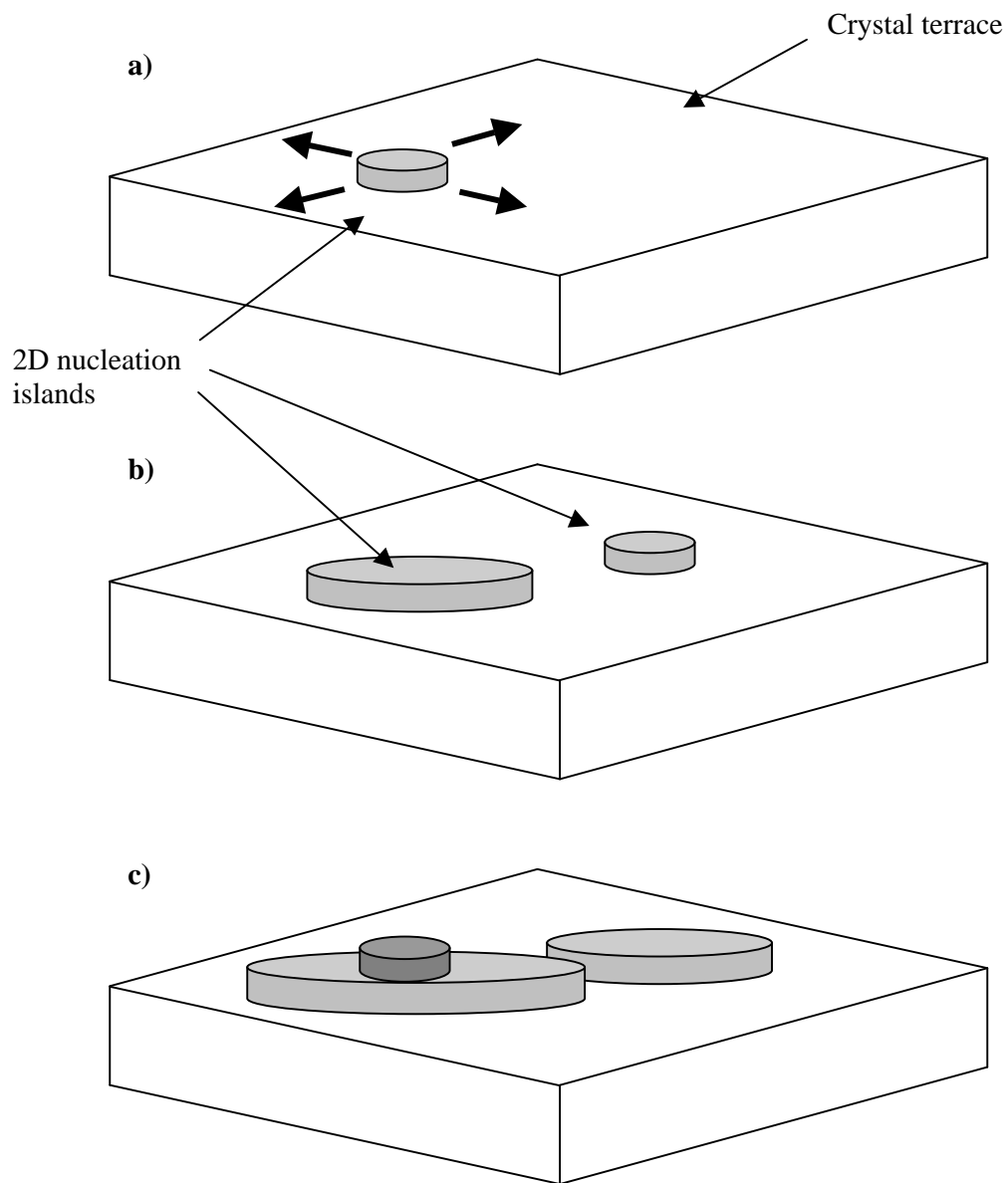


**Figure 1.3.** The formation and expansion of two-dimensional (2D) nucleation islands on a crystal surface. In (a), the island expands in all directions, and is joined by a second island in (b). Growth proceeds by solute addition to both of these islands, and eventually a completely new growth layer will be formed by nucleation on top of one of these islands, as illustrated in (c).

region of the crystal is pushed up through one (or more) unit cells relative to another region. This 'cut' then acts as a step to which solute molecules can attach, thus permitting the continuation of growth, even at reduced levels of supersaturation. The most important feature of such dislocations is that they are not annihilated as the dislocation propagates radially in a spiral, thus imposing a permanent step at the crystal surface (Frank, 1949; Atkins, 1998; Plomp, 1999). This process is illustrated schematically in figure 1.4.

There are a number of different classes of defect, many of which play an important role in certain aspects of crystallization from solution. These are discussed in greater depth throughout this thesis.

#### 1.2.4.4 Other step sources

There are a small number of less common mechanisms by which step sources are formed. The first is a type of surface nucleation termed three-dimensional (3D) nucleation. This mechanism is believed to be unique to macromolecular crystal growth (McPherson *et al.*, 2001). At higher levels of supersaturation in such systems it appears that large quantities of solute molecules are able to aggregate in solution and subsequently adsorb to the crystal surface, at which point they form misaligned microcrystals or multilayered stacks. This mechanism is discussed in further detail in chapter 3.

Defects that are able to propagate through crystals are known to occasionally form step sources, as are foreign molecules that can act as heterogeneous nuclei on the surface of crystals.

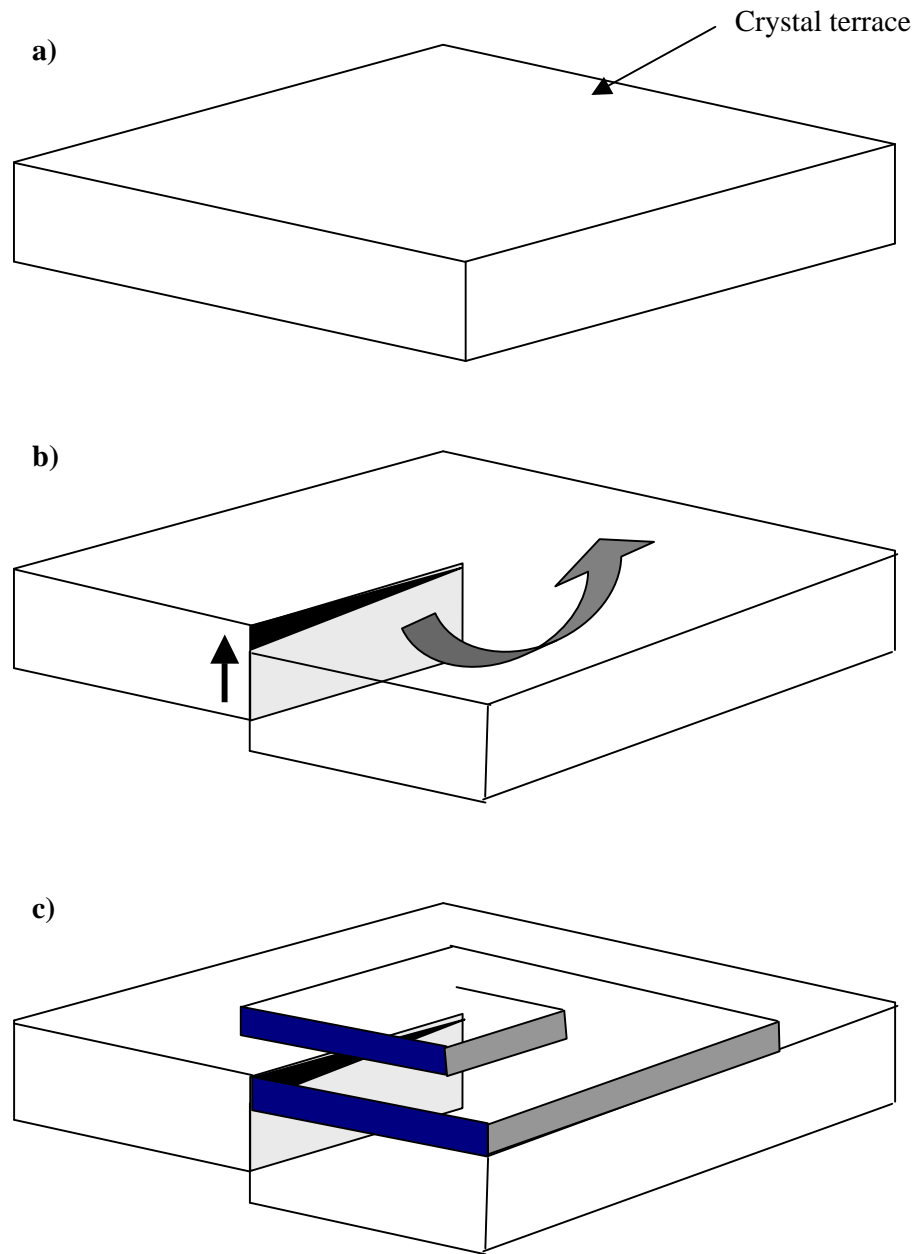


**Figure 1.4.** A schematic representation of spiral crystal growth. (a) A perfect crystal surface, (b) the creation of a screw dislocation by one region of the crystal being pushed up through one (or more) unit cells relative to another region, (c) spiral growth at the dislocation outcrop.

### 1.3 The physical appearance of crystalline solids

#### 1.3.1 Crystal morphology

The overall shape of a crystal, often termed its habit, form or morphology, is determined by a combination of two factors – the internal crystal structure, and the relative growth rates of the faces bounding the crystal (Davey and Garside, 2000).

The pioneering work of Hartmann & Perdok led to the development of the Periodic Bond Chain (PBC) theory, which was the first quantitative theory linking the internal crystal structure to the final 3D crystal morphology (Hartman and Perdok, 1955). They were able to show that the structure and morphology of crystalline entities are inextricably linked as the structure dictates which crystal growth directions offer the largest energy gain (termed attachment energy or  $E_{att}$ ). In these directions, growth will be rapid. As such, over time these surfaces essentially grow themselves out of existence, making the slower growing faces morphologically more important.

This effect also applies to step patterns observed on the crystal faces, leading to anisotropy in the development of 2D nucleation islands and screw dislocations. This effect is particularly prominent during the growth of macromolecular crystals because of their size – depending on which position on an advancing step edge a molecule occupies, it will form a different set of intermolecular interactions with its neighbours, thus exposing a different portion of its surface to the solvent. Consequently, molecules are able to join the lattice at different rates, depending on which direction the step edge is moving. This plays a major part in determining the shape of the growing crystal face, and subsequently the gross morphology of the crystal (McPherson, 1999).

In combination with various energetic calculations and theories, the PBC theory provides a means by which the crystal morphology can be predicted from the structural information of the solute. However, the predictions generated by PBC theory are occasionally flawed as the rates of growth of crystal faces are not exclusively determined by the internal crystal structure – they can also be susceptible to the conditions that prevail in the growth medium. The three main environmental factors that are known to influence crystal morphologies are supersaturation, solvent and the presence of impurities/additives. Indeed, the PBC theory can neglect these factors as its

theoretical morphology predictions are generated for crystals grown at low values of supersaturation from the vapour phase, at 0 K (Pfefer and Boistelle, 2000).

Whilst not as important in macromolecular crystallization, the overall morphology of crystals of pharmaceutical relevance is of significant practical importance. Crystals that exhibit certain shapes (such as thin plates) are often very difficult to deal with on a large scale. Crystallization and its importance in the pharmaceutical industry are discussed further in chapter 2 of this thesis.

### 1.3.2 Polymorphism

When a solute is able to adopt more than one internal crystal structure, it is said to exhibit polymorphism. Polymorphs are generally bounded by alternative crystal faces, with each often exhibiting its own combination of mechanical, thermal and physical properties. Polymorphs of crystalline drug substances, whilst being chemically identical, can display vastly different physical properties such as solubility values and dissolution rates. This can, in turn, affect the overall bioavailability of the drug substance. When considering the remarkable frequency with which many drug types exhibit polymorphism (for example, 63% of barbiturates, 67% of steroids and 40% of sulfonamides are known to form polymorphs), it is clear that it is an extremely important consideration in the pharmaceutical industry (Aulton, 1988).

Polymorphism is also commonly observed in macromolecular crystallization. It can be an important consideration as different polymorphs often display significantly different diffraction properties. This is discussed further in chapter 4 of this thesis.

## **1.4 Experimental techniques used to study nucleation and crystal growth processes**

This section contains a review of the key experimental techniques utilized in the investigation of solution grown crystals. As this thesis is primarily concerned with the growth of such crystals, only a brief outline of the techniques used to quantify

nucleation is presented and as such the reader is directed to the comprehensive reviews referenced for further information.

#### 1.4.1 Nucleation

Nucleation phenomena in small molecular crystals are generally described in terms of macroscopic properties due to the scarcity of experimental techniques that permit the direct observation and monitoring of events at a molecular level. Examples of the macroscopic properties that can be monitored to provide information concerning nucleation include (i) changes in temperature caused by the lowering of the free energy in a system post-nucleation, (ii) changes in the optical properties of a solution during nucleation and (iii) the decrease in solute concentration during nucleation (Rodriguez-Hornedo and Murphy, 1999; Davey and Garside, 2000).

However, the majority of data concerning crystal nucleation has originated from studies of macromolecular crystallization. Such studies are easier to perform due to the larger molecule dimensions and thus the larger pre-nucleation clusters. Additionally, the increased molecule dimensions have permitted direct investigations of nucleation in addition to the observations of changes in macroscopic properties as described above. Indeed, Atomic Force Microscopy (AFM), Transmission Electron Microscopy (TEM) and Confocal Laser Scanning Microscopy (CLSM) have all been utilized to observe the initial pathways of crystallization at a near-molecular level (Garcia-Ruiz, 2003)

#### 1.4.2 Crystal growth

The techniques most commonly implemented in the experimental investigation of crystal growth are listed in table 1.1, with each being briefly reviewed in the following sections. AFM, the main technique implemented throughout this thesis, is reviewed in more depth in section 1.5.

<b>Technique</b>	<b>Information that the technique provides about crystal growth</b>
<i>Optical Microscopy</i>	<ul style="list-style-type: none"> <li>- Study crystallization processes <i>in situ</i></li> <li>- Monitor transformations in suspensions</li> <li>- Characterize additive or solvent interactions with specific crystal faces</li> <li>- Measure crystal growth rates</li> </ul>
<i>Interferometry</i>	<ul style="list-style-type: none"> <li>- Examine surface topography</li> <li>- Identify growth mechanisms</li> <li>- Measure tangential and normal crystal growth rates</li> </ul>
<i>Electron Microscopy</i>	<ul style="list-style-type: none"> <li>- Characterize additive or solvent interactions with specific crystal faces</li> <li>- Identify nucleation and growth mechanisms</li> </ul>
<b>Atomic Force Microscopy</b>	<ul style="list-style-type: none"> <li>- Examine surface topography</li> <li>- Study crystallization processes <i>in situ</i> at high resolution, and in real-time</li> <li>- Characterize additive or solvent interactions with crystal faces</li> <li>- Identify nucleation and growth mechanisms</li> <li>- Measure crystal growth rates</li> </ul>

**Table 1.1.** The experimental techniques commonly applied to the study of crystal growth (Rodriguez-Hornedo and Murphy, 1999)

### 1.4.2.1 Optical microscopy

Optical microscopy, in its simplest form, employs a series of lenses to focus a beam of visible light, after it has interacted with a sample. This provides an image of the sample that is usually observed through an eyepiece. However, the resolution obtainable when employing optical microscopy is limited by the relatively long wavelength of light, and image contamination by out-of-focus light.

The main advantage of optical microscopy is that it is a completely non-invasive technique. As such, the addition of a temperature controlled flow cell has permitted the acquisition of accurate growth rates for a number of crystals of pharmaceutical and biological interest such as sulphathiazole (Mehta *et al.*, 1970; Simonelli *et al.*, 1970), methylprednisolone (Mehta *et al.*, 1970), phenytoin (Zipp and Rodriguez-Hornedo, 1993) and lysozyme (Monaco and Rosenberger, 1993). Additionally, the more advanced optical microscopy technique of Confocal Laser Scanning Microscopy (CLSM) has been used to study the micro-topography of macromolecular crystals such as insulin (Muhlig *et al.*, 2001) and lysozyme (Sazaki *et al.*, 2004).

For more detailed account of optical microscopy and related techniques see (Slayter and Slayter, 1992).

### 1.4.2.2 Interferometry

Interferometry is based on the interference of a wavefront of light reflected from a growing crystal face with a reference beam. Phase differences occur in the reflected beam because of height differences on the crystal surface due to growth hillocks and 2D nucleation islands (McPherson, 1999). Indeed the *in situ* and completely non-invasive nature of interferometry, combined with high vertical resolution (<20nm) and rapid image acquisition times (<5s per image), permits the accurate quantitative measurement of both normal and tangential growth rates of steps on the crystal surface, under a strictly controlled growth environment. Interferometry has been used to investigate the surfaces of crystals of pharmaceutical interest such as paracetamol (Shekunov and Grant, 1997; Shekunov *et al.*, 1997), numerous macromolecular crystals including turnip yellow mosaic virus (TYMV), canavalin and thaumatin (Kuznetsov *et al.*, 1995; Kuznetsov *et al.*, 1996b) and, most commonly, lysozyme (Vekilov *et al.*, 1993; Rosenberger, 1996; Vekilov and Rosenberger, 1996; Vekilov *et al.*, 1997).

Interferometry has undoubtedly contributed much to the fundamental understanding of areas such as the kinetics of impurity incorporation into crystals, growth rate fluctuations and step bunching. However, the technique is limited by its relatively poor spatial resolution (Rosenberger, 1996).

For a detailed description of interferometric techniques, with particular emphasis on their application to crystal growth, see (Kuznetsov *et al.*, 1995).

#### 1.4.2.3 Electron Microscopy

Electron Microscopy (EM) is a method that was developed to tackle the limited resolution of optical microscopy. Electron Microscopes (EMs) function exactly as their optical counterparts except that they use a focused beam of high-energy electrons to ‘image’ the specimen, which is enclosed in a vacuum. There are four basic steps that are involved in the operation of all EMs. (i) A stream of electrons is formed (usually from the process of thermionic emission) and accelerated towards the specimen using a positive electrical potential. (ii) This stream is confined and focused using metal apertures and magnetic lenses into a thin, focused beam. (iii) This beam is subsequently focused onto the sample and (iv) the interactions within that irradiated sample effect the electron beam in a way that can be monitored and converted into an image. As the electrons have a much shorter wavelength than light, the resolution of EM can be several hundred-fold higher than that of a classic optical microscope (Slayter and Slayter, 1992)

The two main types of EM are the Transmission Electron Microscope (TEM) and the Scanning Electron Microscope (SEM), and both have played various roles in the study of crystals of pharmaceutical and biological importance.

To the author’s knowledge, TEM was employed to achieve the first molecular resolution images of single macromolecular crystal surfaces in the mid-1980s (McPherson, 1985). Such images were obtained by employing a slightly modified version of ‘freeze-etch’ TEM, which involves the rapid cleaning, freezing and replicating of newly grown seed crystals.

The first quantitative protein crystal growth study employing TEM was performed in 1990 (Durbin and Feher, 1990). In this study the freeze-etch technique was again implemented, which yielded ‘snapshots’ of lysozyme crystals grown under a

variety of conditions at both a microscopic and molecular level. This allowed the authors to compare the microscopic images with previous experimental studies concerning the measurement of lysozyme crystal growth rates under well-defined conditions (Durbin and Feher, 1986).

Whilst this was an innovative investigation, TEM is not ideally suited to the study of crystal growth as there is no possibility of obtaining any *in situ* data. Indeed, the success of interferometry and AFM (see section 1.5) has effectively made the TEM redundant in the study of crystal growth, with only a handful of experiments performed on specific aspects of crystal growth since the work of Durbin and Feher (Michinomae *et al.*, 1999; Braun *et al.*, 2000). However, the development of exceptionally high resolution helium-cooled instruments has meant that cryo-TEM has become an important tool in the angstrom-resolution structural analysis of certain membrane proteins that have been crystallized in a 2D protein-lipid membrane (Kuhlbrandt and Williams, 1999; Breyton *et al.*, 2002; Werten *et al.*, 2002).

SEM exhibits similar limitations to TEM when performing crystal growth studies. The acquisition of *in situ* data is not possible as the sample is typically studied under vacuum, and non-conducting samples may need to be gold-coated prior to analysis to reduce surface charging effects.

SEM operates differently to TEM in that the output signals (those that make up the image) are reflected from an opaque surface rather than being transmitted through the semi-transparent sample. The result is that SEM images are formed by topographic contrast. This makes the SEM a useful tool in observing morphological aspects of pharmaceutically important crystals without the need for the often time consuming and difficult specimen preparation generally required for TEM. For examples of such images, see chapter 2 of this thesis.

The techniques outlined above all have various advantages and drawbacks. Optical microscopy is completely non-invasive, but has limited resolution because of the physics of light. Electron microscopy is capable of extraordinarily high resolution, but is unable to provide information on dynamic processes *in situ*, as imaging is generally carried out under vacuum. Interferometry is a valuable tool for investigating various kinetic aspects of crystal growth, as it permits the study of microscopic morphologies across whole macroscopic facets. However, as with optical microscopy, interferometry has limited spatial resolution.

Over the past decade a powerful new microscopical technique has come to the fore in the study of crystal growth. Atomic Force Microscopy (AFM) incorporates many of the advantages of the techniques described above in that it is virtually non-invasive and is capable of achieving molecular resolution images of crystals in their native growth environment. A detailed description of the principles of AFM, and its role in the study of solution crystallization phenomena are presented below.

### 1.5 Atomic Force Microscopy (AFM)

AFM is one of a number of microscopical techniques broadly referred to as the Scanning Probe Microscopies (SPM). The first SPM-based technique was invented in the early 1980s and was called Scanning Tunnelling Microscopy (STM) (Binnig and Rohrer, 1982; Binnig *et al.*, 1982).

STM operates by employing a sharp, conducting probe that is brought to within ~1 nm of a conductive sample surface. A bias voltage applied across the probe-sample gap, causing a tunnelling current to flow between the two conductors. In the standard operating mode of STM, a specified level of current is maintained as the probe is raster scanned across the sample surface. If an increase or decrease in current is detected during scanning, the voltage supplied to the piezo is adjusted, thus maintaining a constant pre-set current. These changes in piezo voltage are stored and converted into what is essentially a 'trace' of the electron density across the sample surface, which can, for a homogeneous surface, be approximated to topography data.

The invention of the STM represented a huge step forward in microscopical analysis. However, the instrument is limited to the investigation of electrically conducting samples only. It was this drawback that led to the successful development of AFM, an instrument that is capable of investigating samples in either ambient air conditions or, most importantly for biologists, in liquid.

AFM was developed throughout the early 1980s, and was first reported in 1986 (Binnig *et al.*, 1986). Like all SPM techniques, AFM employs a sharp probe that is positioned in close proximity to a sample surface. Such probes are constructed of a tip mounted at the end of a short flexible cantilever, which is typically 100-250  $\mu\text{m}$  in length. The tip itself generally has a radius in the range of 5-40 nm, although efforts are

being made to dramatically decrease this figure by incorporating carbon nanotubes into the AFM probe (for example see Hafner *et al.*, 2001).

As with the STM, the AFM probe is raster scanned (in the x & y directions) by means of a piezo-electric scanner. As the probe is translated laterally across the sample, it interacts through ‘aggregate atomic forces’ with structural features on the surface (McPherson *et al.*, 2003). These interactions cause the probe to be displaced vertically (in the z direction). Often, these detectable movements are minute (<1 nm), so the AFM incorporates an extremely sensitive detection mechanism. Generally, this takes the form of an ‘optical lever system’, in which a laser beam is focused onto the end of the AFM cantilever and reflected onto a spatially sensitive photodiode detector that is split into four quadrants. As the cantilever moves in response to the sample topography, the angle of the reflection of the laser beam also changes, altering the position of the laser within each of the photodiode quadrants. Indeed, this relatively simple system is sensitive enough to detect atomic-scale movement of the tip as it traverses the sample (Morris *et al.*, 1999). A simplified diagram depicting the typical set-up of an AFM is presented in figure 1.5.

### 1.5.1 AFM imaging modes

Modern AFMs are able to produce images in a number of different modes, depending on the nature of the interaction between the probe and the surface. Figure 1.6 presents a schematic representation of how force varies with distance between tip and sample, together with an indication as to the different regions of the force curve, which correspond to the three main imaging modes (contact, intermittent contact and non-contact). These are briefly discussed in the following section.

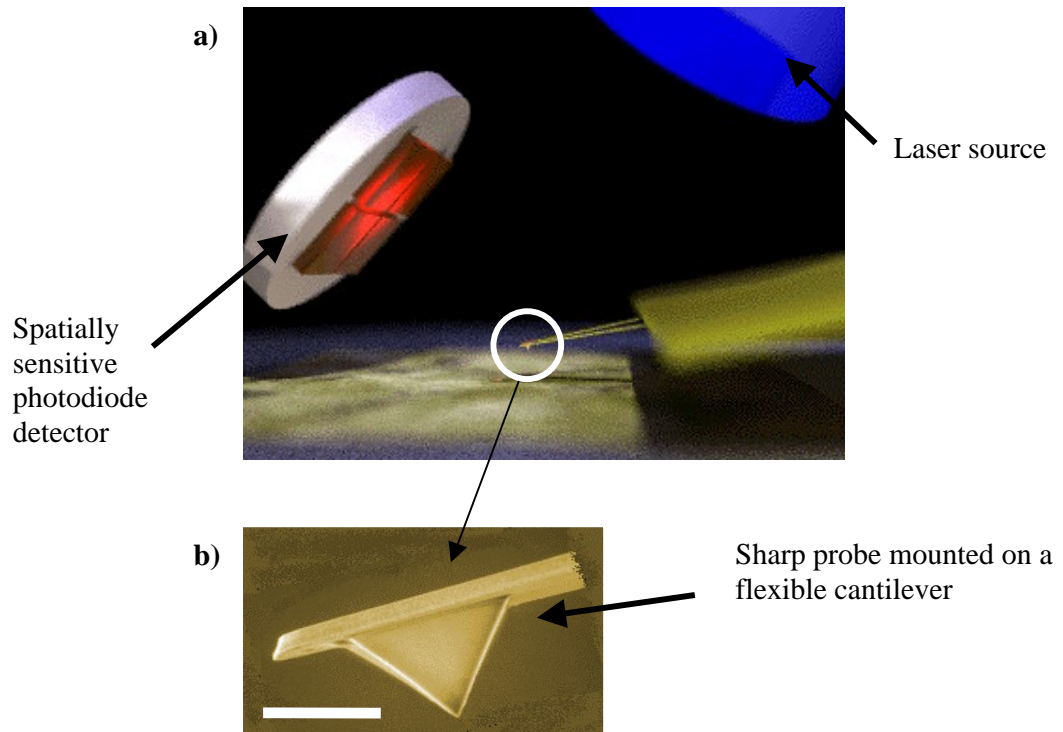


**Figure 1.5.** A schematic representation of a typical AFM set up in (a). An SEM micrograph in (b) shows an AFM tip. Scale bar, 3  $\mu\text{m}$ .

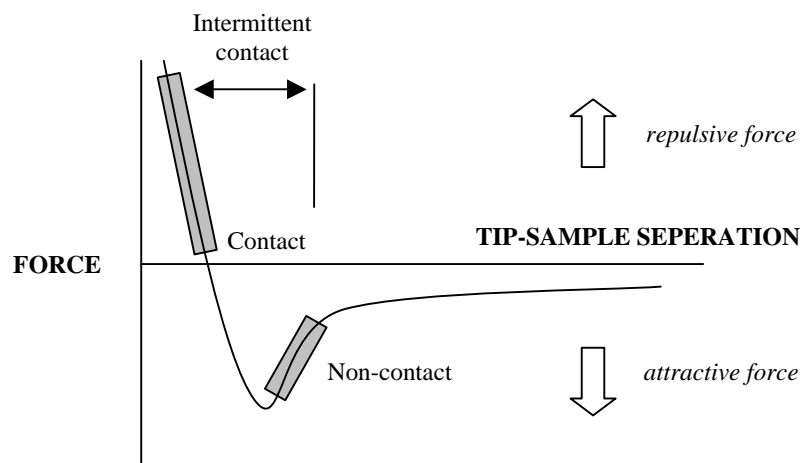


**Figure 1.6.** How force varies with tip-sample separation during the three main AFM imaging modes.

### 1.5.1.1 Contact mode

Contact mode is regarded as the original imaging mode developed in AFM. In this mode, the microscope can be operated in either ‘height’ or ‘deflection’ mode. The former utilizes an electronic feedback mechanism to continually adjust the height of the tip (or sample, depending on the AFM set-up) to maintain a constant force on the sample whilst the tip is raster scanned across the surface. When operated in this mode, the system monitors the changes in piezo height, subsequently using this information to form accurate three-dimensional images of the surface.

When operated in deflection mode, the z-piezo remains stationary whilst the deflection data from the movement of the laser in response to changes in topography are recorded. Images produced in deflection mode are not quantifiable in the z-direction, but often highlight rapid changes in topography in greater detail, such as is seen at step edges, and are occasionally used for that purpose throughout this thesis.

Contact mode imaging is almost always preferred when imaging hard and stable samples. Additionally, as contact mode imaging involves applying a relatively high force to the sample (see figure 1.6) it generally offers the best option for achieving higher resolution images, as the probe is continually in contact with the sample surface. However, the inevitable offset to this is the higher applied force, the greater the likelihood of damage occurring to the surface via unwanted lateral tip-sample effects such as frictional forces. Whilst such forces may not degrade harder samples, they are often of a magnitude sufficient to cause damage to softer, biological samples. These problems led to the development of intermittent and non-contact modes.

### 1.5.1.2 Tapping (or intermittent) mode

Tapping mode (TM-AFM) was developed to help alleviate some of the problems associated with contact mode imaging (Zhong *et al.*, 1993; Hansma *et al.*, 1994). It uses an oscillating tip (frequency in the range 50-500kHz in air, ~10kHz in liquid) at an amplitude of tens of nanometers if not in contact with the surface. As this oscillating tip, which is driven at, or close to, its resonant frequency by a separate oscillation piezo, is moved towards the surface, it begins to touch (or ‘tap’) the surface intermittently. As with contact mode, the AFM feedback system constantly adjusts the z-piezo to maintain the amplitude of the freely oscillating probe as a constant pre-set value (Jandt, 2001;

McPherson *et al.*, 2003), subsequently using this data to form accurate three-dimensional images.

TM-AFM greatly reduces lateral forces involved in imaging, thus minimizing sample damage. As such, it has been widely implemented in the study of easily deformable materials such as polymers, proteins and cells (for relevant examples see Radmacher *et al.*, 1995; Thompson *et al.*, 1996; Camesano *et al.*, 2000).

### 1.5.1.3 Non-contact mode

The magnitude of the forces applied to the sample by the AFM tip can be further reduced by applying non-contact mode (NC-AFM) (Martin *et al.*, 1987; Luthi *et al.*, 1994). This mode operates by bringing a probe, which is vibrating at its resonant frequency, into the attractive force region (see figure 1.6). It does not come into physical contact with the surface, but is able to detect ‘force gradients’ as it is raster scanned across the surface by either shifts in the resonant frequency or amplitude of the cantilever. NC-AFM is desirable as it offers a means of investigating the sample topography with a complete lack of sample damage. However, the long range attractive forces that operate between the sample and probe are relatively low and less sensitive to probe-sample separation – as such, images obtained from NC-AFM inevitably display a lower spatial resolution.

## 1.5.2 Force-distance measurements

In addition to its imaging capabilities, AFM is also able to quantitatively measure the forces that exist between the probe and sample. Experiments of this nature are commonly referred to as force-distance measurements (Burnham and Colton, 1989).

Force-distance measurements are recorded by monitoring the deflections of the cantilever as the probe is first brought into contact with the sample at a constant z-piezo velocity, and subsequently separated from the sample. Figure 1.7 displays a schematic of a typical force-distance plot, which is constructed from the cantilever deflection force in nN (y-axis) versus the distance traveled by the z-piezo measured in nm (x-axis). At (A) the probe-sample distance is considerable and, as such, there is zero cantilever

deflection. From this position, the probe approaches the sample at a constant velocity until the probe is close enough to the surface to begin experiencing weak long-range attractive forces. When the magnitude of these forces exceed the stiffness of the cantilever spring, the probe ‘jumps’ into contact with the sample surface (**B**). Further advancement of the tip towards the sample results in repulsive forces between the two, thus bending the cantilever in the opposite direction. This forward motion continues until (**C**), which represents the predetermined point of maximum load. At this point the probe begins to retract from the surface. The tip often remains engaged beyond the jump to contact distance and the force required for disengagement at (**D**), commonly referred to as the ‘pull-off’ or adhesion force, exceeds that obtained at jump-to-contact. Eventually the tip disengages completely and returns to its original start position (**E**).

By using the AFM as a force-sensing instrument, considerable progress has been made in the understanding of the forces that govern the fundamental properties of all materials. The majority of these investigations are beyond the scope of this thesis and as such, the reader is directed to the numerous review articles on the subject for further information (Allen *et al.*, 1997; Cappella and Dietler, 1999; Best *et al.*, 2003).

### 1.5.3 The role of AFM in the study of crystallization phenomena

Since its inception, AFM has emerged as the method of choice for characterizing the growth and surface structure of a range of crystalline materials. It holds a number of advantages over more conventional techniques, making it ideally suited to the study of such materials.

Most important is the AFMs ability to provide *in situ* data whilst retaining excellent spatial resolution. It can be applied to scan fields ranging in size from less than 50 nm up to approximately 150  $\mu\text{m}$ , with a height resolution as great as 0.1 nm. Thus, it can provide precise visual detail over a size range out of the reach of more conventional techniques (McPherson *et al.*, 2000). Additionally, the non-perturbing nature of the probe interaction with the surface under study allows the dynamic processes that underlie all aspects of crystallization to be investigated under carefully controlled conditions.

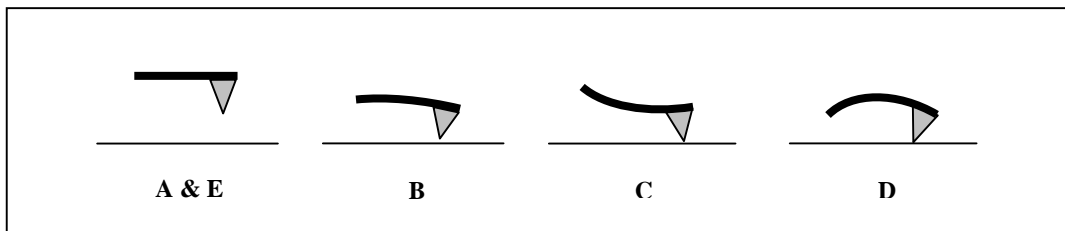
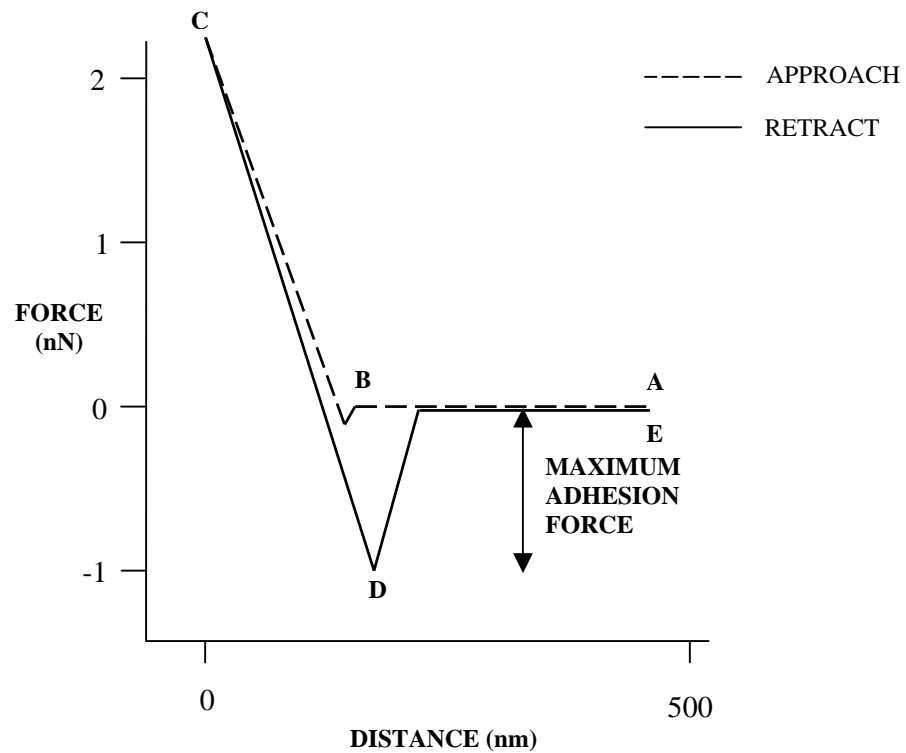


**Figure 1.7.** Schematic of a typical force-distance curve observed with the AFM. (A) Tip approaches sample surface, (B) ‘jump to contact’ due to long range attractive forces, (C) point of maximum load, which is set by the user, (D) disengagement (or ‘pull-off’) as tip is retracted from surface and (E) tip returns back to it’s starting position out of the range of any surface forces.

Inevitably, these advantages have led to AFM being implemented in the study of a huge range of crystalline samples from almost all fields of science and technology. Examples include studies of single diamond crystals (Yin *et al.*, 2002), inorganic crystals such as potassium sulphate (Mauri and Moret, 2000) and calcium oxalate monohydrate (Guo *et al.*, 2002), and investigations into polymer crystallization (Hobbs *et al.*, 2001).

However, the main focus of this thesis is the application of AFM to the study of crystals of pharmaceutical and biological importance. As such, overviews of these fields are presented in the following sections.

### 1.5.3.1 Macromolecular crystallization

First introduced into the field of macromolecular crystallization in 1992 (Durbin and Carlson, 1992), the *in situ* capabilities of AFM have since been successfully implemented in the study of the growth and structure of numerous macromolecular crystals including  $\alpha$ -amylase (Astier *et al.*, 2001; Aquilano *et al.*, 2003), apoferritin (Petsev *et al.*, 2000; Yau *et al.*, 2000; Yau and Vekilov, 2000; Yau and Vekilov, 2001), Bence-Jones protein (Plomp *et al.*, 2003), canavalin (Land *et al.*, 1995; Land *et al.*, 1997; Land and DeYoreo, 2000; Ko *et al.*, 2001), catalase (Malkin *et al.*, 1997), cucumber mosaic virus (CMV) (Malkin and McPherson, 2002), insulin (Yip and Ward, 1996; Yip *et al.*, 1998a; Yip *et al.*, 1998b; Gliko *et al.*, 2003), lysozyme (Durbin and Carlson, 1992; Durbin *et al.*, 1993; Konnert *et al.*, 1994; Chernov *et al.*, 1999; Li *et al.*, 1999a; Li *et al.*, 1999b; Nakada *et al.*, 1999; Rong *et al.*, 2000; Hondoh *et al.*, 2001; Mollica *et al.*, 2001; Rashkovich *et al.*, 2001; Wiechmann *et al.*, 2001; Yoshizaki *et al.*, 2001; Matsuzuki *et al.*, 2002; Rashkovich *et al.*, 2002; Yaminsky *et al.*, 2002), thaumatin (Malkin *et al.*, 1996a; Kuznetsov *et al.*, 1999a; Kuznetsov *et al.*, 2001), trypsin (Plomp *et al.*, 2001), tRNA (Ng *et al.*, 1997), satellite tobacco mosaic virus (STMV) (Malkin *et al.*, 1995b), turnip yellow mosaic virus (TYMV) (Malkin *et al.*, 1999a) and xylanase (Malkin *et al.*, 1999b).

By utilizing such macromolecules as ‘models’ of crystallization, the fundamental understanding of crystal growth has been improved considerably, particularly in areas concerning the mechanisms that promote crystal growth (Malkin *et al.*, 1995a; Malkin *et al.*, 1995b; Kuznetsov *et al.*, 1996a; Malkin *et al.*, 1996c; Kuznetsov *et al.*, 1998; Kuznetsov *et al.*, 1999b), impurity incorporation and defect

structure of macromolecular crystals (Malkin *et al.*, 1996b; McPherson *et al.*, 1996; Malkin *et al.*, 1999b; Nakada *et al.*, 1999; Malkin and McPherson, 2002) and crystal packing and symmetry (Kuznetsov *et al.*, 1997; Plomp *et al.*, 2002).

Indeed, the clear visualization of such crystals offered by AFM has helped indicate that the crystallization of macromolecules and inorganic molecules from solution obey the same fundamental laws (Chernov, 1997). Issues surrounding the fundamental understanding of macromolecular crystallization are discussed further in chapter 3 of this thesis.

### 1.5.3.2 Pharmaceutical crystallization

Whilst not implemented as often as seen in the study of macromolecular crystals, AFM has played a central role in a number of innovative investigations into various aspects of pharmaceutical crystallization.

The dissolution of single aspirin crystals has been investigated by *in situ* AFM on a number of occasions (Wilkins *et al.*, 2000; Danesh *et al.*, 2001; Wilkins *et al.*, 2002), as has the growth of paracetamol crystals in the presence of various additives (Thompson *et al.*, 2004). *Ex situ* AFM has also been performed on paracetamol crystals to investigate the effects of solvent on the formation of etch pits on the crystal surface (Li *et al.*, 2000). Additionally, functionalized AFM cantilevers have been utilized to characterize the different planes of the aspirin crystal (Danesh *et al.*, 2000b), and TM-AFM has been used to distinguish between polymorphs of the drug cimetidine (Danesh *et al.*, 2000a).

## 1.6 Project Aims

Crystallization from solution clearly plays a key role in both the production and processing of pharmaceutically important materials, and in the elucidation of structural information from biological macromolecules. However, because of difficulties associated with their study, many of the phenomena governing the crystallization of such materials are still relatively poorly understood.

In this project, we aim to utilize *in situ* AFM to investigate a number of important issues surrounding molecular and macromolecular crystallization, with a particular view to developing experimental protocols that will enable us to prepare and study poorly diffracting macromolecular crystals.

The studies presented in chapter 2 of this thesis are concerned with the crystallization and habit modification of the pharmaceutical excipient adipic acid. Adipic acid has long been known to exhibit a variety of interesting crystallization properties, many of which have been attributed to the extremely hydrophilic nature of the dominant (100) surface. However, many of these theories have never been proved experimentally. As such, we aim to investigate the (100) face with *in situ* AFM in both air and liquid environments with a view to furthering experimental knowledge of this system. To achieve this aim, protocols will first be developed to grow large seed crystals suitable for study by AFM. Such crystals will initially be characterized in air, followed by studies carried out on crystals that have been doped with specific quantities of the structurally related habit modifier, octanoic acid. Finally we will attempt to investigate the growth, dissolution and habit modification of adipic acid crystals *in situ* to uncover exactly how the chemical nature of the (100) dictates the development of the crystal.

The next study is concerned with the AFM analysis of the model macromolecular crystal system, tetragonal lysozyme. This system has been chosen because lysozyme is readily available and, most importantly, relatively straightforward to crystallize in the tetragonal form. These facts will allow us to develop the experimental protocols necessary to successfully study the smaller, more fragile assemblies of molecules produced during macromolecular crystallization.

Although lysozyme crystallization has been studied with AFM on a number of occasions in the past, there are still conflicting reports concerning certain aspects of the lysozyme molecules assembly into the crystalline state, such as the size of the growth unit and mechanisms employed during growth. As such, we also aim to use *in situ* AFM to add existing microscopical data to the subject, thus addressing some of the outstanding questions concerning the crystallization of lysozyme.

The crystallization of the monoclinic polymorph of lysozyme is presented in chapter 4 of this thesis. Lysozyme has long been known to crystallize in a number of different modifications, often from very similar crystallizing solutions. In this chapter, we aim to investigate this unusual property of lysozyme by studying the rarely observed monoclinic form of the crystal with *in situ* AFM. Initially, the crystal growth conditions will be optimized to be as close as possible to those responsible for the formation of the tetragonal form. The dominant (101) face of the crystal will then be studied at varying protein and precipitant concentrations, with the overall aim being to unambiguously distinguish between the tetragonal and monoclinic crystal lattices.

The final chapter of this thesis is concerned with the study of a macromolecular crystal that displays poor diffraction properties. By utilizing the experimental protocols developed in the preceding chapters, we aim to study the surface of a form of a *S. pneumoniae* protein that is known to diffract X-rays to a low resolution, and relate our AFM observations to crystals known to diffract X-rays well. If successful, this approach may offer considerable promise in identifying problems with certain macromolecular crystals.

## Chapter

## 2

## Crystallization, habit modification and microscopical analysis of a pharmaceutical excipient, adipic acid

---

Atomic force microscopy (AFM) has been used to investigate the (100) face of crystalline adipic acid, both in air and liquid environments. In air, surface reorganization occurred during scanning of the AFM probe, which has been investigated using single point force-distance analysis under a controlled relative humidity (RH) environment. We suggest such reorganization can be attributed to the influence of a network of water molecules bound to the hydrophilic (100) surface permitting local AFM tip-enhanced dissolution and reorganization of the solute. *In situ* imaging was also carried out on the crystals, revealing etch-pit formation during dissolution, and rapid growth at higher levels of supersaturation ( $\sigma$ ), both of which are direct consequences of the hydrophilic nature of the (100) face. Also presented here are nanoscale observations of the effect of octanoic acid, a structurally-related habit modifier, on crystalline adipic acid. Using AFM, we have been able to show that the presence of octanoic acid at low concentration has little observable affect on the development of the (100) face; however, as this concentration is increased, there are clear changes in step morphology and growth mode on the (100) face of the crystal. At a concentration of  $1.26 \text{ mmol dm}^{-3}$  (a concentration corresponding to a molar ratio of approximately 1:175 octanoic acid : adipic acid), growth on the (100) face is inhibited, with *in situ* AFM imaging indicating this is a direct consequence of octanoic acid binding to the surface, and pinning the monomolecular growth steps.

The experiments described in this chapter have been the subject of an article currently in press in the *International Journal of Pharmaceutics* (Keel *et al.*, 2004).

---

## 2.1 Introduction

### 2.1.1 Crystallization and the pharmaceutical industry

The physical properties of the solid state of both drugs and excipients are of considerable importance in the pharmaceutical industry as they can effect both the production of effective and safe dosage forms, and the biological behaviour of the finished form (Florence and Attwood, 1988).

Crystallization from solution plays a vital role in a number of stages in the production of pharmaceutical materials. Initially, purification and separation define a material's chemical purity and physical properties. Further downstream in the manufacturing process, crystal properties can influence a range of industrial formulation factors such as bioavailability, milling and tableting behaviour, agglomeration and flow properties of powders.

Over 90% of all pharmaceutical products contain a drug in crystalline form (Shekunov & York, 2000), and so the characterization of solid-state drugs is an essential element of pre-formulation and formulation research. However, in many dosage forms the drug itself often accounts for only a small percentage of the overall mass of that dose. For example, in 1992 two-thirds of all marketed tablet formulations contained 100 mg or less of bioactive drug, with excipients such as binders, diluents, disintegrants, glidants and lubricants making up the remaining mass of the dose (York, 1992). Due to the relatively large quantities found in certain dosage forms, the physical properties of excipient materials as well as the drug become extremely important to the overall stability and efficacy of the drug formulation, making thorough characterization of such materials essential.

### 2.1.2 Crystal morphology and structure of pharmaceutical materials

In the pharmaceutical industry, the gross morphology exhibited by any crystalline material is an extremely important consideration, as certain crystal habits

such as thin plate crystals and needles can promote poor flow characteristics, and/or give rise to difficulties in the handling or packaging of the material (Mullin, 2001). Such problems can seriously affect manufacturing rate, making the understanding of what affects crystal habit vital.

As previously discussed in chapter 1 of this thesis, all crystals have a natural habit, which is determined by both the internal crystal structure and the attachment energies of molecules to the various faces. However, this natural habit is susceptible to modification by the environment from which the crystal is growing (Wood, 2001). The three main environmental factors linked to morphological control - supersaturation, solvent nature and impurity/additive incorporation - are discussed below.

### 2.1.2.1 Supersaturation

As previously discussed, crystallization from solution can be considered to be the result of three successive processes, (i) supersaturation of the solution, (ii) the formation of a crystal nucleus, and (iii) crystal growth around that nucleus.

Creating supersaturation (and subsequently crystallization) in solutions containing pharmaceuticals is often straightforward because the majority of such materials are well-defined small molecular entities whose structural and physico-chemical properties remain constant over a wide range of conditions – generally speaking, such molecules are stable, difficult to damage and will therefore undergo crystallization from a wide range of experimental conditions such as evaporation, dramatic temperature variations and the use of harsh organic solvents.

A typical solubility diagram for the crystallization of conventional organic molecules from solution is presented in figure 2.1. If the starting composition of an undersaturated solution containing the required product is  $i$ , then it can easily be brought into a supersaturated state by two routes – cooling (route  $x$ ) or solvent evaporation (route  $y$ ). However, whilst these routes are simple to achieve experimentally, they must be carefully controlled as the size and habit of many crystalline products are particularly sensitive to supersaturation (Ristic *et al.*, 2001; Boerrigter *et al.*, 2002). For example, a system at very high supersaturation may produce a vast quantity of small, elongated ‘microcrystals’ over a very short timescale, whilst a low supersaturation solution is likely to produce larger, granular-shaped crystals over a longer period (Haleblian, 1975).

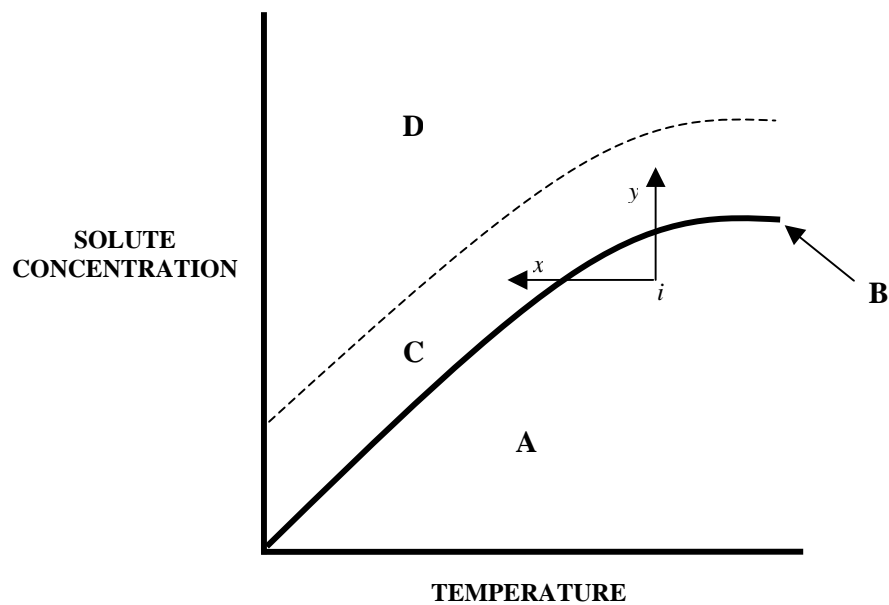


**Figure 2.1.** The two main routes used to bring a solution containing conventional organic molecules into a supersaturated state. As in figure 1.1, this solubility diagram plots solute concentration versus temperature and is split into 4 sections – **A**: undersaturation, **B**: saturation limit, **C & D**: supersaturation, with **C** representing the metastable zone. When starting from an undersaturated solution (*i*), the system can be brought into a supersaturated state by either cooling (*x*) or solvent evaporation (*y*). Adapted from Davey and Garside, 2000.

Such differences in crystal shape are undesirable as bioavailability and dissolution may be influenced by crystal dimensions (Chow *et al.*, 1984), along with a variety of manufacturing factors such as separation, flow and compaction (Ristic *et al.*, 2001). Such formulation problems can sometimes be overcome by normal pharmaceutical processing such as drying and milling (Florence and Salole, 1976). However, such processes may affect the overall crystallinity of the material, potentially further altering the material's solid-state physical properties (Chow *et al.*, 1986).

#### 2.1.2.2 Crystallizing solvent

The solvent utilized in a crystallizing system may associate with specific faces on the crystal by hydrogen bonding or  $\pi$ - $\pi$  interactions, and slow the growth rate of these faces. Such interactions often lead to examples of severe habit modification, such as the case of resorcinol (Haleblian, 1975), succinic acid (Davey *et al.*, 1982) and more recently that of NMBA (4-nitro-4'-methyl benzylidene aniline) crystals, where three alternative habits were grown from ten different organic solvents (Srinivasan *et al.*, 2000). Altering solvent composition to effect crystal habit has also been shown to improve the compression behaviour of molecules such as nitrofurantoin (Marshall and York, 1991). The importance of the crystallizing solvent has also led to the development of computational methods that predict the shape of organic crystals grown from both polar and non-polar solvents (Winn and Doherty, 1998; Li *et al.*, 2000; Winn and Doherty, 2002).

#### 2.1.2.3 Impurities and additives

The incorporation of guest molecules (impurities, additives or crystallizing solvent) into host crystals is inevitable during crystallization from solution (Zhang and Grant, 1999). Generally it can be assumed that there is some form of affinity between an active impurity and the crystallizing species of interest. With organic molecules, affinity between the 'guest' and 'host' molecule often stems from a structural similarity, which has led to the use of the term 'tailored' crystal growth (Weissbuch *et al.*, 1985; Mullin, 2001).

Structurally related additives commonly act as impurities during the crystallization of organic compounds. These substances may be additives that are

introduced to the crystallization medium for a specific purpose, or may be impurities resulting from the synthesis or degradation of the desired product. Such guest molecules may affect the nucleation and growth of molecular crystals in a number of ways. These mechanisms can be split into three distinct groups that have, for example, previously been applied to the crystallization of paracetamol in the presence of structurally related substances (Hendriksen *et al.*, 1998). The first is the ‘blocking’ ability of the guest molecules. Blocking is the ability of an already adsorbed molecule to hinder subsequent adsorption of further layers of host molecules, an effect that will manifest itself as morphological change, as the growth rates of the faces are altered, relative to one another. An effective blocker should present a template that is sterically and energetically different to that of the host.

‘Docking’ is the second proposed mechanism utilized by structurally related guest molecules. Docking is the ability of a molecule in solution to be adsorbed onto the growing crystal surface in an orientation appropriate for inclusion into the host crystal lattice. The level of uptake of such molecules also depends on the molecule’s ability to block subsequent host molecule uptake.

Finally, structurally related guest molecules can have a nucleation inhibitor affect. The ability of such molecules to ‘disrupt’ nucleation is a well-documented occurrence, but is relatively poorly understood. The inhibition of nucleation is probably due to a combination of steric and energetic disruption of the hydrogen bonding networks that are often present in small molecular crystals.

The degree of habit modification observed in any system relies heavily on the concentration of impurity present. Concentrations as low as several parts per million have been reported to have an observable effect on crystal habit (Shekunov and Grant, 1997), making the study and understanding of such interactions a vital part of crystallization research in the pharmaceutical industry. Inevitably, the literature is replete with references to the additive-induced effects on crystalline drug compounds. Some of the reported additives are polymeric molecules that act as nucleation inhibitors, allowing the successful topical delivery of drugs in a supersaturated state (Davis and Hadgraft, 1991; Raghavan *et al.*, 2000; Raghavan *et al.*, 2001). Other reports concern the effect of small molecule inhibitors on the growth and dissolution of pharmaceutical compounds such as  $\alpha$ -lactose monohydrate (Garnier *et al.*, 2002), paracetamol (Chow *et al.*, 1985a; Chow and Grant, 1988a; Chow and Grant, 1988b; Hendriksen and Grant, 1995; Hendriksen *et al.*, 1998; Thompson, 2003; Thompson *et al.*, 2004) and salicylic

acid (Wilkins *et al.*, 2000; Wilkins *et al.*, 2002). Another widely studied pharmaceutical compound of this type is adipic acid, the main topic of this chapter.

### 2.1.3 Adipic acid

#### 2.1.3.1 Crystal structure & morphology

Adipic acid (hexanedionic acid) is a pharmaceutical excipient used as an acidulent in effervescent tablet formulations and as a tablet lubricant. The crystal structure of adipic acid was initially determined in 1941 (MacGillavry, 1941). This structure was refined on a number of occasions by various researchers up until 1965, when Housty and Hospital published their version of the structure of adipic acid that is now recognized to be wholly accurate (Housty and Hospital, 1965). They reported it is in the monoclinic crystal system, with two molecules in the unit cell. The unit cell parameters are  $a = 10.01$ ,  $b = 5.15$  and  $c = 10.06$  Å, with  $\beta = 136.75$ . Figure 2.2 illustrates the positioning of the adipic acid chains in the unit cell.

The actual structure of the crystal is primarily reliant on hydrogen bonding, which occurs between molecules aligned parallel to the a-axis. These chains are in turn held together by van der Waals contacts, with CH $\cdots$ O interactions between the hydroxyl oxygen of one chain and the closest carbon of the next. This interaction is thought to be feasible due to the unusually close lateral approach between the carbon and oxygen (Fairbrother, 1981; Davey *et al.*, 1992). Figure 2.3 illustrates this diagrammatically.

#### 2.1.3.2 Polymorph formation

In the pharmaceutical industry, polymorphism is an extremely important property exhibited by many crystals and can have considerable adverse affects on a number of stages of formulation and manufacture of drug products. As previously mentioned, polymorphism occurs when a substance exists in more than one crystalline form with different lattice arrangements. These different forms will often vary in physical properties such as solubility, solid-state stability as well as processing

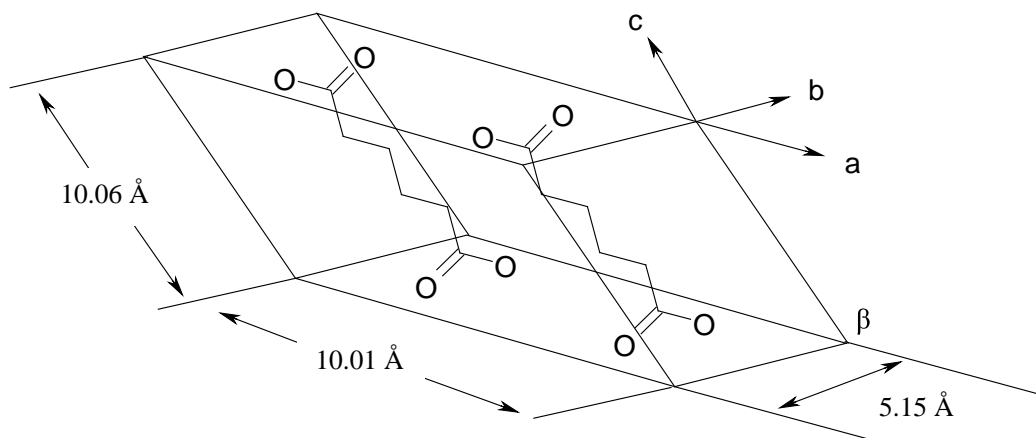


**Figure 2.2.** Diagrammatic representation of the positioning of the two adipic acid chains within the unit cell.

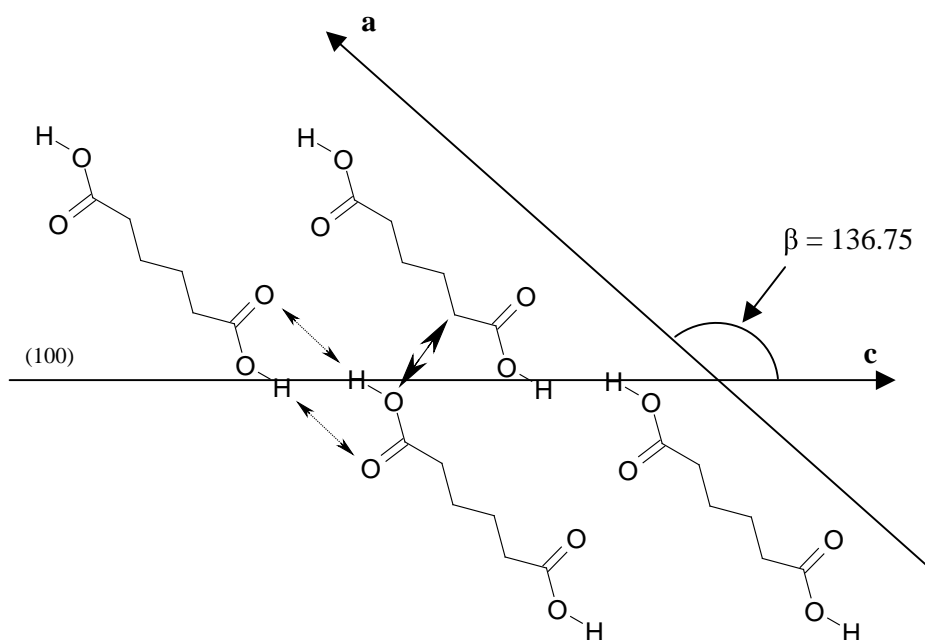


**Figure 2.3.** Hydrogen bonding and van der Waals forces present within the adipic acid crystal. Adapted from Davey *et al.*, 1992.

behaviour in terms of powder flow and compaction during tableting (Aulton, 1988).

Habit modification and polymorphism can be affected by the same environmental parameters, for example supersaturation and solvent nature. Severe habit modification can easily be mistaken for polymorphism; hence it is important that polymorphic transitions are either well understood and easily controlled, or non-existent within the experimental parameters. In the case of adipic acid, the latter is true. Exhaustive experiments carried out by Fairbrother (Fairbrother, 1981) indicate that there is no evidence of the existence of polymorphic forms of crystalline adipic acid under the conditions likely to be encountered in the work presented here.

### 2.1.3.3 Habit modification

The habit modification of crystalline adipic acid was first quantitatively observed in the presence of anionic and cationic surfactants (Michaels and Colville, 1960; Michaels and Tausch, 1961). The three primary crystal faces display very different surface chemistries – the (100) face is composed entirely of –COOH groups, whilst the (001) and (011) are considerably less hydrophilic, being partially carboxyl and partially hydrocarbon in nature. It was shown that the cationic surfactant slowed the rate of growth of the (001) and (011) faces, increasing the relative size of the (100) face. The opposite effect was observed with the anionic surfactant, as illustrated in figure 2.4.

However, it is the effect of a series of *n*-alkanoic acids on the crystal habit that has received most attention. Simple molecules such as caproic, heptanoic, octanoic and decanoic acids are structurally similar to adipic acid making such molecules ideal to act as relevant habit modifiers. The effect of such molecules on the crystallization of adipic acid has been the subject of numerous structural and kinetic studies (Fairbrother and Grant, 1978; Fairbrother and Grant, 1979; Fairbrother, 1981; Davey *et al.*, 1992; Williams-Seton *et al.*, 2000). These studies have indicated that crystals grown in the presence of small quantities of various *n*-alkanoic acids regularly display a range of characteristic morphological changes such as an elongation of the crystals along the *b*-axis, narrowing of the central region in the [100] zone and pronounced curvature of the faces.

Other studies have concentrated on the effects of doping on dissolution rate, crystal energy and density, and melting point (Chow *et al.*, 1984; Chow *et al.*, 1985b;

Chow *et al.*, 1986; Chan and Grant, 1989). Molecular modeling techniques have also been employed to calculate both the theoretical morphology of adipic acid crystals (Pfefer and Boistelle, 2000) and the binding energies present between various long chain alkanolic acids (octanoic acid and above) and the (100) face of adipic acid (Myerson and Jang, 1995).

#### 2.1.4 Chapter aims

Adipic acid has long been known to exhibit a variety of interesting crystallization properties, many of which have been theoretically attributed to the extremely hydrophilic nature of the dominant (100) surface. As such, we aim to investigate the (100) face with *in situ* AFM in both air and liquid environments with a view to furthering experimental understanding of this system. To achieve this, protocols will first be developed to grow large seed crystals suitable for study by AFM. Such crystals will initially be characterized in air, followed by studies carried out on crystals that have been doped with specific quantities of the structurally related habit modifier, octanoic acid. Finally we will attempt to investigate the growth, dissolution and habit modification of adipic acid crystals *in situ* to uncover exactly how the chemical nature of the (100) face dictates the development of the crystal.

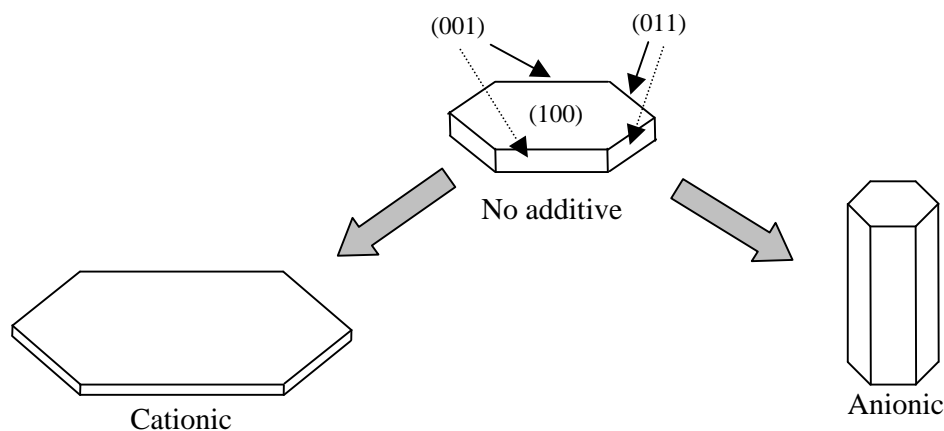


**Figure 2.4.** The effects of cationic and anionic surfactants on the habit of crystalline adipic acid. Adapted from Michaels and Tausch, 1961.

## 2.2 Materials & Methods

### 2.2.1 Preparation of adipic acid crystals

Commercially available adipic acid (99.5 %) (Sigma-Aldrich, Gillingham, U.K) was used throughout. Recrystallization of adipic acid was carried out from both HPLC grade water and ethanol (Sigma-Aldrich) in an attempt to further purify the solute. However, subsequent AFM scans showed little difference in surface properties of the crystals post-recrystallization. This process also seemed to alter the solubility of the adipic acid, which had a negative impact on the repeatability of the crystallization experiments. For these reasons, adipic acid was used throughout without further purification and always from the same batch to encourage reproducibility. The solvent used throughout was HPLC grade water (18.2 M $\Omega$ cm resistivity).

Initially, four methods were investigated to identify suitable conditions to encourage the growth of larger adipic acid crystals. These are briefly described below.

#### 1) Cooling to 34 °C (Fairbrother, 1981).

A total of 9 g of adipic acid were dissolved in 200 ml water at 45 °C. To ensure complete dissolution the solution was stirred at 238 rpm for 1 hour at this temperature, after which the temperature was lowered to 34 °C. Nucleation was rapid and the bulk of the crystallization was complete after 2 hours. Crystals were then rapidly vacuum filtered, washed and dried lightly with absorbent tissue paper. The crystals were subsequently dried overnight in an oven at 60 °C and stored in a desiccator until required.

#### 2) Cooling to room temperature – stagnant system.

As outlined in method 1, 9 g of adipic acid were dissolved in grade water at 45 °C. To ensure complete dissolution the solution was stirred at 238 rpm for 1 hour at this temperature. At this point, the heat and stirrer were removed and the solution was left

to return to room temperature and crystallize overnight. The resulting crystals were dealt with as specified in method 1.

### 3) High temperature & slow solvent evaporation (Davey, 2001).

Water (100 ml) was heated to 60 °C, whilst being stirred at 60 rpm. 10 g of adipic acid was subsequently added and the crystallizing vessel covered. When dissolution of the solute was complete, the cover was removed and the stirred solution left overnight at 60 °C to crystallize through solvent evaporation. The resulting crystals were dealt with as specified in method 1.

### 4) Low temperature cooling

A lack of solubility data for adipic acid at low temperature led to a range of experiments being carried out to identify appropriate low-temperature crystallization conditions. The optimized protocol was as follows. 2.05 g of adipic acid was added to 200 ml of water and dissolved by sonication to make a 0.07 mol dm<sup>-3</sup> solution. This undersaturated solution was filtered and placed in the refrigerator at 4 °C to crystallize. The resulting crystals were dealt with as specified in method 1.

## 2.2.2 Preparation of imaging solutions

The relative supersaturation of all imaging solutions was calculated using equation 1.1.

$$\sigma = \ln (c/c_0) \quad \text{equation 1.1}$$

where  $c_0$  is the solubility of adipic acid at a given temperature, and  $c$  is the concentration of adipic acid dissolved in the solvent (water). Solubility data for this system has been published on numerous occasions (for example see Davies and Griffiths, 1953), but we

have used data obtained from a University of Nottingham PhD thesis (Fairbrother, 1981)

All AFM experiments were carried out at room temperature ( $\sim 25\text{ }^{\circ}\text{C}$ ). However, it must be noted that the temperature within the AFM liquid cell is slightly elevated when compared to the room temperature due to the heat generated by the AFM piezoelectrics and laser light (Kipp *et al.*, 1995). Inevitably, this raises the solubility of adipic acid, causing the calculated values of supersaturation to be artificially high. This explains why, for example, dissolution was observed in an apparently supersaturated solution (section 2.3.3). This effect is difficult to quantify, especially when dealing with a material such as adipic acid whose solubility is highly dependent on temperature. As such, the values of supersaturation quoted throughout have been calculated using the solubility of adipic acid in water at  $25\text{ }^{\circ}\text{C}$  (23.45 g/1000 ml), and are accurate relative to one another at this temperature.

The following protocol was utilized to make up the imaging media. The calculated quantity of adipic acid was dissolved in 5 ml of water by stirring at 238 rpm, at  $50\text{ }^{\circ}\text{C}$ . If the solution was to contain a habit modifier, the desired quantity was added at this point. The solution was stirred for approximately 60 minutes to ensure complete dissolution, after which it was filtered and left to cool to  $25\text{ }^{\circ}\text{C}$  prior to being introduced into the AFM liquid cell. All values of supersaturation and quantities of habit modifier will be quoted and discussed in the results section.

### 2.2.3 AFM analysis

Suitably faceted crystals (diameter  $>1\text{ mm}$ ) were selected for AFM analysis by optical microscopy. Once a suitable crystal had been identified, it was mounted on a 10 mm glass coverslip (Agar Scientific, Stansted, UK) using Tempfix (Agar Scientific), which in turn was fixed to a magnetic AFM stub. Being the crystal face of interest during the present study, the (100) face was mounted parallel to the glass coverslip.

All images were recorded using a DI Multimode atomic force microscope equipped with a Nanoscope IIIa controller (Veeco, Santa Barbara, CA). Silicon nitride NP-S cantilevers with a nominal spring constant of  $0.1\text{ Nm}^{-1}$  were used throughout (Veeco). The DI multimode was equipped with an E-scanner with a maximum scan

size of 13  $\mu\text{m}$  x 13  $\mu\text{m}$ . Images were collected in both tapping and contact mode, using a minimum contact force at all times to avoid damaging the crystal face. All images were collected at either 256 x 256 or 512 x 512 pixel resolution, at a scan rate in the range of 2-8 Hz.

Experiments carried out in solution utilized a liquid cell (Veeco), equipped with a small O-ring to prevent solvent evaporation. Prior to each experiment in liquid the selected crystal was imaged in air to ensure the tip was of good quality and the area of crystal to be investigated was representative of a typical adipic acid crystal.

The images presented throughout this study are in the form of either topography or deflection data. Topography micrographs are constructed from the movement of the z-piezo in response to the AFM controller feedback system, and contain accurate three-dimensional data. The deflection images are constructed directly from the movement of the laser on the AFM photodiode. These images often highlight rapid changes in topography in greater detail, such as is seen at step edges, and are used for that purpose throughout this chapter.

Force-distance data presented herein were also collected using the DI Multimode AFM. The same cantilever, which was initially cleaned in weak argon plasma for five seconds, was used throughout the experiments, allowing direct comparison of data. Curves presented are corrected from deflection vs. piezo deflection, to true force (nN) vs. probe-sample separation data.

#### 2.2.4 SEM Analysis

All samples were gold-coated using a Balzers SCD 030 Sputter Coater (Balzers Union Limited, Liechtenstein), operated at 0.1 mbar with a sputtering current of 30mA. The duration of coating was 2 minutes. A Philips 505 SEM (Philips Electron Optics, Eindhoven, Netherlands) was used to image all samples under a range of magnification settings at a voltage of 23 keV, with a spot size of 50 nm.

## 2.3 Results and Discussion

### 2.3.1 Seed crystal optimization

Of the 4 different methods employed, low temperature cooling was found to be the most successful in the production of large (>1 mm) adipic acid crystals. The SEM micrographs contained in figure 2.5 illustrate the importance of selecting the correct crystallization conditions if larger single crystals are desired.

The crystals produced by the 3 alternative methods (cooling to 34 °C, cooling to room temperature and solvent evaporation) all display the signs of rapid, poorly controlled growth. Such crystals are indicative products of solutions that have reached a highly supersaturated state in a short timescale. Without exception, the single crystals produced were small and poorly defined. The (100) face was identifiable in many cases, however its edges were rounded and often littered with smaller crystals that had nucleated on the face in the highly unstable growth conditions. Similar cases of severe secondary nucleation have also previously been reported in adipic acid crystals grown from ethanol (Doki *et al.*, 2003).

The advantages of the low temperature cooling method are numerous. Supersaturation is reached gradually by cooling an undersaturated solution from room temperature to 4 °C, and optimization of the protocol allowed crystals to be grown within 72 hours. Spurious nucleation, a problem in the three other methods, was not observed when employing optimized low temperature cooling. This is of vital importance when large single crystals are desired as rapid nucleation removes vast quantities of solute from solution, effectively limiting the size of each crystal. The initial preparation of an undersaturated rather than a supersaturated solution was in itself an advantage. Heating, which was a pre-requisite in the alternative methods, can seriously affect experimental reproducibility if not accurately controlled, as the solubility of adipic acid is heavily reliant on temperature. We were also able to filter all solutions before cooling to minimize the likelihood of heterogeneous nucleation from any large impurities such as dust particles.

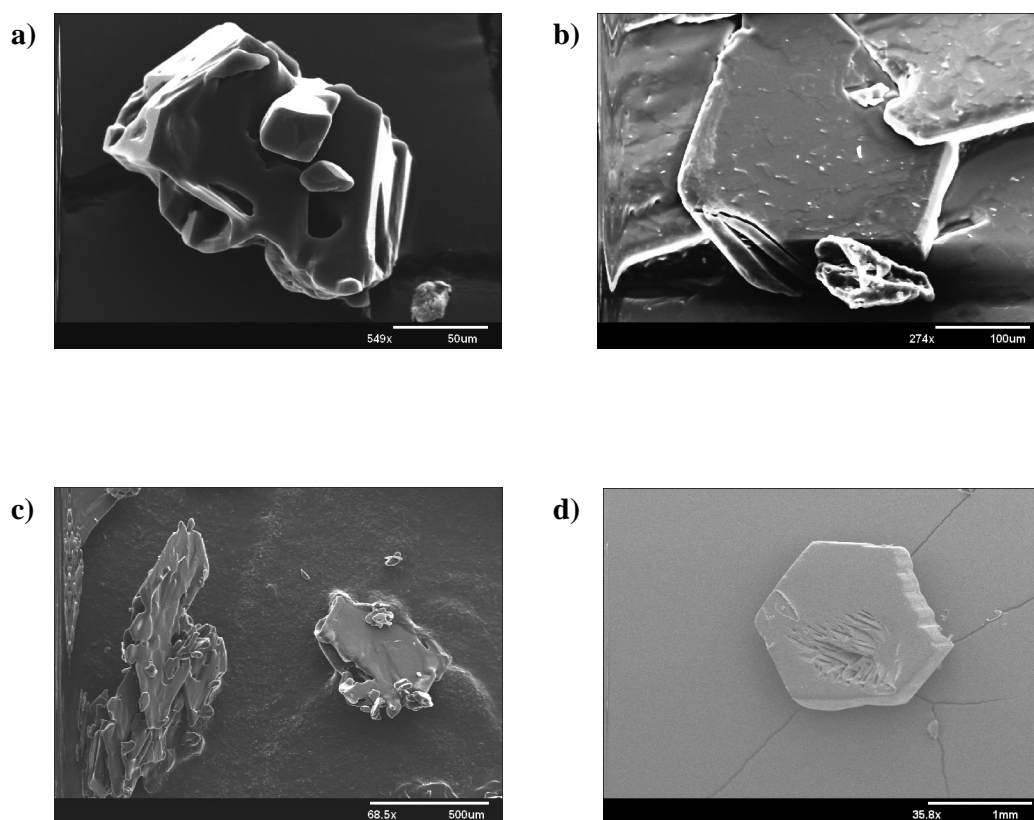


**Figure 2.5.** SEM micrographs of typical adipic acid crystals grown by 4 different methods. **(a)** – Cooling to 34 °C, **(b)** – Cooling to room temperature, **(c)** – Solvent evaporation and **(d)** – Low temperature cooling. Micrographs **(a)**-**(c)** all display common features. The crystals are small, poorly defined and generally of low optical quality. This is quite probably a consequence of spurious nucleation and poor control of the supersaturation in the system. However, optimized low temperature cooling (micrograph **(d)**) produced large, well-defined crystals that make ideal candidates for AFM experimentation. **(a)** – x 549 magnification, **(b)** – x 274 magnification, **(c)** – x 274 magnification & **(d)** – x 35.8 magnification.

### 2.3.2 Surface restructuring on the (100) face of un-doped adipic acid crystals

To our knowledge, no AFM studies have previously been carried out on crystalline adipic acid, so initial experiments were carried out in air in an attempt to characterize the (100) face of the crystal. Two typical AFM topography images are shown in Figure 2.6. The surfaces of the crystals are dominated by step edges that have been pinned by foreign particles adsorbed on the crystal surface (Cabrera and Vermilyea, 1958). The single-molecule steps were consistently around 0.7nm in height ( $\pm 0.15$  nm), a figure that is directly comparable to 0.685 nm, the interplanar distance normal to the (100) face deduced from crystallographic studies (Housty and Hospital, 1965).

On a number of separate occasions during the preliminary characterization experiments presented here, an apparent reorganization of adipic acid on the surface of the crystal was observed. Figure 2.7 shows four consecutive tapping mode images. These images illustrate a clear change in surface morphology in a short space of time. Solute is clearly nucleating on the step terraces in 2.6(b), and subsequently being incorporated into the advancing monomolecular steps in 2.6(c).

To our knowledge, such solute reorganization has only previously been observed on crystals of cadmium mercury thiocyanate (CMTC), a nonlinear optical material (Jiang *et al.*, 2001; Jiang *et al.*, 2002a; Jiang *et al.*, 2002b). These reports detailed a variety of phase transitions and surface morphology transformations, including the transformation of amorphous aggregates to microcrystals, and alteration of step shapes and defects. The authors attributed the apparent restructuring of the crystal surface to the inevitable increase in internal energy of the lattice after prolonged periods of contact mode imaging, which in turn promoted the gradual formation of increasingly stable states of the crystal.

Our observations are somewhat different to the report of Jiang *et al.* Reorganization has been observed after just a few minutes scanning in one area, in both contact (data not shown) and tapping mode. Tapping mode scanning negates many of the unfavourable probe-sample interactions associated with contact mode, and can lower lateral forces exerted on the sample surface to an almost negligible level, although contact forces can still be considerable at maximum loading. The observation of

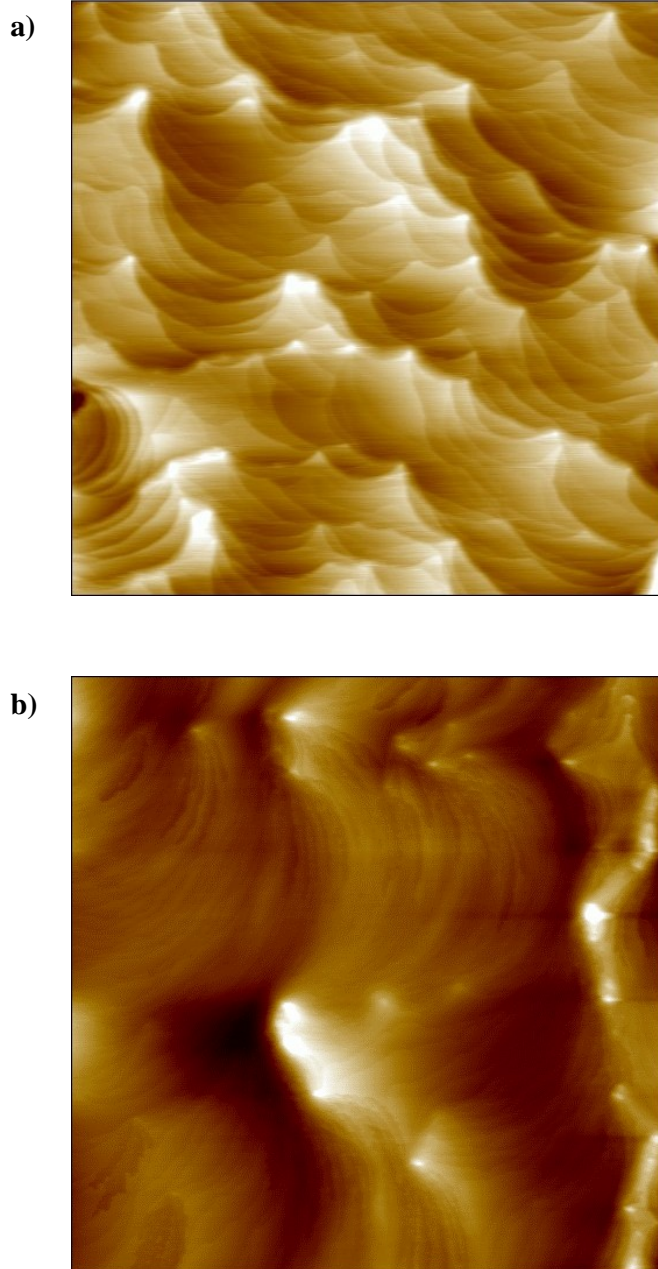


**Figure 2.6.**  $5\mu\text{m} \times 5\mu\text{m}$  topographical AFM images of adipic acid crystals grown by the low temperature cooling method. Z-ranges, **a)** 32.8 nm, **b)** 50 nm

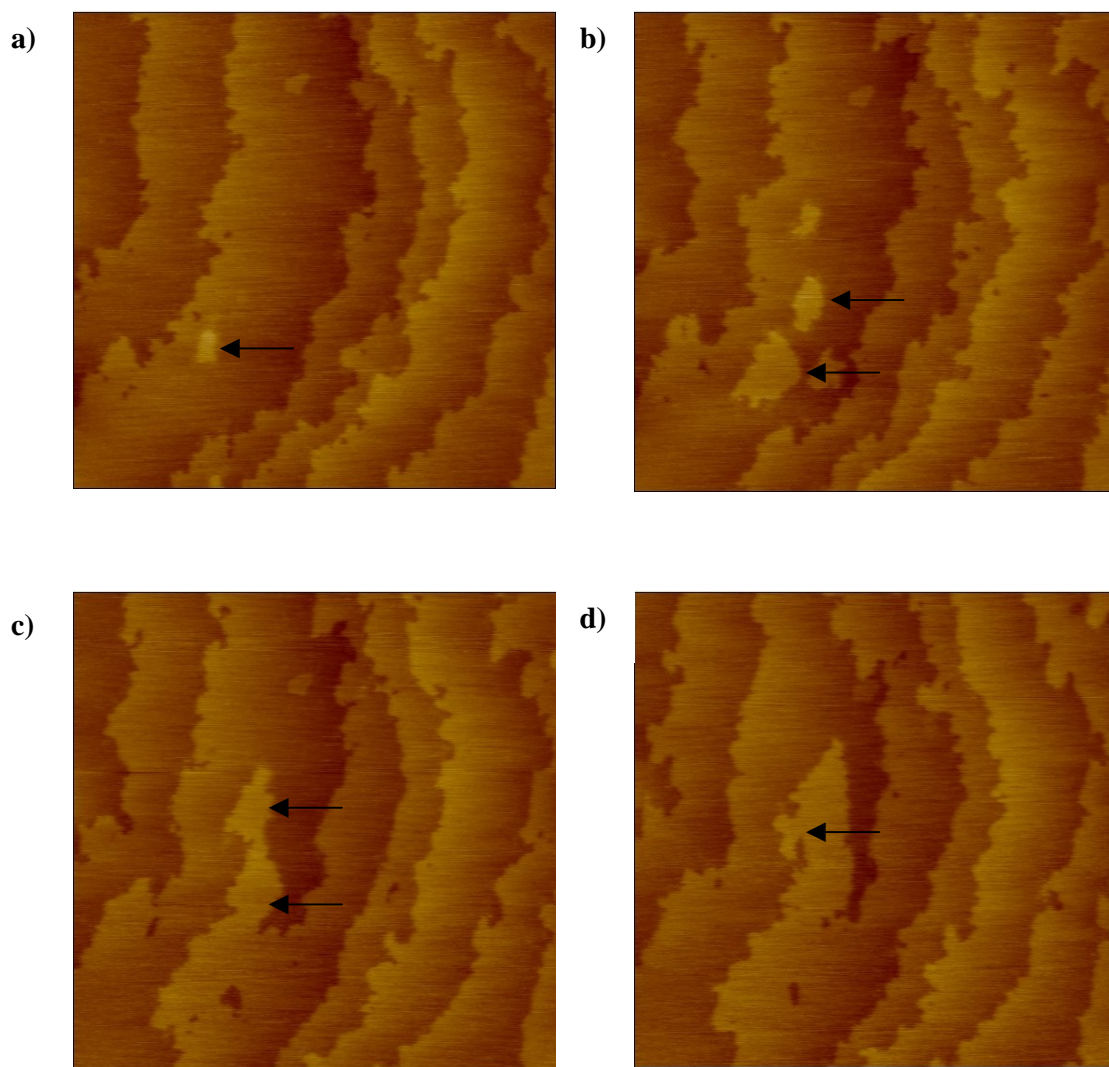


**Figure 2.7.** Consecutive  $1.5\ \mu\text{m} \times 1.5\ \mu\text{m}$  tapping mode images of an adipic acid crystal, recorded in air at a scan speed of 3Hz. Widespread solute reorganization on the crystal surface is clearly evident, some of which is highlighted by arrows. z-ranges of (a-d), 8 nm.

reorganization so rapidly after the onset of scanning indicates that, in addition to any tip-sample interaction, the surface chemistry of the crystal may be playing a significant part in the apparent solute mobility.

To further investigate these observations a series of single point force-distance experiments were carried out, the results of which are displayed in figure 2.8. Figure 2.8(a) is characteristic of a typical force-distance curve acquired on a crystal of adipic acid in ambient air conditions (RH ~30 %). The jump-to-contact on tip approach to the crystal surface is relatively small, whilst the jump-off-contact is considerably larger. Such a comparatively large adhesion is due to the meniscus force exerted by layers of water adsorbed on the sample surface. Indeed, when the crystal and the AFM tip were immersed in a saturated aqueous solution of adipic acid, the large capillary-induced adhesion force was negated (data not shown).

In the case of adipic acid, the presence of a significant meniscus force on the (100) face in ambient conditions is inevitable as it is constructed entirely of carboxylic groups (see figures 2.2 & 2.3). The hydrophilic nature of such groups is likely to induce strong attractive forces between the sample surface and the thin water layer covering it. Theoretically, perturbation of this bound water layer by the raster motion of the tip may induce local dissolution and reorganization of the solute molecules on the crystal surface, giving rise to the effects observed during scanning.

In an attempt to further investigate the likelihood of dissolution and reorganization occurring on the crystal surface, force-distances curves were also carried out on the crystals in a 0 % relative humidity (RH) environment and a typical curve is displayed in figure 2.8(b) (this curve has been translated 50nm on the z-displacement axis for clarity). There have been numerous studies previously investigating the dependence of pull-off forces on RH, many of which have been covered in Cappella's comprehensive review article (Cappella and Dietler, 1999). Generally, as the RH is lowered toward 0 %, the pull-off force decreases in magnitude due to the removal of lesser-bound water molecules at the sample surface. However, when comparing figures 2.8(a) & 2.8(b) there appears to be a negligible decrease in pull-off force when lowering the RH from ambient conditions of ~30 % to 0 %. This suggests that a significant layer of water is *strongly* adsorbed to the (100) surface. It seems feasible that such conditions may, when promoted by the interaction of the AFM tip on the surface, facilitate dissolution and reorganization of the solute within the bound 'network' of water molecules on the surface as observed in the sequence of images in figure 2.7.

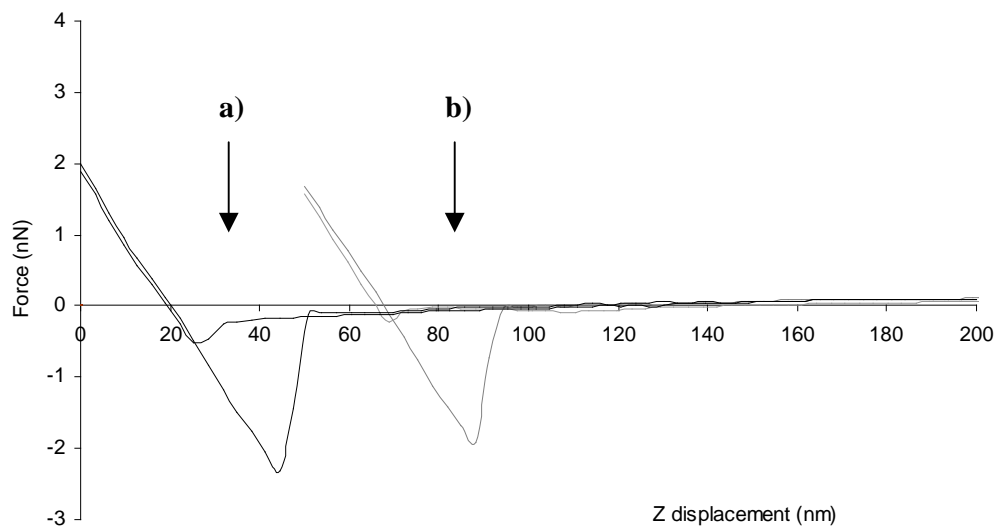


**Figure 2.8.** Force-Z displacement data obtained from the (100) face at ambient (**a**) and low (**b**) relative humidity. Curve (**b**) has been translated 50 nm to the right for clarity.

The hydrophilic nature of the (100) face demonstrated here is of utmost importance in a number of aspects of the growth and morphology of adipic acid crystals. Theoretically, the formation of the (100) face should be rapid due to the hydrogen bonding which occurs between adipic acid chains to construct that face (see figure 2.3). In fact, it is the slowest growing of all the faces, which is the reason the crystal takes the shape of a thin plate rather than a needle-like morphology. The slow growth rate is generally believed to be due to adipic acid molecules effectively having to compete with the occupying water molecules to bind at the crystal surface. This leads to a situation where desorption of the water molecules may play a significant role in determining the relative growth rate of the crystal faces (Davey *et al.*, 1982; Davey *et al.*, 1992).

### 2.3.3 Growth and dissolution of adipic acid crystals

As previously discussed, there have been numerous reports of the bulk dissolution and growth behaviour of crystalline adipic acid. One of the main advantages of AFM is the ability to perform experiments *in situ*, which allows data to be collected in real time under conditions directly relevant to the system of interest. In the case of adipic acid, *in situ* AFM allows the investigation of growth and dissolution of the (100) face of single crystals under controlled imaging media.

Initially, experiments were conducted to identify conditions suitable for such investigations. Imaging solutions with  $\sigma > 0.45$  promoted the spontaneous nucleation of microcrystals of adipic acid in the imaging solution, which rapidly coated the cantilever and sample surface, effectively prohibiting scanning. Conversely, at  $\sigma < 0.2$ , dissolution and etch pits became apparent on the seed crystal surface.

The formation of etch pits was in itself an interesting observation. Figure 2.9 contains a typical light microscopy image and *ex situ* AFM image of etch pits formed on the crystal surface after being immersed for approximately 30 minutes in solution,  $\sigma = 0.15$ . It has been established that etch pits form at the site of an emergent dislocation (Shimon *et al.*, 1985), and the etching only becomes apparent when the surface is 'poisoned' by an impurity. However, under the conditions created in these experiments, the only other substance present in the crystallization medium is the solvent, water.

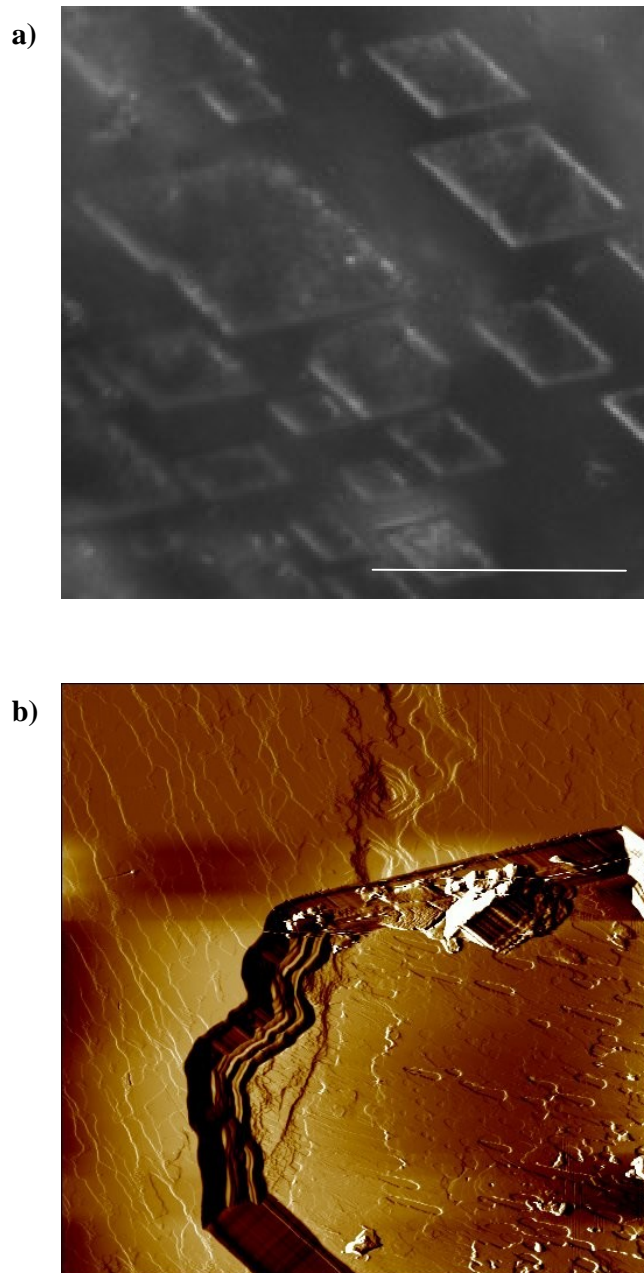


**Figure 2.9.** Etch pits formed on the (100) face of seed crystals immersed for approximately 30 minutes in solution,  $\sigma = 0.15$ . **(a)** light microscopy image, scale bar 50  $\mu\text{m}$ , **(b)** AFM deflection micrograph, 13  $\mu\text{m} \times 13 \mu\text{m}$

Indeed, the solvent-crystal interaction has previously been shown to affect the formation of etch pits on paracetamol crystals, and plays an important role in the detachment and surface diffusion of surface molecules (Li *et al.*, 2000).

As we have shown in section 2.3.2, water is bound to the hydrophilic (100) surface and the presence of etch pits on this face may indicate that the bound water discourages dissolution by ‘poisoning’ the horizontal surfaces within and around a dislocation. However, the less hydrophilic surfaces initially exposed by dissolution at the emergent dislocation will not be protected by such tightly bound water molecules and dissolve more freely, leading to the formation of the observed pits.

To investigate this theory, *in situ* AFM was performed on a seed crystal at  $\sigma = 0.15$ , and images obtained shown in figure 2.10. The large step (~150 nm in height) represents the edge of an etch pit, and is dissolving freely across the image from left to right. However, the terrace to the right of the widening etch-pit boundary is completely unchanged throughout imaging, with the smaller steps showing no indication of dissolution normal or parallel to the crystal surface. We believe this represents strong microscopical evidence of the ‘masking’ role played by the bound water to the hydrophilic (100) surface of crystalline adipic acid.

To encourage growth, the imaging medium had to be at a relatively high supersaturation, presumably to disrupt the bound water molecules at the (100) surface. When this condition was met ( $\sigma > 0.3$ ) growth occurred rapidly, both tangentially and normally to the surface. Typical images obtained during such experiments are shown in figure 2.11. Whilst secondary nucleation was occasionally observed at higher supersaturation (2.11(a)), the surfaces tended to be dominated by large macrosteps that swept rapidly across the crystal surface, incorporating vast quantities of solute molecules into the crystal lattice. However, growth always came to a halt quickly probably because the rapid incorporation of solute forced the relative supersaturation below the required threshold for growth to proceed. Presumably as the supersaturation fell below this value, significant quantities of water molecules were able to re-adsorb to the surface, and interfere with growth again.

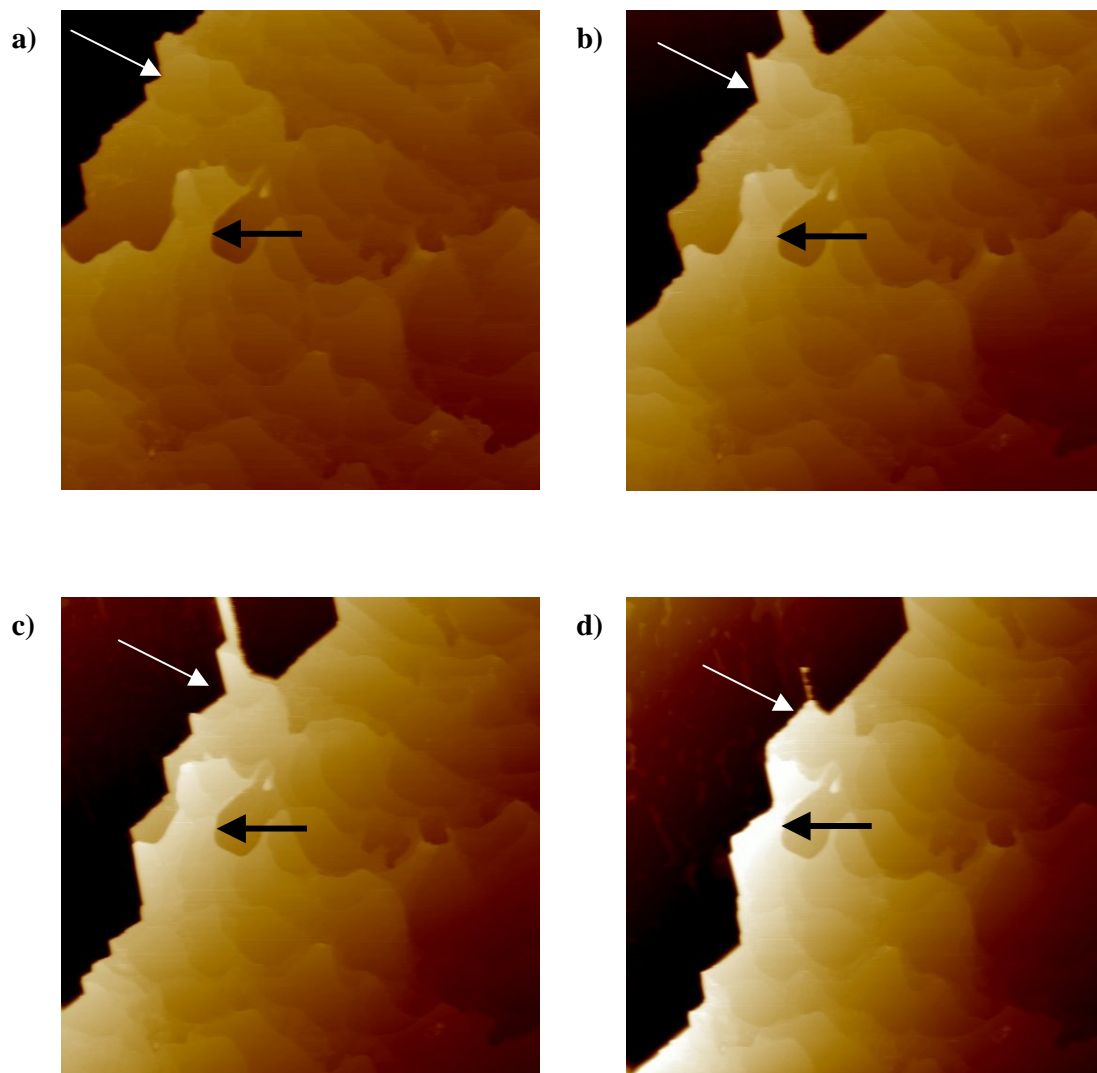


**Figure 2.10.** Dissolution and etch-pit formation on un-doped adipic acid crystals. **(a)-(d)** Consecutive  $10\ \mu\text{m} \times 10\ \mu\text{m}$  topography images illustrating selective dissolution on the crystal surface. The etch pit edge is approximately 150 nm in height, with dissolution proceeding from left to right as indicated by the white arrows. The terrace to the right of the advancing etch pit is not undergoing dissolution, an area of which is highlighted with black arrows. Z-range, 200 nm in **(a)-(d)**

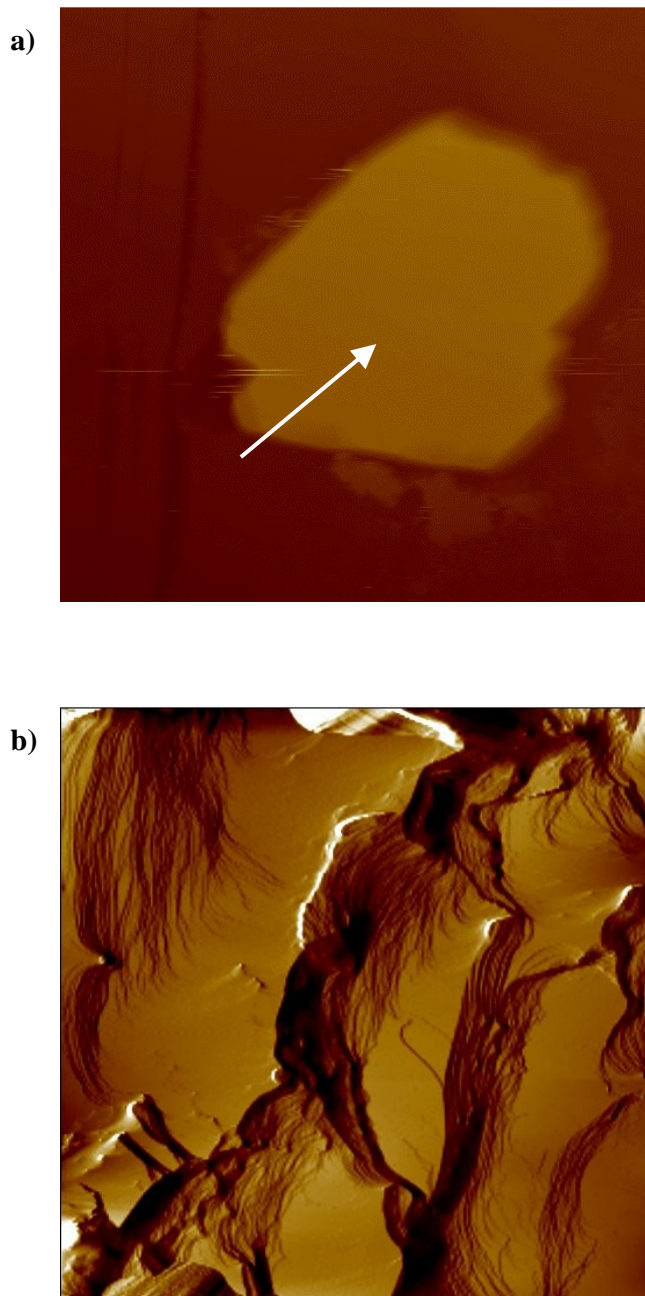


**Figure 2.11(a)**  $13\ \mu\text{m} \times 13\ \mu\text{m}$  raw topography micrograph illustrating secondary nucleation observed at high supersaturation. z-range, 3000nm. **(b)** A typical  $10\ \mu\text{m} \times 10\ \mu\text{m}$  deflection image captured during un-doped adipic acid growth, relative supersaturation = 0.4. The two large macrosteps running through the center of the image are approximately 300-400 nm in height.

### 2.3.4 Crystallization of adipic acid in the presence of octanoic acid.

As previously discussed, the effect of the family of *n*-alkanoic acids on the crystallization of adipic acid has been the subject of numerous structural and kinetic studies (Fairbrother and Grant, 1978; Fairbrother and Grant, 1979; Fairbrother, 1981; Davey *et al.*, 1992; Williams-Seton *et al.*, 2000). Crystals grown in the presence of small quantities of various *n*-alkanoic acids regularly display a range of characteristic morphological changes such as an elongation of the crystals along the b-axis, narrowing of the central region in the [100] zone and pronounced curvature of the faces.

Davey *et al.* (1992) found octanoic acid to be the most effective growth disrupter of the series of *n*-alkanoic acids due to its size – an eight carbon chain causes maximum steric disruption to the (001) surface when incorporated into the growing face, subsequently preventing the next adipic acid molecule occupying its lattice site. Inevitably, this slows crystal growth, giving the (001) surface increased morphological importance. Williams-Seton *et al.* (2000) reported similar observations in the case of decanoic acid. However, these experimental studies also indicated that the growth of the (100) surface is largely unaffected by the presence of such structurally related habit modifiers. This is generally believed to be another consequence of the hydrophilic nature of this face – presumably, the strongly adsorbed water layer is able to reject the majority of the hydrophobic alkanolic acid molecules. Consequently, the (100) surface is still morphologically dominant at low additive concentration.

In an attempt to microscopically assess this effect, we have performed both *in situ* and *ex situ* studies of the (100) face of adipic acid grown in the presence of the structurally related habit modifier, octanoic acid.

Seed co-crystals were grown for *ex situ* AFM analysis in the presence of 0.034 mmoldm<sup>-3</sup> octanoic acid (a concentration corresponding to a molar ratio of approximately 1:2000 octanoic acid: adipic acid) and 0.048 mmoldm<sup>-3</sup> octanoic acid (1:1400). It immediately became obvious that octanoic acid had a considerable nucleation inhibitory effect, with similarly sized crystals taking an additional 48 hours and 168 hours to grow in the presence of 0.034 mmoldm<sup>-3</sup> and 0.048 mmoldm<sup>-3</sup> octanoic acid respectively. Such increases in induction time when growing co-crystals of adipic acid and alkanolic acids have previously been well documented (Davey *et al.*, 1992).

Figure 2.12 contains SEM micrographs of crystals grown in the presence of the two concentrations of octanoic acid. As expected, the co-crystals displayed both an elongated morphology about the *b*-axis and pronounced curvature on the crystal faces, whilst the (100) face maintained its morphological dominance.

AFM imaging in air was performed on the crystals grown in the presence of  $0.034 \text{ mmoldm}^{-3}$  of the inhibitor, and typical images are displayed in figure 2.13. The surface topography appears quite different to that of the un-doped crystals shown in figures 2.6 & 2.7. The pronounced curvature observed in the SEM micrographs is evident on the individual step edges, as highlighted by the white arrows. Another important observation is the existence of numerous hollow dislocations scattered across the surface of the crystal, which are highlighted with black arrows (Frank, 1951). Hollow cores were not observed on the surface of the un-doped crystals, indicating the possibility of increased stress of the dislocations as a consequence of the progressive incorporation of octanoic acid into the crystal lattice throughout growth.

To build up a more thorough picture of the interaction of octanoic acid on crystalline adipic acid, *in situ* AFM imaging was carried out. From experiments carried out in section 2.3.3, it was known that imaging solutions in the range  $0.3 < \sigma < 0.4$  were suitable for observing growth on the (100) face of crystalline adipic acid. An un-doped seed crystal was mounted in the AFM, and a solution of  $\sigma = 0.4$  adipic acid was injected into the cell with octanoic acid present at a variety of concentrations.

Low concentrations of octanoic had no observable affect on the growth of the (100) surface, with AFM imaging problematic because of growth occurring rapidly, both tangentially and normally to the surface. However, as this concentration was raised, the affect of the impurity started to become clear. Figure 2.14 shows four consecutive images of the crystal growing in a solution containing  $0.63 \text{ mmoldm}^{-3}$  octanoic acid at  $\sigma = 0.4$  (a concentration corresponding to a molar ratio of approximately 1:350 octanoic acid : adipic acid).

The macrosteps typically observed in the un-doped system (see figure 2.11) appear to have been eradicated, with single molecular steps now dominating the crystal surface. Some step bunching is apparent; however this is insignificant when compared to the un-doped system. The step edges move noticeably slowly, and dislocations are clearly observable on the crystal surface.

Whilst this level of impurity is not sufficient to completely eradicate tangential growth, it is clear that the octanoic acid is now affecting the development of the (100)

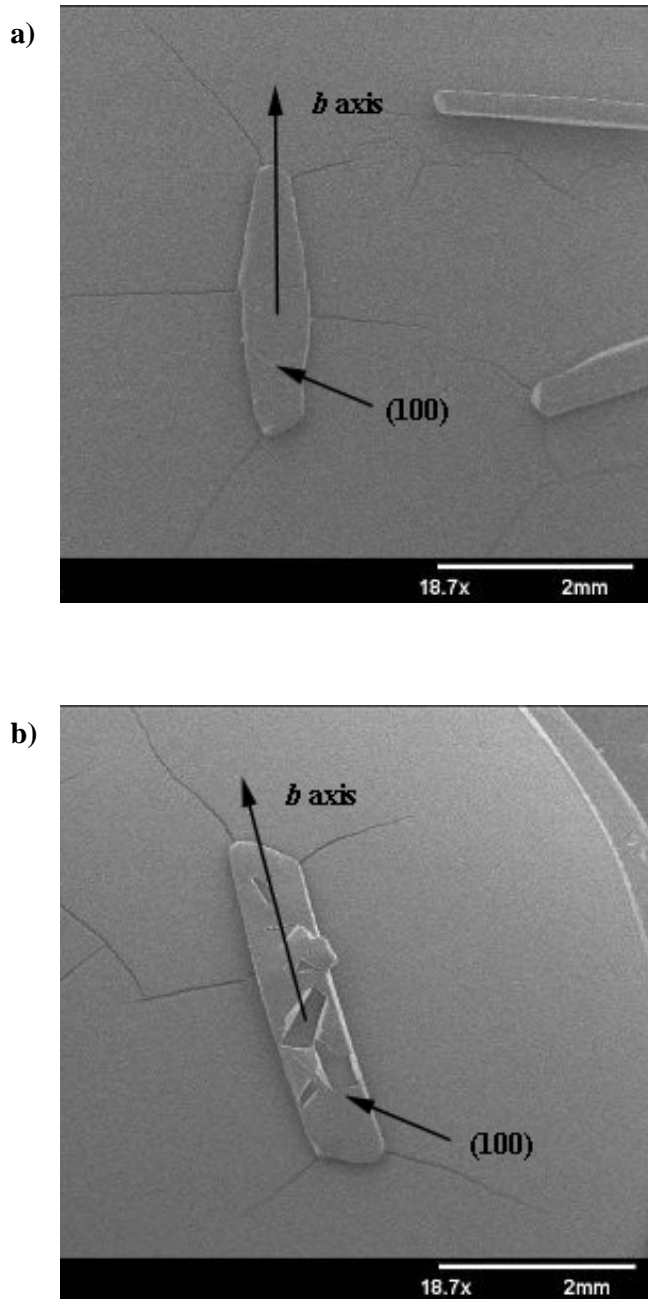


**Figure 2.12.** SEM micrographs of crystals grown the presence of 0.034 mmoldm<sup>-3</sup> octanoic acid (a) and 0.048 mmoldm<sup>-3</sup> octanoic acid (b). (a) – x 18.7 magnification, (b) – x 18.7 magnification.

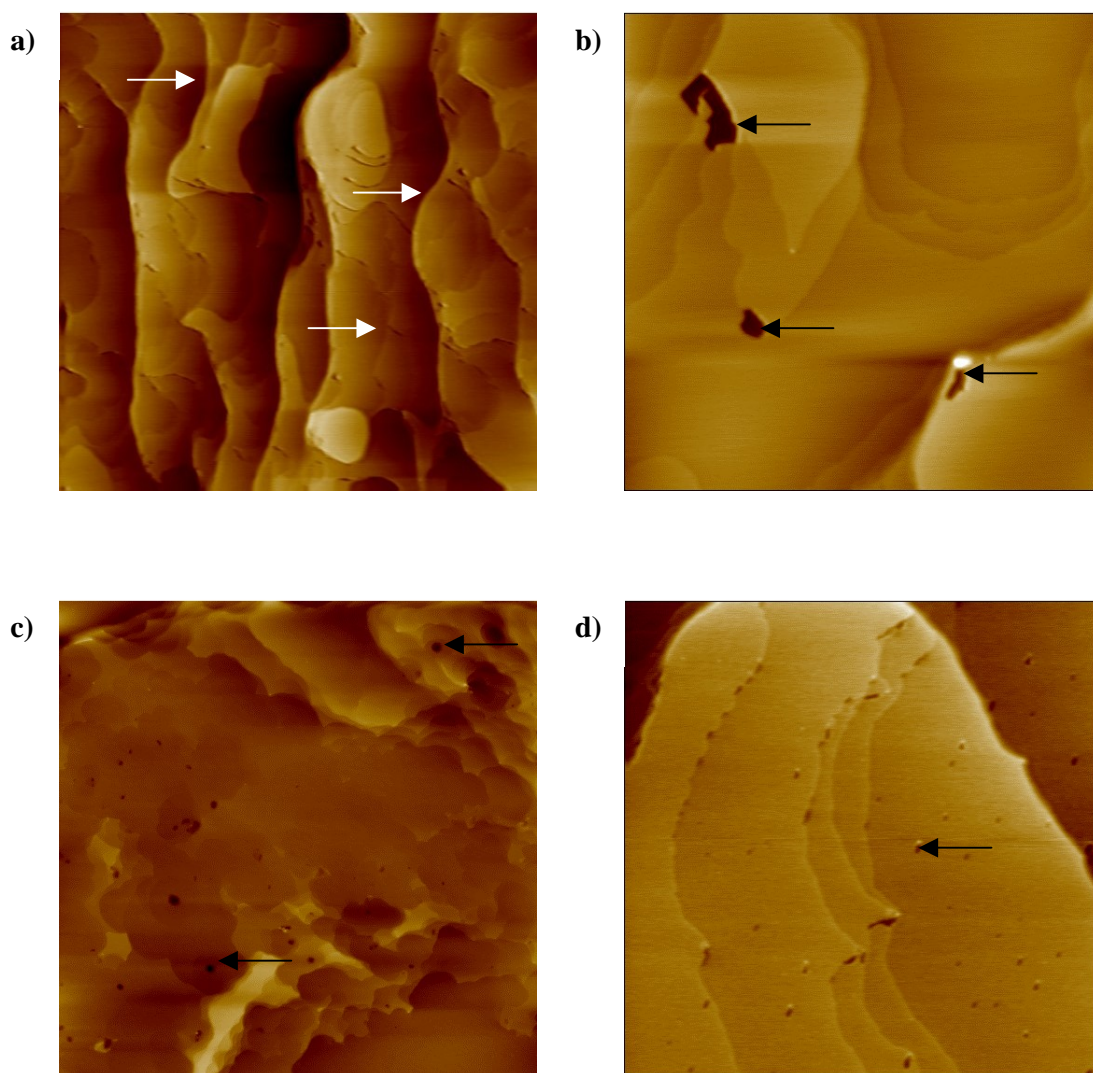


**Figure 2.13.** AFM topographical images of the (100) face of adipic acid crystals grown in the presence of  $0.034 \text{ mmoldm}^{-3}$  octanoic acid. Hollow cores are clearly visible in all images, a few of which are highlighted with black arrows. Scan sizes & z-ranges **a)**  $10 \mu\text{m} \times 10 \mu\text{m}$ , 25 nm; **b)**  $2.7 \mu\text{m} \times 2.7 \mu\text{m}$ , 20 nm; **c)**  $13 \mu\text{m} \times 13 \mu\text{m}$ , 100 nm; **d)**  $5 \mu\text{m} \times 5 \mu\text{m}$ , 20 nm

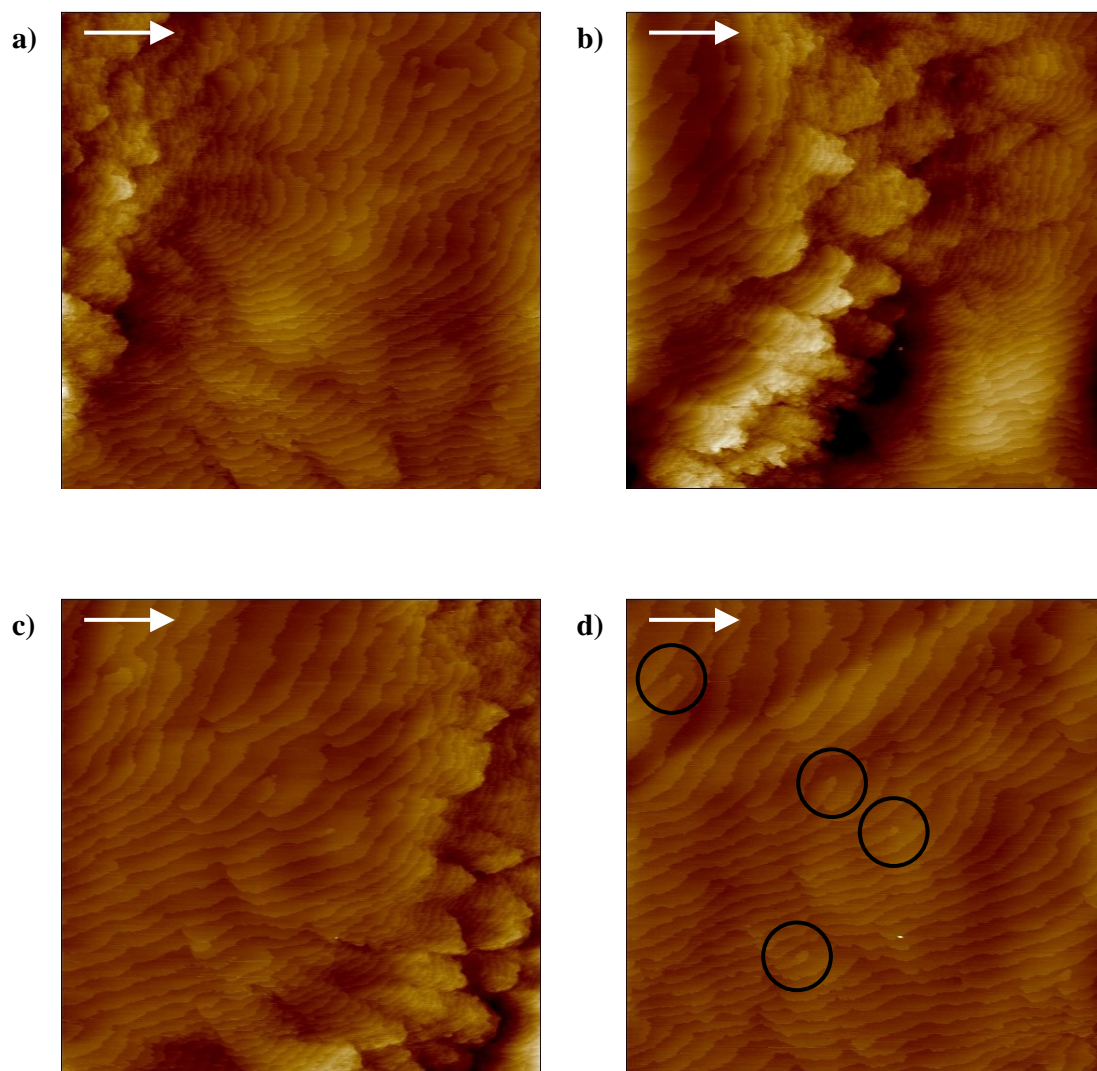


**Figure 2.14.** Sequential 10 μm x 10 μm topographical images of crystalline adipic acid growing in the presence of 0.63 mmoldm<sup>-3</sup> octanoic acid, at a supersaturation of ~0.4. Growth is occurring from left to right in the images as indicated by the white arrows. Defects are indicated in (d) with black circles. The z-range of all four images is 10 nm, with a scan rate of 5.5 Hz.

surface. The reasons for this are probably two-fold. Firstly, the higher concentrations of impurity may act to lower the system supersaturation slightly – indeed, this would account for the apparent annihilation of the large macrosteps and appearance of screw dislocations on the surface. Secondly, it is possible that the octanoic acid is now at a concentration sufficient to adsorb sporadically to the (100) surface and thus directly interfere with growth, but of insufficient concentration to completely pin the advancing steps.

To investigate this further, the concentration of the guest molecule was doubled to  $1.26 \text{ mmoldm}^{-3}$  (a concentration corresponding to a molar ratio of approximately 1:175 octanoic acid : adipic acid) and numerous images were taken at various points over the whole crystal surface, two of which are displayed in figure 2.15. The concentration of octanoic acid was now apparently sufficient to inhibit tangential step-wise growth on this face completely, as sequential images displayed negligible signs of growth. Figure 2.15(b) displays a section of the crystal at higher resolution and here the steps appear to be extremely rough, which is indicative of a high level of incorporation of impurity to the crystal surface.

These observations correlate well with previous modeling and experimental studies. Although it exhibits signs of increased lattice stress, the growth of the (100) face appears to be minimally affected at low concentrations of the additive. Presumably, this is due to the hydrophilic surface rejecting the comparatively hydrophobic monocarboxylic additive molecules (Williams-Seton *et al.*, 2000), whilst the less hydrophilic faces that bound the (100) face incorporate the additive, thus altering the gross morphology of the crystal. However, as the concentration is raised, it is clear that octanoic acid begins to effect the development of the (100) surface, with growth being inhibited at an additive concentration of  $1.26 \text{ mmoldm}^{-3}$ . This may be due to the binding energy between the octanoic acid molecule and the (100) surface of crystalline adipic acid being significantly larger than that exhibited by the surface and water, ethanol and even adipic acid (Myerson and Jang, 1995). The modelling studies of Myerson & Yang indicate that octanoic acts as a growth inhibitor on this face because of the increased binding that occurs between the (100) surface of adipic acid and octanoic acid. This indeed appears to be the case, but only at elevated concentrations of additive – below this, the (100) face appears to be largely protected by water bound to its hydrophilic surface.

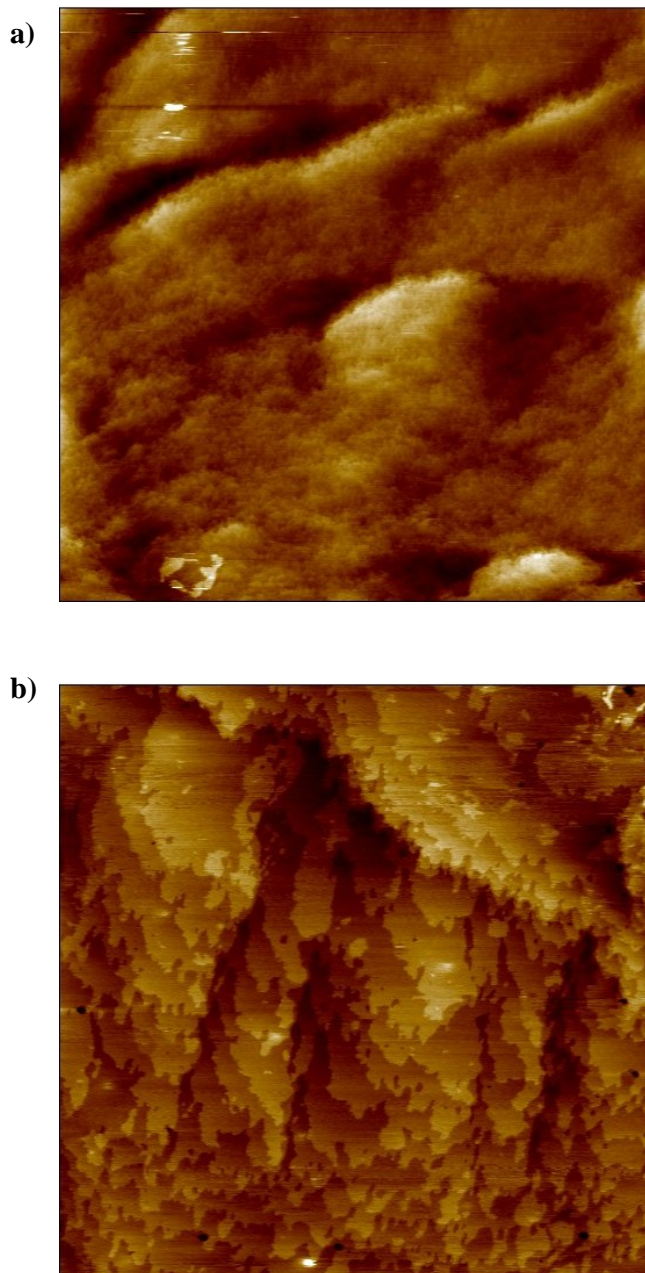


**Figure 2.15.** Topographical images captured in the presence of  $1.26\text{mmoldm}^{-3}$  octanoic acid, at a supersaturation of  $\sim 0.4$ . **(a)**  $10\ \mu\text{m} \times 10\ \mu\text{m}$ , z-range 20 nm, **(b)**  $3\ \mu\text{m} \times 3\ \mu\text{m}$ , z-range 5 nm.

## 2.4 Conclusions

The hydrophilic nature of the (100) surface of crystalline adipic acid has long been known to play an important role in determining the gross morphology of the crystal. By utilizing Atomic Force Microscopy (AFM), we have been able to directly observe the (100) face of adipic acid in both air and liquid environments, and in doing so, provide direct microscopical evidence of the importance of hydrophilic nature of this surface.

Initially optimization experiments were carried out in order to identify suitable conditions to allow the reproducible growth of crystals large enough to act as seeds during the AFM experiments. This was achieved by implementing slow cooling of an undersaturated solution to 4 °C over a period of 72 hours.

Preliminary characterization experiments revealed the (100) face of the crystal to be composed of both single-molecular and bunched step edges that had often been pinned by foreign impurities adsorbed on to the crystal surface. The single-molecule steps were consistently around 0.7 nm in height ( $\pm 0.15$  nm), a figure that is directly comparable to 0.685 nm, the interplanar distance normal to the (100) face deduced from crystallographic studies.

Solute reorganization was observed during scanning in air, in both contact and tapping mode. This is a rarely reported phenomenon which, using the force-distance capabilities of AFM, we investigated and explained as a possible consequence of the hydrophilic nature of the surface permitting local tip-enhanced dissolution and reorganization of the solute. *In situ* imaging carried out on the seed crystals also revealed the formation of etch pits during dissolution, which can also be attributed to the presence of bound water on the (100) face.

Also presented here are nanoscale observations of the effect of octanoic acid, a structurally related habit modifier, on the (100) surface of crystalline adipic acid. Initially, doped seed crystals were grown and studied using AFM and SEM. These studies showed that although there seemed to be an increased level of stress within the lattice, the development of the (100) face was apparently unaffected by the presence of relatively low levels of the additive, with the (100) surface retaining its morphological dominance. This observation was confirmed by carrying out *in situ* experiments, which showed that the presence of low levels of additive had little effect on the development

of the (100) surface, presumably because the strongly adsorbed water layer is able to reject the majority of the more hydrophobic alcanoic acid molecules. However, as the concentration of octanoic acid was increased during these *in situ* experiments, the surface began to exhibit clear changes in step morphology and growth mode. Indeed, at the elevated concentration of  $1.26 \text{ mmoldm}^{-3}$  octanoic acid (a concentration corresponding to a molar ratio of approximately 1:175 octanoic acid : adipic acid), growth on the (100) face was completely inhibited.

## Chapter

# 3

## The surface characterization of a model protein crystal

---

The (110) and (101) faces of the tetragonal lysozyme crystal have been investigated at both a microscopic and nanoscopic level using *in situ* AFM. Initially, the (110) surface was imaged at a range of supersaturations: high ( $\sigma > 1.0$ ), medium ( $0.99 > \sigma > 0.8$ ) and low ( $\sigma < 0.79$ ). As expected, lowering the value of supersaturation progressively lowered both the quantity and tangential growth velocity of the steps in the  $\langle 001 \rangle$  direction from  $11.0 \text{ nms}^{-1} \pm 1.6 \text{ nms}^{-1}$  at  $\sigma = 1.6$ , to  $3.3 \text{ nms}^{-1} \pm 1.2 \text{ nms}^{-1}$  at  $\sigma = 0.67$ . Contrary to a number of recent reports, the generation of the step edges on the (110) surface was apparently a consequence of a number of distinct growth mechanisms – 3D nucleation, 2D nucleation and screw dislocations. Additionally, one of the mechanistic observations made during this study (the promotion of multilayered stacks by the edges of adsorbed microcrystals) has not, to the author's knowledge, previously been reported for any crystal system. A number of molecular resolution features were also obtained using AFM data. The step edge heights for both the (110) and (101) surfaces were measured to be  $5.3 \text{ nm} \pm 0.5 \text{ nm}$  and  $3.6 \text{ nm} \pm 0.5 \text{ nm}$  respectively, indicating the growth units for both faces are dimeric in height, rather than monomeric. Both surfaces were also imaged at molecular resolution. After performing Fast Fourier Transformation (FFT) analyses, the periodic features on the (110) face were shown to be  $11.5 \text{ nm}$  and  $3.8 \text{ nm}$ , with the (101) face displaying periodicities of  $7.9 \text{ nm}$  and  $7.9 \text{ nm}$ , all of which conform precisely to the known 2D unit cell measurements for the respective crystallographic faces.

---

## 3.1 Introduction

### 3.1.1 Macromolecular crystal growth – A brief history

Many advances of our understanding of biological systems at the molecular level have been made possible through knowledge of the detailed structures of biological macromolecules such as proteins, viruses and nucleic acids. Indeed, such information provides the cornerstone of many modern fields of research including protein engineering and rational drug design (Durbin and Feher, 1996).

Obtaining the atomic structure of a macromolecule is a complicated and often time-consuming process, and is reliant on many different factors. One of the most important stages in this process is the production of crystals of suitable size and perfection for X-ray diffraction studies.

Hünefeld first achieved macromolecular crystallization around 160 years ago (McPherson, 1991) when he pressed the blood of an earthworm between two glass slides, and allowed it to dry very slowly. Essentially, he was permitting the controlled evaporation of a concentrated protein solution (in this case, hemoglobin), which resulted in the formation of protein crystals. In fact, most crystal growth techniques in use today are based on the fundamental physical chemistry involved in this relatively simple experiment.

Until the 1930s the growth of macromolecular crystals was associated with purity alone. However, advances in X-ray crystallography techniques at this time meant the macromolecular crystal became seen as not just a purification tool, but also a possible source of structural information (McPherson, 1999). The first X-ray diffraction pattern of a macromolecule, pepsin, was produced in 1934 (Bernal and Crowfoot, 1934), and then in the early 1960s the first atomic structures of hemoglobin and myoglobin were published (Cullis *et al.*, 1962) with two of the researchers, Max Perutz and John Kendrew, being awarded the Nobel Prize for chemistry in 1962. Since this time, over 23,000 unique structures have been deposited in the Protein Data Bank (PDB), the vast majority of which have been determined from data accrued during X-ray crystallography studies (Berman *et al.*, 2000).

The last 40 years have seen huge advances in molecular biology and biochemistry (for example the discovery and application of the Polymerase Chain Reaction (PCR) to DNA synthesis, and the success of the human genome project), and all aspects of X-ray crystallography technology and computing have improved beyond reckoning. However the discipline of macromolecular crystal growth has not advanced at this rate, in either fundamental understanding or technique. Inevitably, a ‘bottleneck’ has formed at this critical stage of the structural biology process, the severity of which is clear when considering the results of recent structural biology pilot studies – a mere 30 % of cloned, purified macromolecules produce crystals of a quality suitable for X-ray analysis (Chayen, 2002).

The underlying reasons behind the relatively slow advancement in the techniques and understanding of macromolecular crystal growth are numerous, and almost all linked to the nature of biological macromolecules and physical characteristics of the crystals that they produce.

Crystallizing a macromolecule is generally regarded to be a difficult task. When compared to conventional small molecules, macromolecules are considerably more sensitive to their environment. To avoid denaturation, they have to be maintained in a completely hydrated state at (or very near to) physiological pH and temperature. Additionally, biological macromolecules of interest are generally only available in minute quantities (~milligrams) due to biochemical complications, or difficulties with purification. Purity has to be of ‘crystallography grade’, which requires not only a protein solution with a marked lack of contaminants (< 5 %), but also a conformationally pure solute free from denatured molecules. Inevitably these requirements make the purification step difficult and often costly in terms of pure-protein yield

As such, conventional large-scale solution crystallization methods such as evaporation, dramatic temperature variations, or the addition of strong organic solvents are simply not suitable for the crystallization of fragile macromolecules (McPherson, 1985).

The strategy generally employed to bring about crystallization of such molecules is to guide the system very slowly toward a state of minimum solubility by modifying the properties of the solvent, or the character of the macromolecule itself (McPherson, 1999). This is most commonly achieved by using salt molecules as ‘precipitants’. By using such molecules, supersaturated solutions can be achieved gently, without

denaturing the fragile macromolecules with high temperatures or organic molecules. A typical solubility diagram for such a macromolecule/precipitant crystallizing system is presented in figure 3.1

Until the mid-1980s these experimental difficulties were compounded by an almost complete lack of theoretical knowledge concerning protein crystals and their growth. In fact, the understanding of macromolecular crystallization still consisted more of a set of ‘trial and error’ recipes rather than a set of general principles (Durbin and Feher, 1996). Indeed, this situation was in stark contrast to that of most other types of crystal growth, where understanding was far more advanced (Chernov, 1984). The reason for this considerable lack of fundamental knowledge at this time was quite simple – the physical characteristics of biological crystals made them extremely difficult to study.

Whilst the contacts within macromolecular crystals are comparable in energy to those found in small molecule crystals, far fewer contacts are present because of the larger molecular weight, which tends to make the crystal mechanically weak when compared with its small molecule counterpart. Macromolecular crystals rarely exceed one millimeter on an edge and extensive solvent channels within the lattice mean that 20 % - 80 % of the crystal mass is actually solvent, further adding to the inherent fragility (Ducruix and Giege, 1992; McPherson, 1999). The factors above all combine to make such crystals very difficult to manipulate, as they are often small, brittle and can only be kept in a solvent-saturated environment to prevent dehydration, cracking and ultimately destruction.

Consequently until the mid-1980s there had been only a handful of systematic investigations into the fundamental aspects of macromolecular crystal growth (Durbin and Feher, 1986). This situation was effectively enforced by a lack of techniques suitable for the study of such brittle, elusive crystals – inevitably, the fundamental knowledge of macromolecular crystallization fell far behind that of their small-molecule counterparts. However, the early part of the 1990s saw a number of significant developments in the field of microscopy, many of which provided a means to investigate the phenomena that govern all crystallization processes, including those of biological molecules. Indeed, as detailed in chapter 1 of this thesis, the successful application of techniques such as interferometry and AFM to the study of a handful of model biological crystals had a considerable impact on the overall fundamental understanding of macromolecular crystallization.

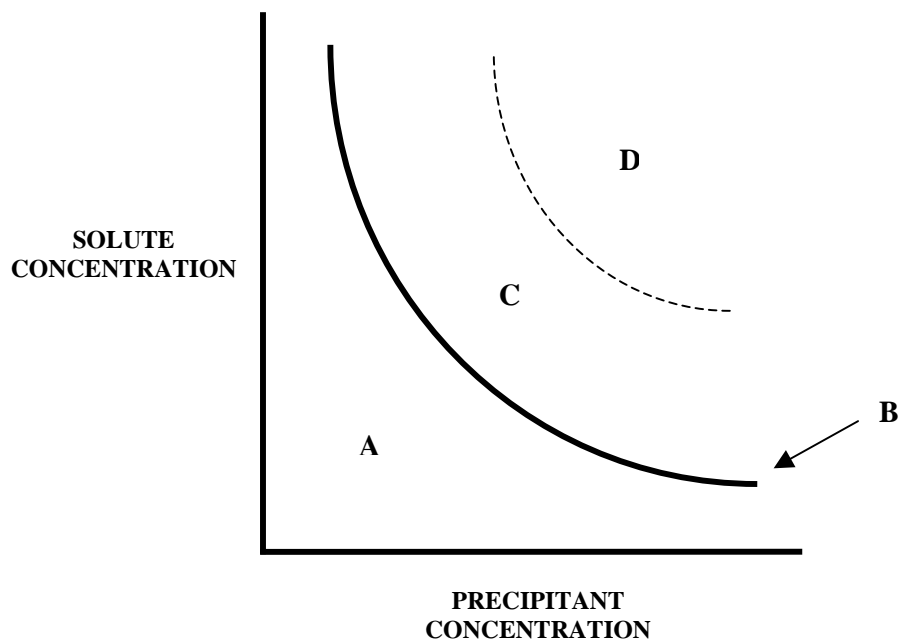


**Figure 3.1.** A typical solubility diagram for the crystallization of a macromolecule, plotting the solute concentration versus the precipitant concentration. The solid line (**B**) represents the limit of solubility, where the solid phase of the macromolecule is in equilibrium with the liquid phase. Beneath this limit (region **A**) the system is undersaturated, and no crystals will grow. Above this limit, the system is supersaturated, with both spontaneous nucleation and crystal growth energetically feasible in **D**, and only crystal growth in **C** (the metastable zone).

Undoubtedly the protein that has yielded the most significant quantity of biological crystal growth data is lysozyme, the main topic of this chapter.

### 3.1.2 Lysozyme

Lysozyme, a globular protein with a relative molecular mass of around 14,400 Da, was discovered in 1922 by Alexander Fleming. It is an antibacterial enzyme that acts by hydrolyzing the polysaccharide portion of the cell wall of certain bacteria. Lysozyme is found in almost all animal and plant life, with one particularly rich source being found in hen egg white (known as HEW lysozyme, or HEWL).

For the last 60 years lysozyme has been synonymous with crystallization. Tetragonal HEWL crystals were first reported in 1946 (Alderton and Fevold, 1946), and the pioneering X-ray crystallographic investigations carried out by David Phillips and Louise Johnson in the 1960s led to the elucidation of both the atomic structure of lysozyme at 2 Å, and its mechanism of action (Blake *et al.*, 1965; Johnson and Phillips, 1965; Blake *et al.*, 1967). Since this time almost 750 unique crystallographic structures of lysozyme (and closely related molecules) have been produced, including an ultra-high resolution structure at 0.94 Å (Sauter *et al.*, 2001). All structures are available in both a dedicated lysozyme structural database (Mohan *et al.*, 2004) and the PDB (Berman *et al.*, 2000). A model of the lysozyme molecule is presented in figure 3.2, with a schematic of the crystal habit adopted by the tetragonal form of lysozyme presented in figure 3.3. Eight molecules of lysozyme make up the unit cell in the tetragonal form, the dimensions of which are  $a = 79.1$ ,  $b = 79.1$ ,  $c = 37.9$  Å (Nadarajah and Pusey, 1996).

### 3.1.3 The study of tetragonal lysozyme crystal growth

Due to its widespread availability, robust nature and relative ease of crystallization, lysozyme has become the preferred model system for the vast majority of protein crystal growth studies.

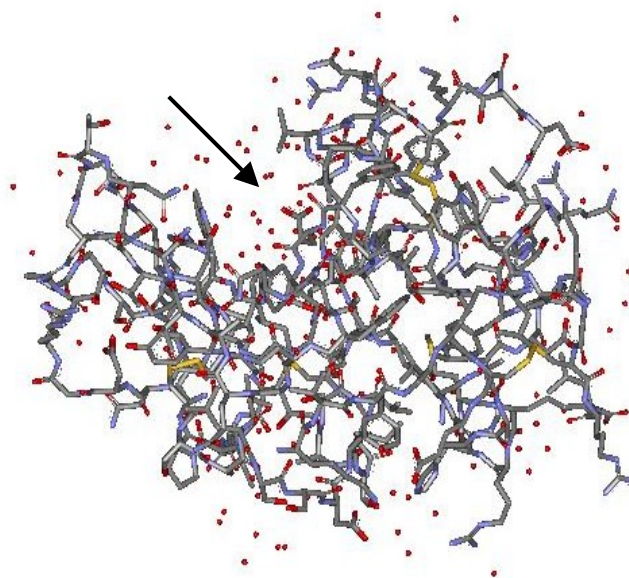


**Figure 3.2.** The lysozyme molecule (PDB ID – 2LYZ), a single polypeptide chain consisting of 129 residues. The active site is located in the cleft indicated by the arrow

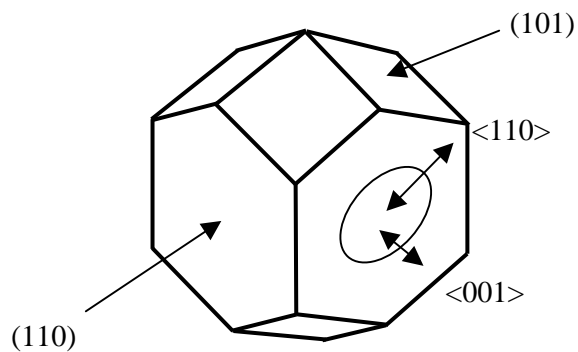


**Figure 3.3.** The habit of lysozyme crystallized in the tetragonal form. The two major faces of the crystal are the (110) and (101). Additionally, the shape and orientation of two-dimensional islands that form on the (110) surface are illustrated.

Durbin & Feher produced the first major report focusing on the post-nucleation growth of lysozyme over a wide range of solute concentrations (Durbin and Feher, 1986). This report was particularly insightful, as the authors were able to relate the supersaturation to both the shape and rate of growth of the crystallographic faces. Additionally, they were later able to favorably compare this crystal growth data with TEM micrographs of lysozyme crystals (Durbin and Feher, 1990), as detailed in chapter 1 of this thesis. The report of Monaco & Rosenberger later furthered these studies by employing high-resolution optical microscopy to probe the growth and etching of lysozyme crystals under stringently controlled conditions (Monaco and Rosenberger, 1993).

In the early 1990s the application of interferometric techniques contributed much to the understanding of the mechanisms and kinetics of lysozyme crystal growth (for an excellent review of this data see Rosenberger, 1996). However, because of its superior resolution and *in situ* capabilities, it was AFM that made the most significant microscopical impact on the study of lysozyme crystals.

AFM was first used to study lysozyme crystallization in the early 1990s (Durbin and Carlson, 1992; Durbin *et al.*, 1993). These early *in situ* studies produced particularly instructive images of growth step generation at screw dislocation outcrops, the nucleation and subsequent development of 2D islands and other growth phenomena such as step bunching. In 1994, Konnert *et al* reported observing the (110) surface of tetragonal lysozyme crystals at a molecular resolution for the first time using AFM (Konnert *et al.*, 1994). Since this time, a number of AFM-based studies have focused on a variety of aspects of the crystallization of tetragonal lysozyme crystals including the determination of the dominant molecular mechanism of growth (Li *et al.*, 1999a; Li *et al.*, 1999b; Wiechmann *et al.*, 2001), the growth rates of the (110) surface under controlled conditions (Rong *et al.*, 2000), the effect of impurities on growth (Nakada *et al.*, 1999) and the effect of the growth supersaturation on the crystal quality (Yoshizaki *et al.*, 2001; Yoshizaki *et al.*, 2002).

### 3.1.4 Chapter Aims

This study aims to tackle a number of issues. As previously discussed, the mechanical nature of macromolecular crystals makes them difficult to investigate – indeed, far more difficult than organic crystals such as adipic acid. For this reason, the first objective of this study will be to develop experimental protocols that will enable such delicate crystals to be investigated by AFM. This involves identifying reliable conditions to both grow and adhere seed crystals on to a substrate suitable for AFM analysis.

The selection of lysozyme as the model system serves two purposes. Firstly, as previously discussed, lysozyme is available in large quantities and crystallizes in the tetragonal form with relative ease. These facts will make the optimization stage of the study more straightforward and ensure the development of valuable *in situ* imaging protocols that will be of use in future investigations of more challenging macromolecular crystals. Secondly, there are still conflicting reports concerning numerous aspects of the crystal growth of lysozyme, such as the size of the growth unit and mechanisms employed during growth (Rong *et al.*, 2000; Wiechmann *et al.*, 2001; Pusey and Nadarajah, 2002; Wiechmann, 2002). Using *in situ* AFM we aim to add to existing microscopical data, and address outstanding questions concerning the crystallization of lysozyme.

## 3.2 Materials & Methods

### 3.2.1 Substrate Preparation

To withstand the forces associated with the raster scanning action of the AFM tip it was imperative that the crystals were firmly fixed to a suitable substrate. Three substrates have been used during the nucleation, growth and subsequent AFM analysis of all macromolecular crystals in this thesis – plain glass coverslides, Poly-L-Lysine (PLL)-coated glass coverslides and nickel-coated Transmission Electron Microscopy (TEM) grids. The various advantages and disadvantages of each, together with a brief discussion on other methods previously reported, are included in the results and discussion section below.

### 3.2.2 Seed Crystal Growth

A range of initial crystallization conditions were investigated and optimised to provide suitably sized crystal seeds within a manageable timescale. For tetragonal HEWL crystals, batch crystallization was employed and found to be a robust, repeatable method. Batch crystallization is the simplest form of macromolecular crystallization and involves mixing the biomolecule of interest with a crystallizing agent at concentrations sufficient to produce an instantaneously supersaturated solution.

All buffers were prepared with ultrapure, HPLC grade water (18.2 M $\Omega$ cm resistivity). All lysozyme solutions were freshly prepared before each crystallization run to avoid the ‘aging effect’ (Chayen *et al.*, 1993).

Unless otherwise stated in the results and discussion section, seed crystals were grown as follows. Three-fold lyophilized HEWL (Fluka, Dorset, UK) at a concentration of 30 mg/ml, and 30 mg/ml sodium chloride (Sigma-Aldrich, Dorset, UK) were dissolved in a 0.1 M NaOAc/AcOH buffer at pH 4.5 by vortexing and low-speed centrifugation. The solution was filtered, and six 4-6  $\mu$ L drops of the crystallizing solution were placed on previously unused substrate, which had been attached to a

magnetic AFM sample stub. The stubs were then all sealed in separate sitting-drop crystallization wells (Hampton Research Corporation, Laguna Niguel, CA), and left overnight at a temperature of approximately 20 °C. Because the drop size was small, nucleation generally occurred within 12 – 16 hours and seed crystals of 50 μm x 50 μm or larger had grown within 24 hours.

### 3.2.3 Preparation of imaging solutions

The relative supersaturations of all imaging solutions were calculated using equation 1.1.

$$\sigma = \ln (c/c_0) \quad \text{equation 1.1}$$

where  $c_0$  is the solubility of lysozyme at a given temperature, and  $c$  is the concentration of lysozyme dissolved in the growth medium. All experiments were carried out at room temperature (~25 °C). All values of supersaturation were calculated in conjunction with published solubility data accurately determined for lysozyme at various values of pH, precipitant concentration and temperature (Cacioppo and Pusey, 1991). However, as discussed in some depth in section 2.2.2 of this thesis, the calculated value of supersaturation may be slightly higher than the actual experimental conditions as a result of localized temperature variations within the liquid cell. As such, the values of supersaturation quoted throughout have been calculated using the solubility data at 25 °C, and are accurate relative to one another at this temperature.

### 3.2.4 AFM analysis

Prior to imaging, all samples were observed by *ex situ* optical microscopy to assess the optical quality of the crystals. The most promising (usually those samples that contained well faceted, crack-free crystals) were removed from the crystallization plate, the mother liquor wicked away and rapidly replaced with a drop of solution

prepared for imaging. The sample was then inserted into the AFM together with the liquid cell, which was equipped with a plastic O-ring to minimize solvent evaporation. The cell was subsequently flooded with imaging solution and, using the optical microscope integrated into the AFM system, the cantilever was positioned above a crystal that displayed a face of interest parallel to the substrate. The sample was then left for ~1 hour to equilibrate before imaging began.

As a consequence of both the high protein concentration in the imaging solution and relatively low growth rate of the crystals, we found it unnecessary to employ a flow-through system to the experimental procedure described above. Using the conditions and data obtained in section 3.3.2.1 as an example (20 mg/ml lysozyme producing a supersaturation of 1.0), the quantity of lysozyme molecules within the liquid cell (volume 50  $\mu\text{l}$ ) is calculated to be approximately  $4 \times 10^{16}$ . In this set of data, the progress of approximately 20 step edges were tracked across a  $10 \mu\text{m} \times 10 \mu\text{m}$  section of crystal face. The average tangential step velocity was calculated as 5.7 nm/s.

The dimensions of a single lysozyme molecule in two dimensions are approximately 3 nm x 3 nm. Hence, a single  $10 \mu\text{m} \times 10 \mu\text{m}$  section of crystal face is constructed of roughly  $1.1 \times 10^7$  molecules. By considering the step velocity, one step edge covers the  $10 \mu\text{m} \times 10 \mu\text{m}$  section in approximately 30 minutes. Thus, as a very basic guide,  $20 \times 1.1 \times 10^7$  molecules are incorporated into this section of the crystal surface in 30 minutes at a supersaturation of 1.0. As the crystals seeds investigated were generally  $\sim 100 \mu\text{m} \times 100 \mu\text{m}$  in two dimensions, this figure can be multiplied by 100 to give a rough guide to the quantity of molecules added to the surface of the entire crystal in 30 minutes. This final figure is calculated as  $2.2 \times 10^{10}$ . When comparing this figure to the quantity of lysozyme molecules in the mother liquor ( $4 \times 10^{16}$ ), it is quite clear that the quantity of lysozyme molecules ‘lost’ to the crystal face is (comparatively) infinitesimally small and will have a negligible effect on the solution supersaturation over the relatively short imaging periods employed throughout this study.

All images were recorded using either a DI Multimode or DI3000 atomic force microscope, both of which equipped with a Nanoscope IIIa controller (Veeco, Santa Barbara, CA). Silicon nitride NP-S cantilevers with a nominal spring constant of  $0.1 \text{ Nm}^{-1}$  were used throughout (Veeco). The DI multimode was equipped with an E-type scanner with maximum scan dimensions of  $13 \mu\text{m} \times 13 \mu\text{m} \times 2 \mu\text{m}$ , and the DI3000 was equipped with G-type scanner, maximum scan dimensions  $100 \mu\text{m} \times 100 \mu\text{m} \times 12 \mu\text{m}$ .

The relatively robust nature of the crystal allowed images to be collected in contact mode throughout. However, care was taken to continually adjust the setpoint voltage to the lowest value for which tip-crystal contact was maintained to minimize the force applied to the crystalline surface. This was particularly important during the molecular resolution scans (see section 3.3.3.2). All images were collected at either 256 x 256 or 512 x 512 pixel resolution, at a scan rate in the range of 3-7 Hz.

The images presented throughout this study are in the form of either topography or deflection data. Topography micrographs are constructed from the movement of the z-piezo in response to the AFM controller feedback system, and contain accurate three-dimensional data. The deflection images are constructed directly from the movement of the laser on the AFM photodiode. These images often highlight rapid changes in topography in greater detail, such as is seen at step edges, and are used for that purpose throughout this chapter.

The tangential step velocities quoted in section 3.3.2 have been calculated from consecutive images by considering the image acquisition time in conjunction with the distance travelled by the step (Rong *et al.*, 2000). This figure was obtained by using the section function available in the DI image processing software. Step anisotropy (as discussed in the introduction of this thesis and illustrated in figure 3.3) was considered, and as such all velocities quoted correspond to growth in the  $\langle 001 \rangle$  direction on the (110) face. All other image analysis and processing were carried out with DI software.

### 3.3 Results & Discussion

#### 3.3.1 Seed crystal immobilization

As briefly mentioned above, to undergo the raster scanning action of the AFM tip it was imperative that the crystals were firmly fixed to a suitable substrate. Four methods have previously been implemented to facilitate AFM data acquisition. Crystals have been physically adhered to a substrate using vacuum grease (Konnert *et al.*, 1994), secured beneath a thin silicon carbide fibre (Malkin *et al.*, 1997), adsorbed to a surface by careful control of both the composition of the imaging medium and physical-chemical properties of the substrate (Lacapere *et al.*, 1992), and nucleated directly onto a substrate (Durbin and Carlson, 1992; Kuznetsov *et al.*, 1997).

The two methods utilizing vacuum grease and a thin carbon fibre were not implemented during this study for the following reasons. To the author's knowledge, both methods have only been utilized in this specific capacity (in published research) once, and on both occasions the crystals of interest were relatively robust (lysozyme and catalase respectively). Whilst this study is concerned with the crystallization of lysozyme, one objective is to develop protocols for future studies of protein crystals that are unlikely to display such robust mechanical properties.

Similarly, the method involving crystal adsorption has rarely been used in this capacity, and has not been implemented during this study. Its major drawback is that to achieve suitable levels of crystal-substrate adhesion, the imaging medium must extremely be carefully controlled, which both detracts from and limits the unique *in situ* capabilities of the AFM. Even if precise conditions were determined and maintained throughout an experiment, the author questions the strength of adhesion over an extended period of imaging.

The technique most commonly and successfully implemented in the literature has been that of nucleation directly onto a substrate. Indeed, heterogeneous nucleation is a common (and generally unwanted) observation in protein crystal growth, and often results in promising crystals being ruined because of their strong adhesion to the containing vessel. However, for the purposes required for AFM imaging such heterogeneous nucleation is advantageous. Crystals can be grown and subsequently

transferred into the AFM cell without the need for awkward manual handling, which often results in damage to the crystal of interest.

Three different substrates were investigated in this study, and their various attributes described below.

#### 3.3.1.1 Plain glass coverslides

Glass is negatively charged in water and as such could be expected to exhibit some degree of electrostatic interaction with lysozyme molecules, which are positively charged at the crystallizing solution pH of 4.5 (the pI of lysozyme is around pH 11 (Rosenberger, 1996)), making this an ideal substrate/sample combination. However, crystals were not always adhered to the plain glass surface, a fact that can probably be attributed to the composition of the crystallizing solution. The precipitant ions in the relatively complex solution are likely to have a screening effect on both the crystal and surface charges, effectively minimizing any electrostatic interactions. Any crystals that were adhered to the substrate surface were observed to be randomly orientated.

#### 3.3.1.2 Nickel-coated TEM grids

In an attempt to improve the quantity of crystals strongly adhered to the substrate, the method developed by Kuznetsov *et al.* was implemented (Kuznetsov *et al.*, 1997). It involves gluing 3 mm diameter TEM grids to clean glass coverslides (which in turn have been attached to the magnetic AFM stub), and placing the drop of crystallizing solution directly on top of the grid. This is illustrated in the photograph in figure 3.4(a).

The comparatively rough surface of the metal grid appeared to strongly encourage the heterogeneous nucleation of lysozyme crystals suitable for long periods of *in situ* imaging. Additionally, the method was reliable, repeatable and applicable to other more fragile samples.

#### 3.3.1.3 Poly-L-Lysine (PLL)-coated glass coverslides

A slight drawback of the two methods discussed above is the random orientation adopted by crystals nucleated on the substrate. Previous reports have indicated that PLL

has an effect on the orientation of lysozyme crystals nucleated on its surface (Tsekova *et al.*, 1999; Nanev and Tsekova, 2000; Fermani *et al.*, 2001; Rong *et al.*, 2002). Such control may be advantageous during AFM studies, as successful imaging relies on obtaining samples with crystal faces parallel to the substrate surface.

The application of PLL to glass coverslides places positive charges at the substrate surface. Inevitably, this causes some repulsion between lysozyme molecules and the substrate, which led to an apparent decrease in nucleation in the optimization experiments carried out here. Indeed, nucleation-inhibiting properties of PLL on lysozyme crystallization have previously been noted (Chayen and Saridakis, 2001; Rong *et al.*, 2002). However, heterogeneous nucleation did still occur (probably due in part to the same charge-screening effect discussed briefly in section 3.3.1.1) and many of the crystals were orientated to the (110) form, as illustrated by the photograph in figure 3.4(b). The lower incidence of nucleation also had the ‘knock on’ effect of the seed crystals growing to be slightly larger due to the increased concentration of solute available in the crystallizing solution.

The reliability of the TEM grid method outweighed the slight advantages offered by the PLL-coated coverslides. Whilst the occasional TEM grid sample was devoid of suitable crystals, the majority always offered at least one surface parallel to the substrate. Although they were significantly more reliable than the plain glass coverslides, the PLL samples did not always immobilize crystals strongly enough to undergo scanning. The increased likelihood of orientation to the (110) face meant there was a corresponding decreased probability of orientation to the other crystallographic surface, the (101) face. Additionally, as previously reported, results obtained with lysozyme concerning heterogeneous nucleation are not always applicable to other proteins (Chayen and Saridakis, 2001), so unless otherwise stated in the text the TEM method was used to encourage the heterogeneous nucleation of protein crystals.

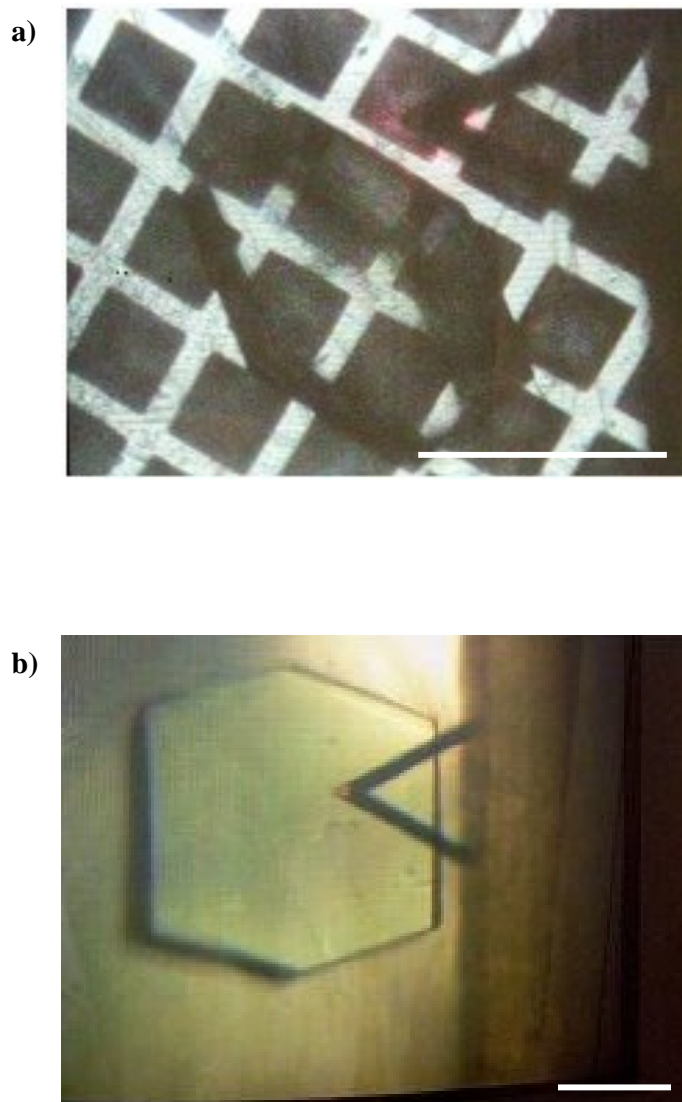


**Figure 3.4.** Photographs taken from the optical microscope integrated into the AFM system. **(a)** A lysozyme seed crystal orientated to the (110) form, nucleated on a TEM grid. **(b)** A crystal again orientated to the (110) form, nucleated on a PLL-coated glass coverslide. The scale bar in both cases is 200  $\mu\text{m}$ .

### 3.3.2 Mechanisms of growth on the (110) face of tetragonal lysozyme crystals

Macromolecules are far more complex in composition, structure, surface features and surface potential than conventional molecules (Malkin *et al.*, 1995a). Inevitably, crystals comprised of macromolecules also display additional complexities and differences when compared with their small-molecule counterparts. One such difference is a large discrepancy in growth rate – indeed, the kinetics of the growth processes of macromolecular crystals are several orders of magnitude slower than seen in conventional crystals (McPherson, 1999). This represents a considerable advantage to microscopists, as the course of events during the growth of macromolecular crystals is more compatible with the temporal resolution of standard atomic force microscopy and interferometry. Obtaining direct evidence of many fundamental aspects of crystallization (such as growth mechanisms) from conventional crystals has proved extremely difficult because of the small dimensions of the molecules, and their rapid growth rates (Vekilov and Alexander, 2000). For example, the author was able to observe dislocations *in situ* on the surface of adipic acid crystals (Chapter 2, section 2.3.4) only because of the presence of a growth-inhibiting molecule within the mother liquor – the pure-grown crystals yielded no such mechanistic detail because of their rapid growth rates.

As such, over the past decade the macromolecular crystal has become the system of choice for microscopical investigations of numerous aspects of crystal growth. However, there having been various conflicting reports concerning the mechanisms of growth employed on the surfaces of such crystals and how these mechanisms are affected by changes in the solution supersaturation. In an attempt to add to existing data available on the crystallization of lysozyme, we have conducted a number of experiments on the (110) surface of tetragonal crystals at a range of supersaturations – high ( $\sigma > 1.0$ ), medium ( $0.99 > \sigma > 0.8$ ) and low ( $\sigma < 0.79$ ). Results from a selection of these experiments are presented below.

#### 3.3.2.1 High supersaturation ( $\sigma > 1.0$ )

The experimental procedure outlined in the materials & methods section above was initially altered slightly in an attempt to observe crystals growing under conditions

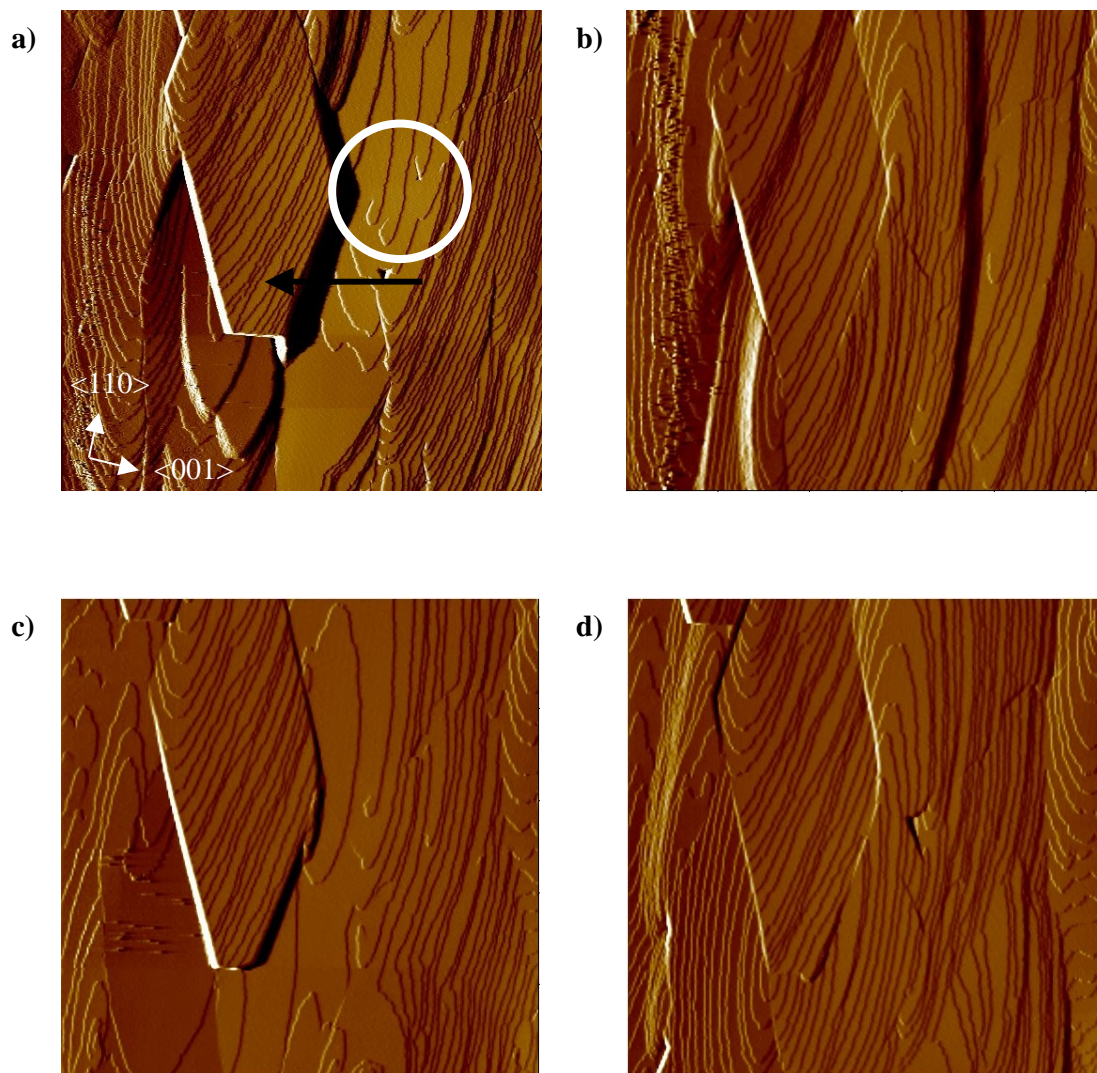
that accurately represented the growth environment of developing tetragonal lysozyme crystals. Rather than preparing a fresh imaging medium, the solution used to grow the seed crystals was transferred into the fluid cell. This effectively allowed the observation of crystals ~24 hours into an experiment in their original mother liquor ( $\sigma = 1.6$ ).

Figure 3.4 shows four images captured during one such experiment. The raster scanning time of each image is approximately 52 seconds and the time of acquisition of each image is indicated in the figure legend. The average tangential step velocity in the  $\langle 001 \rangle$  direction was calculated to be  $11.0 \text{ nms}^{-1} \pm 1.6 \text{ nms}^{-1}$ . The entire sequence of images captured during this experiment is available both as an .avi file on the attached CD (filename lysozyme1), and on the departmental website (Chen, 2004).

The dominant feature present in this series of images is the small ( $\sim 9 \mu\text{m} \times 5 \mu\text{m}$ ) crystalline entity on the surface of the crystal under investigation. Such entities are ‘microcrystals’ that have nucleated in the mother liquor and subsequently adhered to the surface of the seed crystal. Microcrystals have been reported on a few occasions on protein crystals surfaces such as canavalin and thaumatin (Malkin *et al.*, 1996c). Many such microcrystals are rapidly incorporated into the larger seed crystal, particularly when the supersaturation is insufficient to support normal growth by two-dimensional nucleation (Kuznetsov *et al.*, 1998). However, it appears that this microcrystal may have been partially incorporated into the bulk of the crystal and has subsequently developed a source of growth steps that permits its normal development. Interestingly, the microcrystal did appear to have almost become incorporated into the bulk on a number of separate occasions, only to reappear quite clearly a few images later (from figure 3.5(b)-(c) for example). This may indicate some degree of misorientation between the microcrystal and seed crystal surface.

During the periods when the microcrystal was prominent on the bulk crystal surface, a series of interesting growth events took place. Whilst a number of screw dislocations were present on the crystal surface throughout (as indicated in figure 3.5(a)), the major source of growth appeared to be a series of multilayer stacks that emanated from the edges of the un-incorporated microcrystal. The development of one such stack is illustrated in the sequential images in figure 3.6 and the importance of the stacks in the development of this area on the crystal surface is made particularly clear by the movie accompanying this thesis.

Multilayered stacks are believed to arise from liquid-protein phase droplets that exist in protein solutions (Kuznetsov *et al.*, 1999b). These liquid-protein phases are



**Figure 3.5.** Deflection images charting the development of a  $13 \mu\text{m} \times 13 \mu\text{m}$  section of a tetragonal lysozyme crystal at  $\sigma = 1.6$ . In image (a) time  $t = 0$  secs, (b)  $t = 3112$  secs, (c)  $t = 4243$  secs, (d)  $t = 5435$  secs. A number of screw dislocations and a large microcrystal are present throughout and are highlighted in image (a).

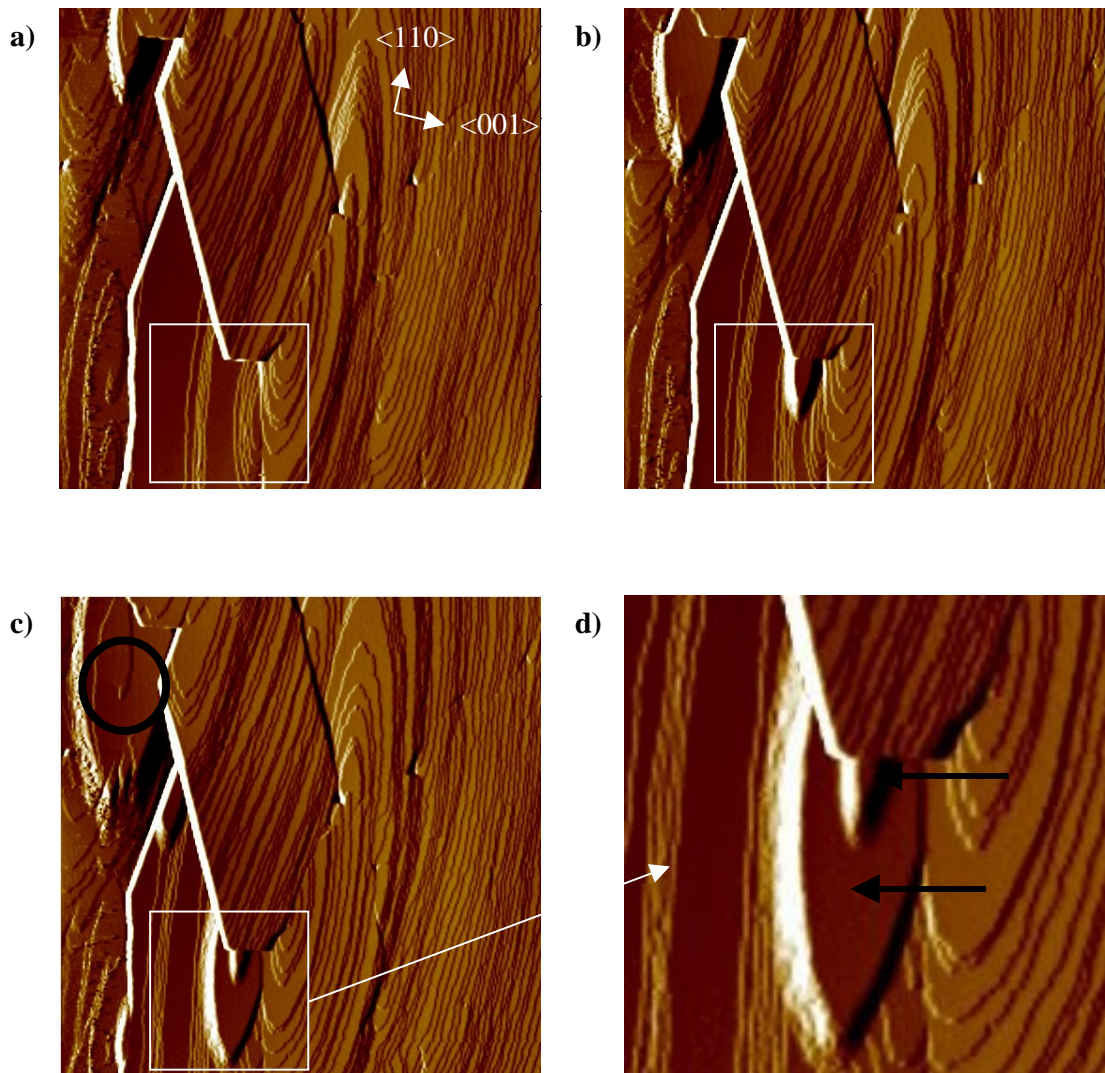


**Figure 3.6.** The rapid, real-time development of a multilayer stack along the perimeter of a microcrystal. Image (d) contains a close-up view of the stack, which has a second stack developing on its surface. An independent multilayer stack is also developing in the top left portion of images (a-c), with a screw dislocation clearly visible on its surface in image (c). All images are deflection images, (a-c)  $13\ \mu\text{m} \times 13\ \mu\text{m}$ , (d)  $4.5\ \mu\text{m} \times 4.5\ \mu\text{m}$ . Taking image (a) as  $t = 0$  secs, the stack highlighted in image (c & d) has developed to this stage in just 103 seconds.

essentially a large aggregate of molecules that display significant levels of short-range order. They adsorb to a crystal surface where the liquid nature of the phase allows the bottom layer of molecules (ie, those in contact with the bulk crystal) to rearrange themselves as to form a congruent layer guided by the underlying lattice. The molecules above this are thus promoted to follow the same pattern, eventually giving rise to a stack of ordered growth layers, rather than a singularly ordered layer as promoted by 2D nucleation.

To the author's knowledge, the promotion of multilayered stacks by the edges of adsorbed microcrystals has never previously been reported. The growth event that bears closest resemblance to this was the apparent generation of 2D nucleation islands from the perimeter of undeveloped microcrystals on the surface of STMV and tRNA crystals (Ng *et al.*, 1997; Kuznetsov *et al.*, 1998). It was postulated that the microcrystal perimeter might provide sites, in conjunction with the underlying lattice, which served as sources of growth steps. Indeed, it follows that if two-dimensional nucleation is possible, then multilayered stack formation must also be feasible as the microcrystal is highly ordered normal to the substrate crystal and will, in some cases, provide steps suitable for more than one layer of tangential growth. This theory is presented schematically in figure 3.7.

The presence of microscopic aggregates in solution did not appear to be limited to experiments carried out in the original mother liquor. The series of images contained in figure 3.8 were recorded during an experiment performed in freshly prepared imaging media at a supersaturation of 1.0, and the step edges displayed an average step velocity of  $5.7 \text{ nms}^{-1} \pm 1.3 \text{ nms}^{-1}$ . The short sequence of images captured during this experiment is available both as an .avi file on the attached CD (filename lysozyme2), and on the departmental website (Chen, 2004).

Throughout imaging, numerous small particles were seen to land on the crystal surface and become incorporated into the lattice. These entities ranged from just a few tens of nanometers to approximately one micrometer in diameter. Almost without exception, the incorporation of these particles led to the formation of a similarly sized inclusion in the crystal surface, which persisted upon growth of additional layers. It is difficult to say with any certainty whether these entities were minute liquid-protein droplets (the precursor of microcrystal formation), or foreign particles/aggregated solute molecules. However, the latter seems more likely as the particle incorporation did lead to the formation of inclusions, which clearly acted as defects during subsequent crystal

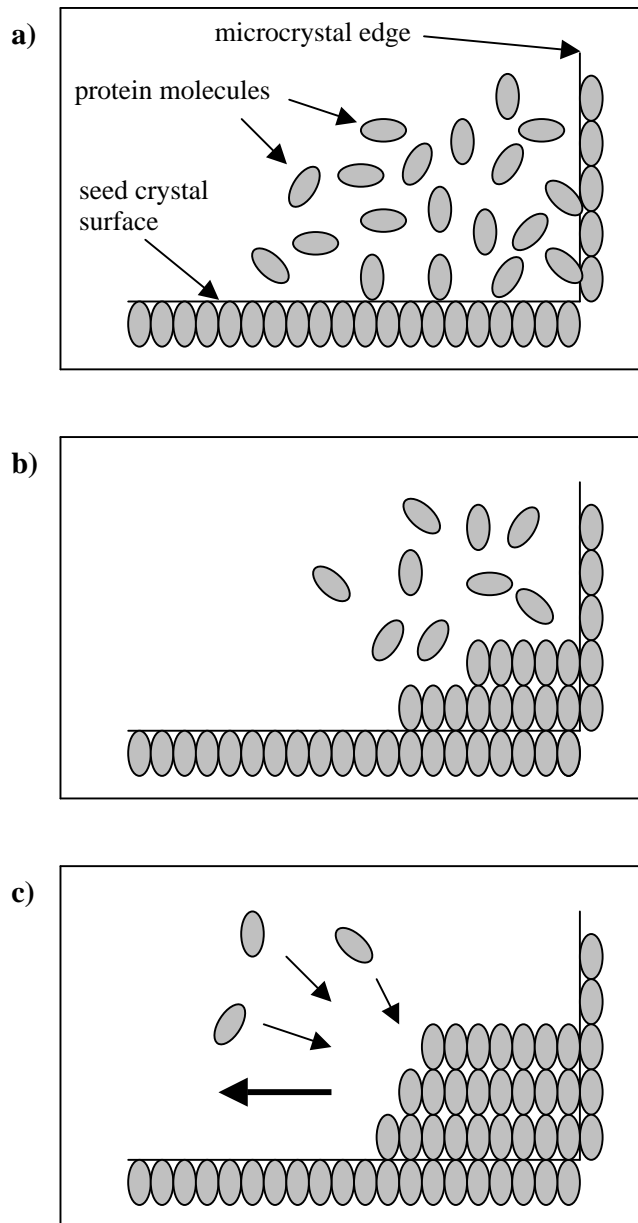


**Figure 3.7.** (a) A large aggregate of molecules adsorb to the surface of the bulk crystal and edge of the microcrystal. (b) Guided by the lattices with which they are in contact, a congruent arrangement of molecules begins to form. (c) This in turn promotes the molecules around them to do likewise, thus forming the rapidly developing multilayer stacks observed in figure 3.6.

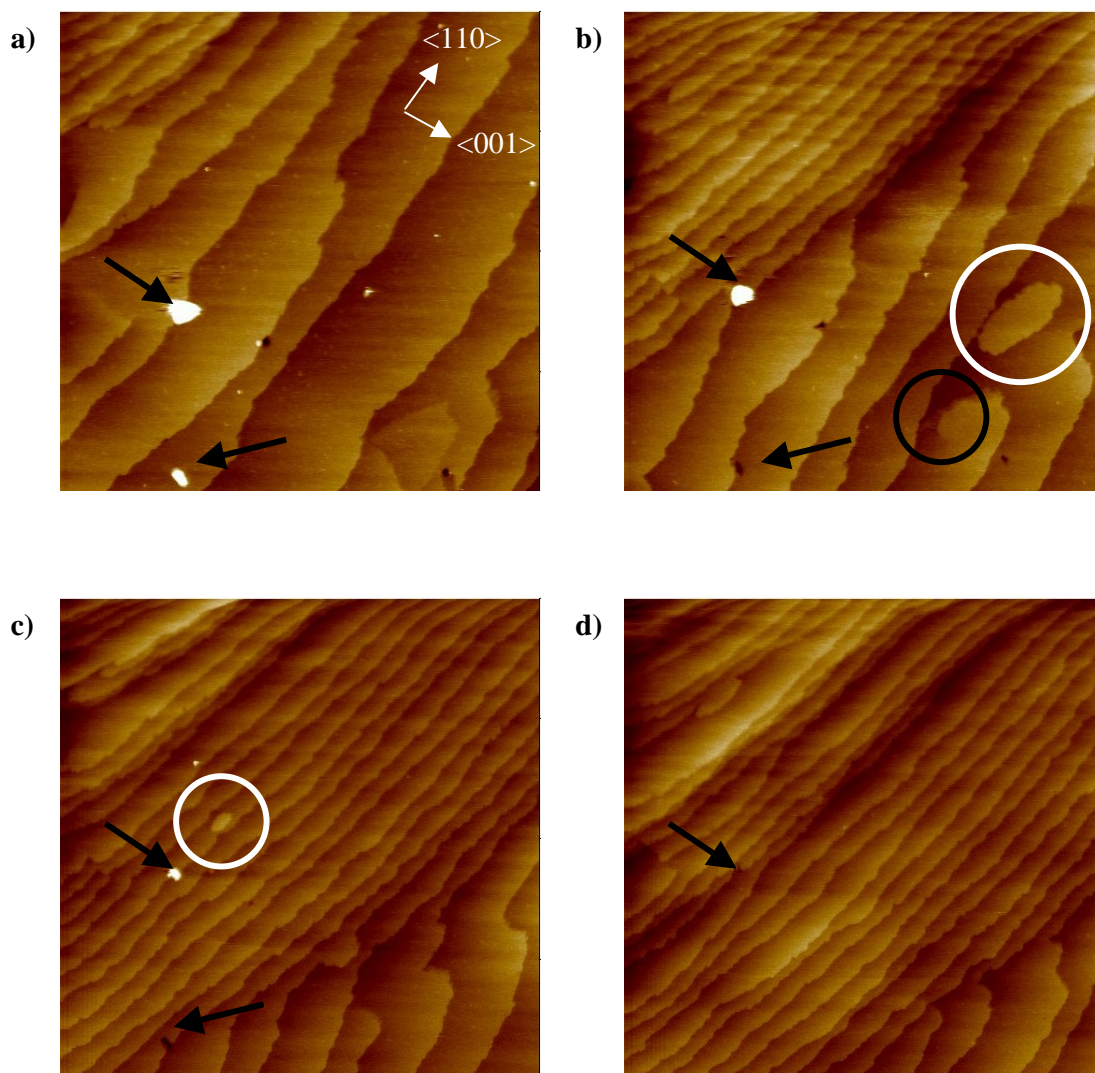


**Figure 3.8.** Topographical images charting the development of a  $10 \mu\text{m} \times 10 \mu\text{m}$  section of a seed crystal at  $\sigma = 1.0$ . In image (a) time  $t = 0$  secs, (b)  $t = 910$  secs, (c)  $t = 1511$  secs, (d)  $t = 1768$  secs. The incorporation of two small particles into the lattice and subsequent formation of inclusions is highlighted with black arrows. Screw dislocations and two-dimensional nucleation islands were observed throughout, as illustrated in images (b & c) with the white and black circles respectively. z-range throughout, 50 nm.

growth. Additionally, the particles displayed no definite morphology and never appeared to develop on the surface of the seed crystal. 2D nucleation islands were clearly observable throughout the experiment. Growth also occurred from spiral dislocations that, as observed with the holes formed after particle incorporation, persisted even after growth of additional layers.

### 3.3.2.2 *Medium supersaturation* ( $0.99 > \sigma > 0.8$ )

The multiple growth mechanisms employed by the developing seed crystal at high supersaturations continued even when the imaging medium was altered to a lower value of supersaturation. A good example of this is presented in figure 3.9. This experiment was conducted with an imaging medium of  $\sigma = 0.89$

Image 3.9(a) displays three single turn screw dislocations, of both right- and left-handed orientation. What is of note here is the existence of a 2D nucleation island in addition to the dislocations. Mirroring the observations of the experiments carried out at higher levels of supersaturation, this crystal also appears to be undergoing growth by two separate and distinct mechanisms during an experiment on a single crystal, at a defined level of supersaturation – in this case screw dislocations and two-dimensional nucleation.

Additionally it is clear that this area, and thus presumably the entire crystal face, is littered with a number of planar defects known as stacking faults. Examples of such faults are clearly illustrated in the deflection image contained in figure 3.9(b). Stacking faults are severe defects that arise from partial unit cell displacements of an entire row of unit cells. Such displacements can affect many molecules in the vicinity of the fault and will often extend through many hundreds of layers of the crystal. Because of this, these particularly severe dislocations can have a significant negative impact on the long-range order of the crystal (McPherson, 1999).

This remarkable ability of stacking faults to propagate throughout growth layers in the normal direction is illustrated by the consecutive images displayed in figure 3.9(c) and (d). A macrostep, which is a rapidly moving ‘wave’ of bunched steps whose existence are believed to be a consequence of three-dimensional nucleation somewhere on the crystal surface and physical fluctuations in the growth medium, becomes apparent in bottom left hand corner of the image and subsequently moves rapidly across the crystal face to the top right. This macrostep, which is made up of many tens of

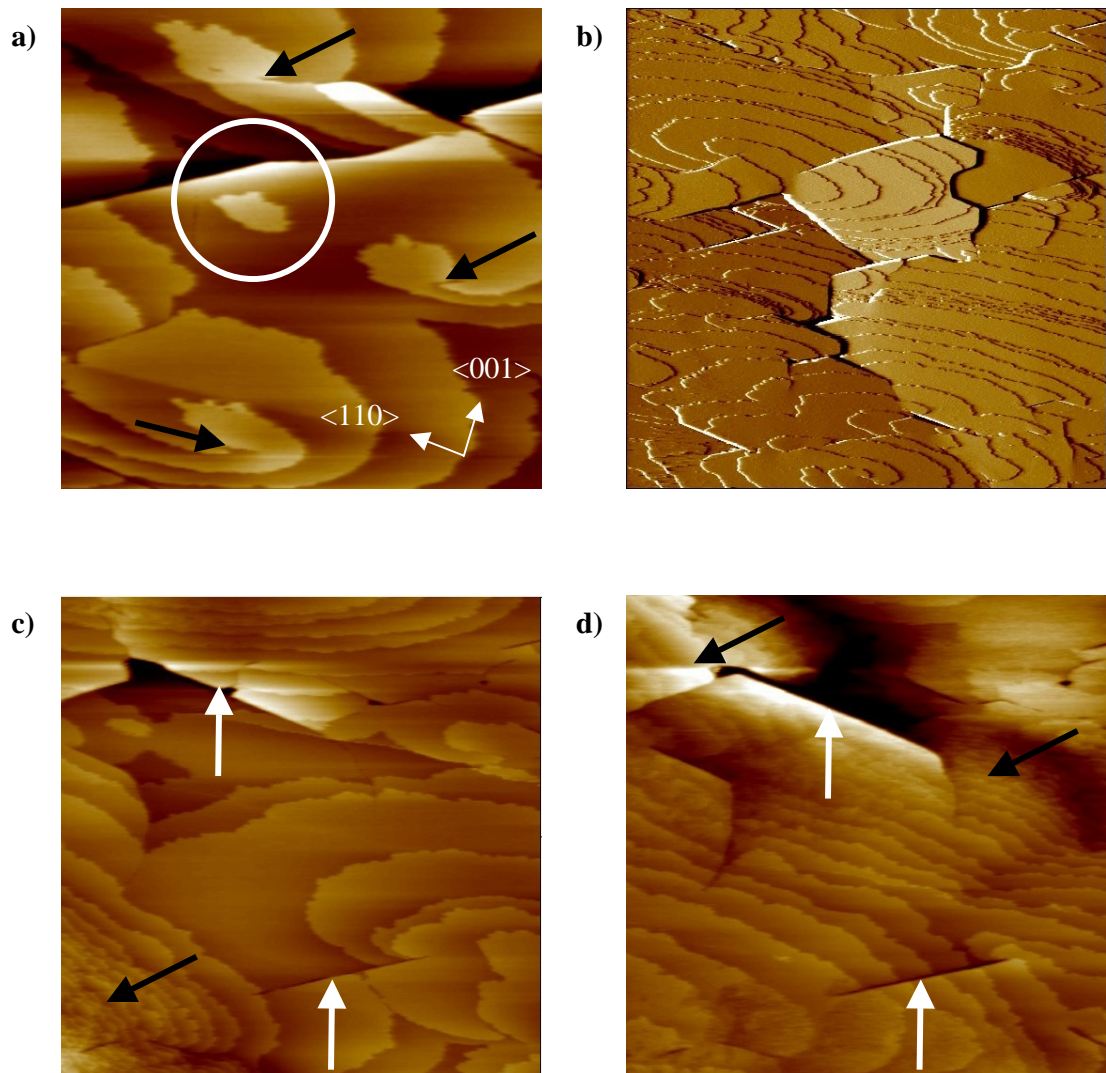


**Figure 3.9.** Images recorded at  $\sigma = 0.89$ . Screw dislocations and growth islands are plainly visible in (a), along with numerous stacking faults in the deflection image contained in (b). (c & d) are consecutive topography images illustrating the appearance of a macrostep (black arrows) in the bottom left hand corner of (c). This step rapidly engulfs the surface, but is unable to annihilate the numerous stacking faults present (white arrows). Scan sizes (a)  $3 \mu\text{m} \times 3 \mu\text{m}$ , (b)  $10 \mu\text{m} \times 10 \mu\text{m}$ , (c & d)  $5 \mu\text{m} \times 5 \mu\text{m}$ . z-ranges, (a) 50 nm, (c & d) 100 nm.

growth layers, is forced to flow around the stacking faults present on the surface of the crystal. As the macrostep passes, it becomes clear that the stacking fault has propagated through the layers in the normal direction, thus ‘surviving’ as a surface feature rather than being incorporated into the crystal lattice.

### 3.3.2.3 Low supersaturation ( $\sigma < 0.79$ )

It was only as the supersaturation of the imaging medium was lowered towards zero that the growth behaviour of the seed crystals became more predictable. Images contained in figure 3.10 are typical of those captured at reduced supersaturation, in this case  $\sigma = 0.67$ .

It immediately became obvious that a significantly lower quantity of step edges were present on the crystal surfaces, which in turn were developing tangentially at a lower rate – in this case at an average of  $3.3 \text{ nms}^{-1} \pm 1.2 \text{ nms}^{-1}$ . At no time during imaging at these lower levels of supersaturation were we able to directly observe either 2D nucleation islands or screw dislocations as a source of the steps. Neither can be discounted, and it is quite feasible that a small quantity of dislocations and sporadic 2D nucleation were occurring in tandem to generate growth normal to the surface.

Growth was found to come to halt at approximately  $\sigma = 0.5$ . This value was determined when three consecutive images did not display any significant change with time. Seed crystals in solutions below this value of supersaturation underwent dissolution (data not shown).

The (110) face of tetragonal lysozyme crystals has been shown here developing by utilizing three quite distinct mechanisms, over a relatively narrow range of supersaturation. These findings are in sharp contrast to recent reports that specified a complete lack of screw dislocations throughout their experiments (Rong *et al.*, 2000; Wiechmann *et al.*, 2001; Yoshizaki *et al.*, 2001; Wiechmann, 2002). Indeed, the report of Rong *et al.* emphasized the complete dominance, without exception, of two-dimensional nucleation at all levels of supersaturation. Indeed, 2D nucleation is generally accepted to be the preferred growth mechanism of numerous protein crystals, including lysozyme, but a complete absence of dislocations is rare.

The formation of screw dislocations and stacking faults in macromolecular

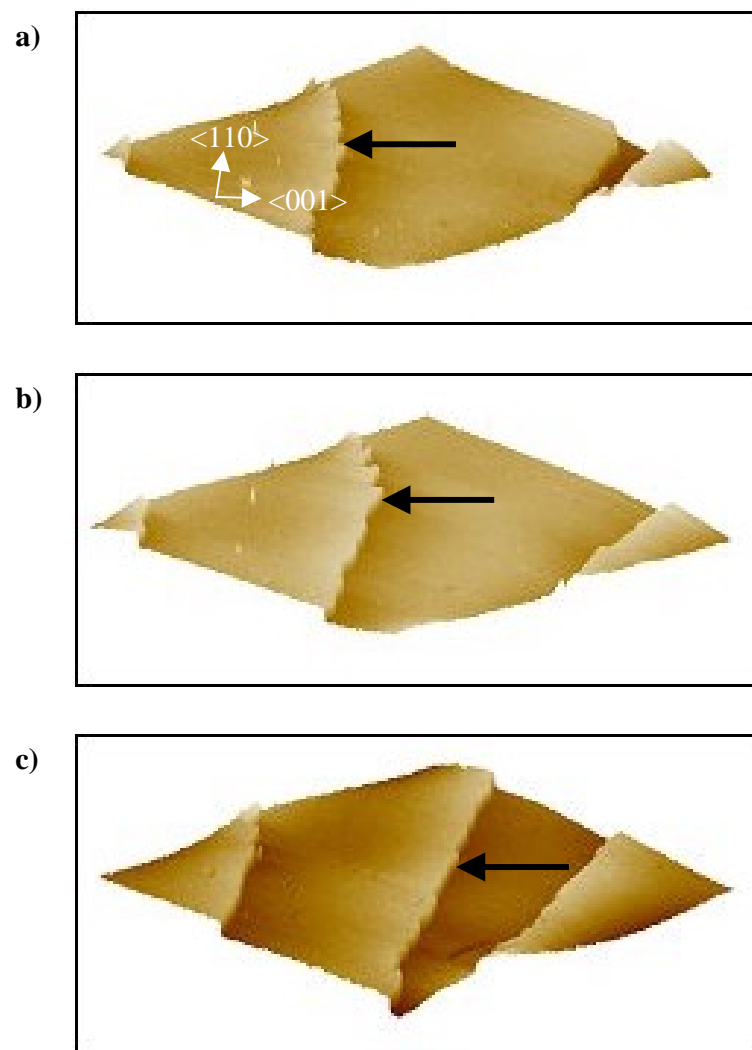


**Figure 3.10.** Consecutive 3D topography images a seed crystal at a relatively low supersaturation,  $\sigma = 0.67$ . Scan sizes  $5 \mu\text{m} \times 5 \mu\text{m}$ , step heights 5-6 nm.

crystals has previously been linked to the mechanical properties of the specific crystal. For example, the incorporation of small microcrystals (<10  $\mu\text{m}$ ) into the lattice of canavalin and thaumatin crystals resulted in the formation of stacking faults and the appearance of dislocations (Malkin *et al.*, 1996a; Malkin *et al.*, 1996b). In contrast, both growth and etching experiments performed on the surface of catalase crystals have illustrated heavy microcrystal incorporation without the resulting defect formation – in fact, no screw dislocations or stacking faults have ever been observed on the surface of catalase crystals (Malkin *et al.*, 1997). This has been attributed to the seemingly more ‘elastic’ mechanical properties displayed by the crystal lattice, which permits the incorporation of misaligned microcrystals without suffering damage in the form of defects. However, there is also evidence suggesting such ‘elastic’ or non-rigorous crystal lattices have a deleterious effect on the diffraction properties of the crystal. This is discussed in further detail in chapter 5 of this thesis.

However, from both the AFM results presented here and elsewhere it is clear that the lysozyme crystal lattice can suffer such damage, (Durbin *et al.*, 1993; Konnert *et al.*, 1994; McPherson, 1999; McPherson *et al.*, 2000). However, defects were not always observed on the crystal surfaces. It is possible that the lysozyme crystal displays similar mechanical properties to thaumatin and canavalin crystals in that the incorporation of foreign particles and microcrystals into its lattice may make a significant contribution to the formation of dislocations and stacking faults on the surface. Inevitably, 2D nucleation would become the preferred mechanism of growth in the absence of such particles – a theory seemingly borne out by the observations reported by Rong *et al.*

### 3.3.3 Molecular-resolution features on the crystal surfaces

The AFM boasts an exceptionally high signal-to-noise ratio that, in combination with the relatively large dimensions of protein molecules (in the case of lysozyme, ~2.8 nm), permits the molecular resolution investigations of protein crystals in both the lateral and vertical directions. However obtaining such data, particularly in the lateral

direction, is by no means a trivial exercise even with a relatively robust crystal such as lysozyme.

This section is split into two parts. The first considers the step heights observed on both the (110) and (101) surfaces, and what details these measurements can provide concerning the molecular growth mechanisms that occur on the surface of the crystal. The second section presents molecular resolution images obtained on both faces of the crystal, and discusses the practical considerations of obtaining such images and how they can subsequently be correlated to elementary crystallographic data.

### 3.3.3.1 Step edge heights

Figure 3.11 contains a typical section analysis of a step edge from both the (110) and (101) faces of a tetragonal lysozyme crystal. Measurements were obtained from twenty single, unrelated growth steps on each face. The average heights were - (110),  $5.3 \text{ nm} \pm 0.5 \text{ nm}$  and (101),  $3.6 \text{ nm} \pm 0.5 \text{ nm}$ .

The figure of  $\sim 5.3 \text{ nm}$  on the (110) surface indicates that growth layers on this face are of bimolecular height. A number of previous AFM studies on the (110) face of tetragonal lysozyme crystals have also made this assertion (Durbin and Carlson, 1992; Durbin *et al.*, 1993; Konnert *et al.*, 1994; Li *et al.*, 1999a; Rong *et al.*, 2000), which indicates one of two processes must be occurring: (i) either there is some element of monomer association in the bulk growth solution to form the growth unit that subsequently adds to the growing crystal or (ii) growth occurs by rapid monomer association on the crystal surface.

Numerous studies have been performed on this system to unravel the molecular growth mechanisms involved, with the majority favouring the former process. Several theoretical studies based on the periodic bond-chain (PBC) theory of Hartman & Perdok (Hartman and Perdok, 1955) have indicated that growth proceeds by the addition of units pre-formed in solution of at least a tetramer in size (Nadarajah and Pusey, 1996; Nadarajah *et al.*, 1997; Strom and Bennema, 1997a; Strom and Bennema, 1997b). Experimental findings have also repeatedly shown the presence of associated species in solution (Wilson *et al.*, 1993; Schaper *et al.*, 1997; Michinomae *et al.*, 1999). A series of comprehensive AFM and growth rate studies carried out in 1999 specified a complete lack of single molecule attachment throughout (Li *et al.*, 1999a) and these results, in

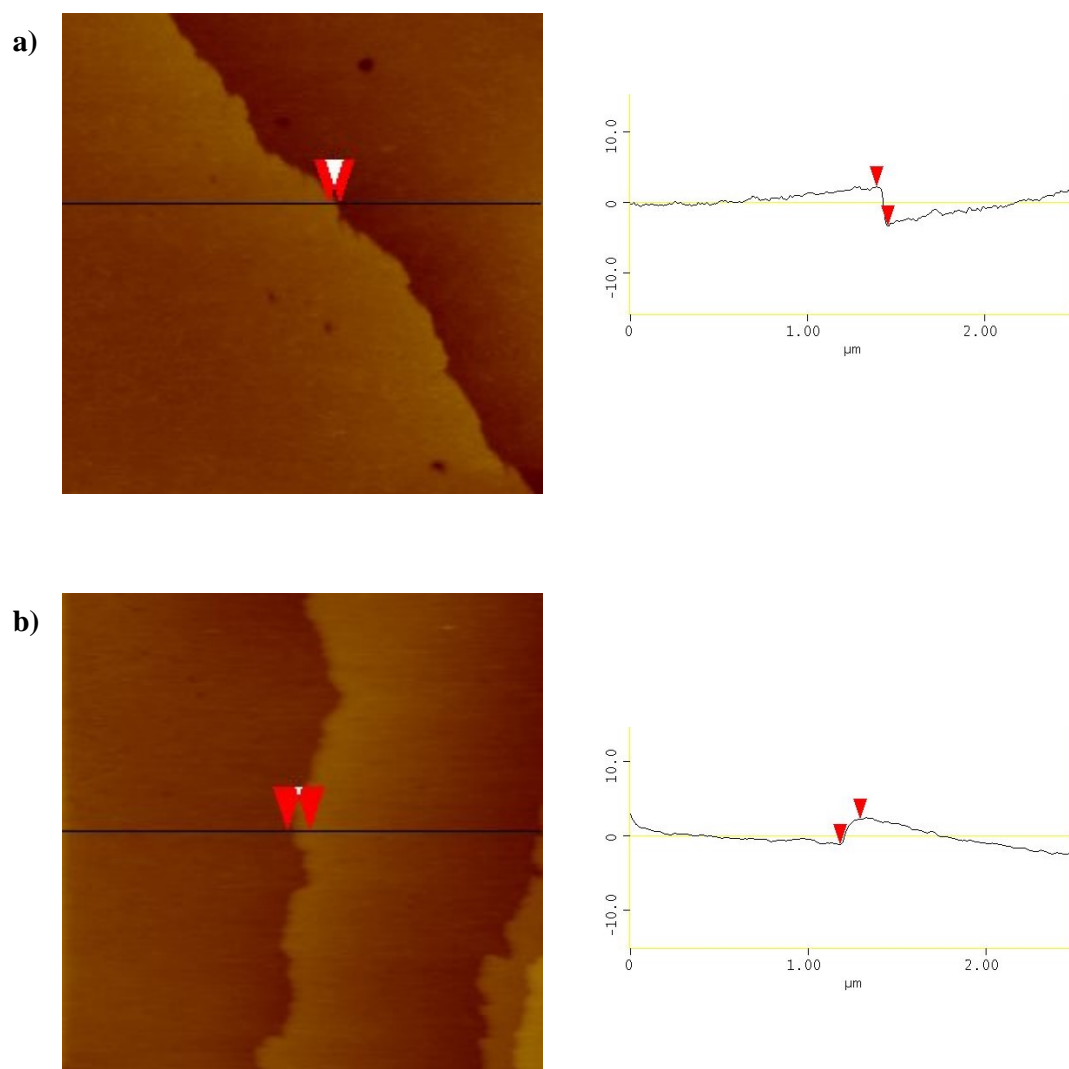


**Figure 3.11.** Step height measurements on the two faces of the tetragonal lysozyme crystal. **(a)** A  $2.5\ \mu\text{m} \times 2.5\ \mu\text{m}$  image of the (110) face, with a single step of height 5.6 nm. **(b)**  $2.5\ \mu\text{m} \times 2.5\ \mu\text{m}$  image of the (101) face, with a single step of height 3.4 nm.

combination with the results from three other related reports (Forsythe *et al.*, 1999a; Li *et al.*, 1999b; Li *et al.*, 1999c) and various theoretical studies, were used to model the molecular mechanisms utilized in the growth of both the (110) and (101) faces of tetragonal lysozyme crystals. Simplified versions of these models are illustrated schematically in figure 3.12.

However, the recent report of Wiechmann *et al.* (Wiechmann *et al.*, 2001) described the appearance of single molecule step heights on the (110) face during rapid raster scanning. As such, they cannot be completely discounted as growth units. It does seem, however, to be an extremely rare occurrence, indicating the preferred growth unit size is a tetramer or larger as suggested by the results presented here and elsewhere.

As the majority of evidence points to tetrameric building blocks acting as the preferred growth unit of the (110), it is unlikely that growth of the (101) will be different. Indeed, the results obtained for this face also correlate well to the model presented in figure 3.12. The average step height observed was 3.6 nm, which corresponds accurately to the inter-planar distance of 3.4 nm on this face (Li *et al.*, 1999c; Nakada *et al.*, 1999).

### 3.3.3.2 Molecular resolution imaging

There are a number of additional considerations that must be taken into account when attempting to obtain molecular resolution images of a protein crystal. Firstly, it is important to carry out experiments at low levels of supersaturation to limit the movement of steps edges over the face of interest. If the crystal is growing rapidly, there is a good chance that obtaining molecular-resolution data will be difficult, if not impossible. An example of this is shown in figure 3.13(a)

Secondly, the smaller scan size required during such experiments is more likely to cause damage to the crystal surface, even with relatively robust crystals such as lysozyme. This is due to the inevitable increase in tip-sample contact time that subsequently results in an increase in energy imparted by the tip over that small sample area. As such, it is extremely important to operate at the minimum possible force at all times during such experiments. However, this in itself can sometimes be problematic. Figure 3.13(b) contains a typical single-point force-displacement curve taken on the (110) face of a tetragonal lysozyme crystal. The ideal imaging force for such experiments is  $< 1$  nN, however at this low force there is clearly a significant level of

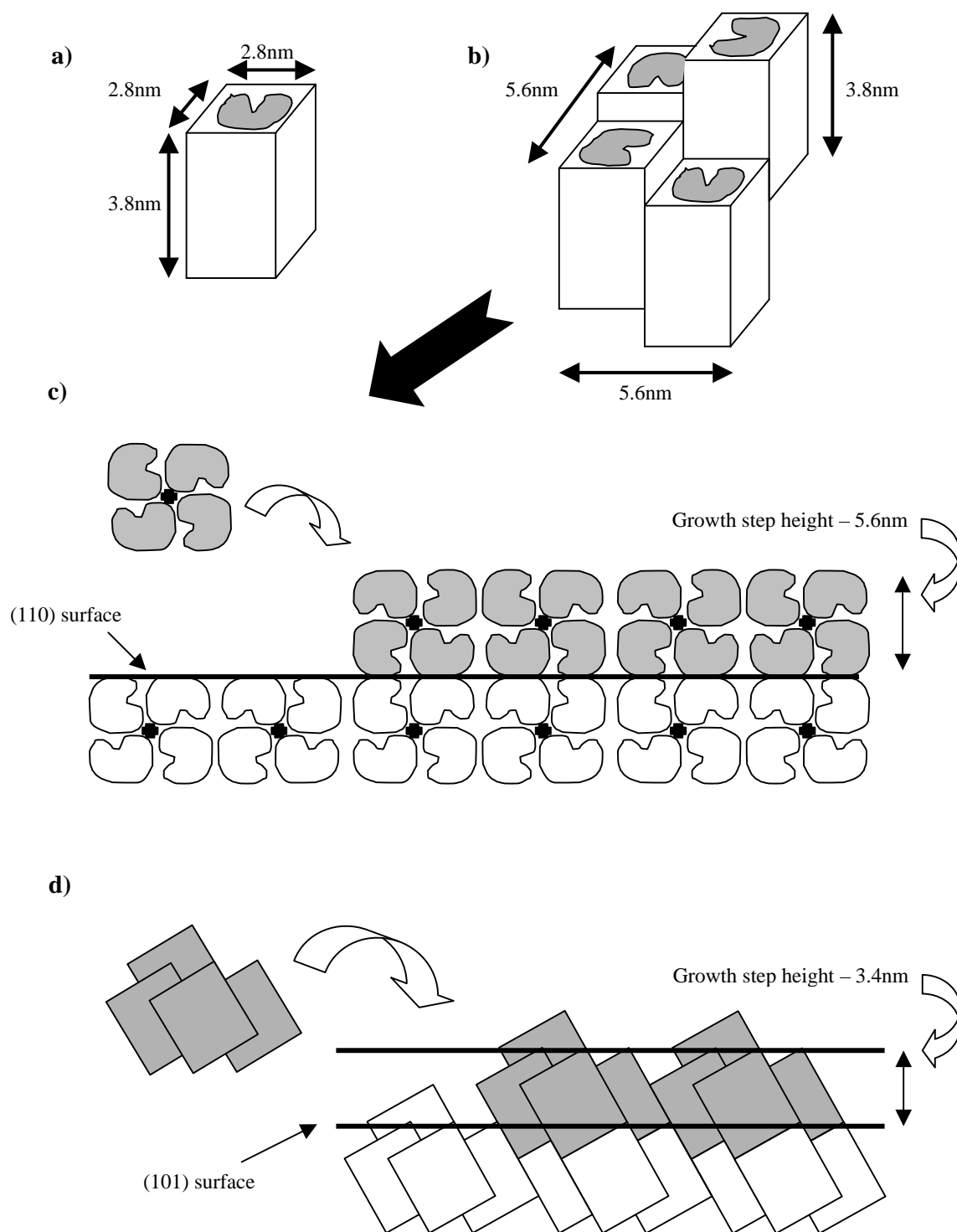


**Figure 3.12.** (a) The dimensions of the asymmetric unit in the tetragonal crystal. (b) The four molecule helical growth unit and its incorporation into the (110) face (c) and the (101) face (d). Adapted from Li *et al.*, 1999a & Li *et al.*, 1999c.

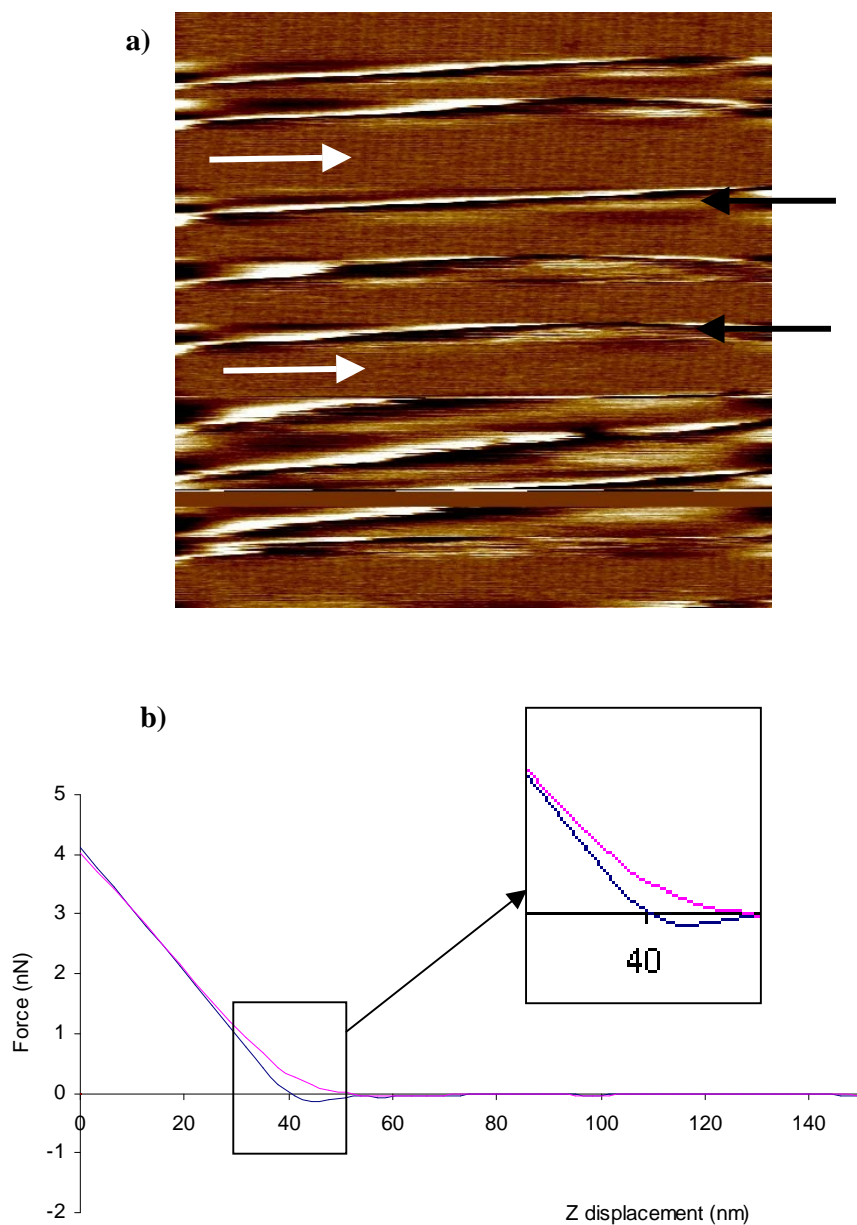


**Figure 3.13.** (a) A 200 nm x 200 nm scan of the (110) face of a lysozyme crystal. The movement of steps across the crystal surface repeatedly disturbs the scanning, leading the areas of the surface at molecular resolution (white arrows) and areas of noise (black arrows). (b) A single-point force curve on the same crystal surface. The repulsive forces present between tip and sample are clearly observable.

repulsion present between the tip and sample. In liquid, the  $\text{Si}_3\text{N}_4$  AFM tip exhibits an isoelectric point (pI) of approximately pH 6 (Rossell *et al.*, 2003) and therefore at pH 4.5 the resulting charge on the tip is positive. The surface of the crystal will also exhibit a significant positive charge as the lysozyme molecule has a pI of approximately pH 11. Hence these two positively charged surfaces electrostatically repel one another as observed in the force-displacement curve presented in figure 3.13(b).

Such interactions can often be advantageous when imaging biomolecules, as careful manipulation of the imaging conditions can alter the interactions between tip and sample, subsequently improving imaging resolution and thus the quality and quantity of information contained within the image (Muller *et al.*, 1999; Scheuring *et al.*, 2001; Rossell *et al.*, 2003). Unfortunately however, manipulating the imaging conditions in this way is generally not possible with 3D protein crystals. The reason for this is that crystals tend to crack when moved into a solution exhibiting an alternative salt concentration to the crystals original mother liquor (Kuznetsov *et al.*, 2001).

Whilst there were a number of difficulties involved in obtaining molecular resolution data, it was achieved on both faces of the crystal. Figures 3.14 & 3.15 contain images obtained from the (101) and (110) surfaces respectively. The periodic nature of the crystal surfaces permitted them to be analyzed and filtered using power spectral density (PSD) plots and 2D fast fourier transformations (FFT).

PSD plots are able to identify periodic surface features by essentially calculating which wavelengths in an image impart the greatest influence or ‘power’ to the surface’s topography. An example of this feature is displayed in figure 3.14. Figure 3.14(b) contains a PSD plot of the raw image contained in 3.14(a). Such tapered PSD plots are characteristic of flat, isotropic surfaces. However, there is a cluster of spikes at a wavelength corresponding to approximately 8nm, a figure that is almost precisely the expected periodicity of the (101) face of the tetragonal lysozyme crystal (Li *et al.*, 1999c).

The clarity of the periodic features is tempered by the influence of both high frequency electrical noise and lower-frequency mechanical noise, both of which are inherent to all higher magnification scans performed under such conditions. However, by using the spectrum 2D function to transform the image into a 2D FFT, the frequencies corresponding to the noise in the image can be removed whilst retaining the frequencies responsible for the periodic features of interest. After selecting the desired

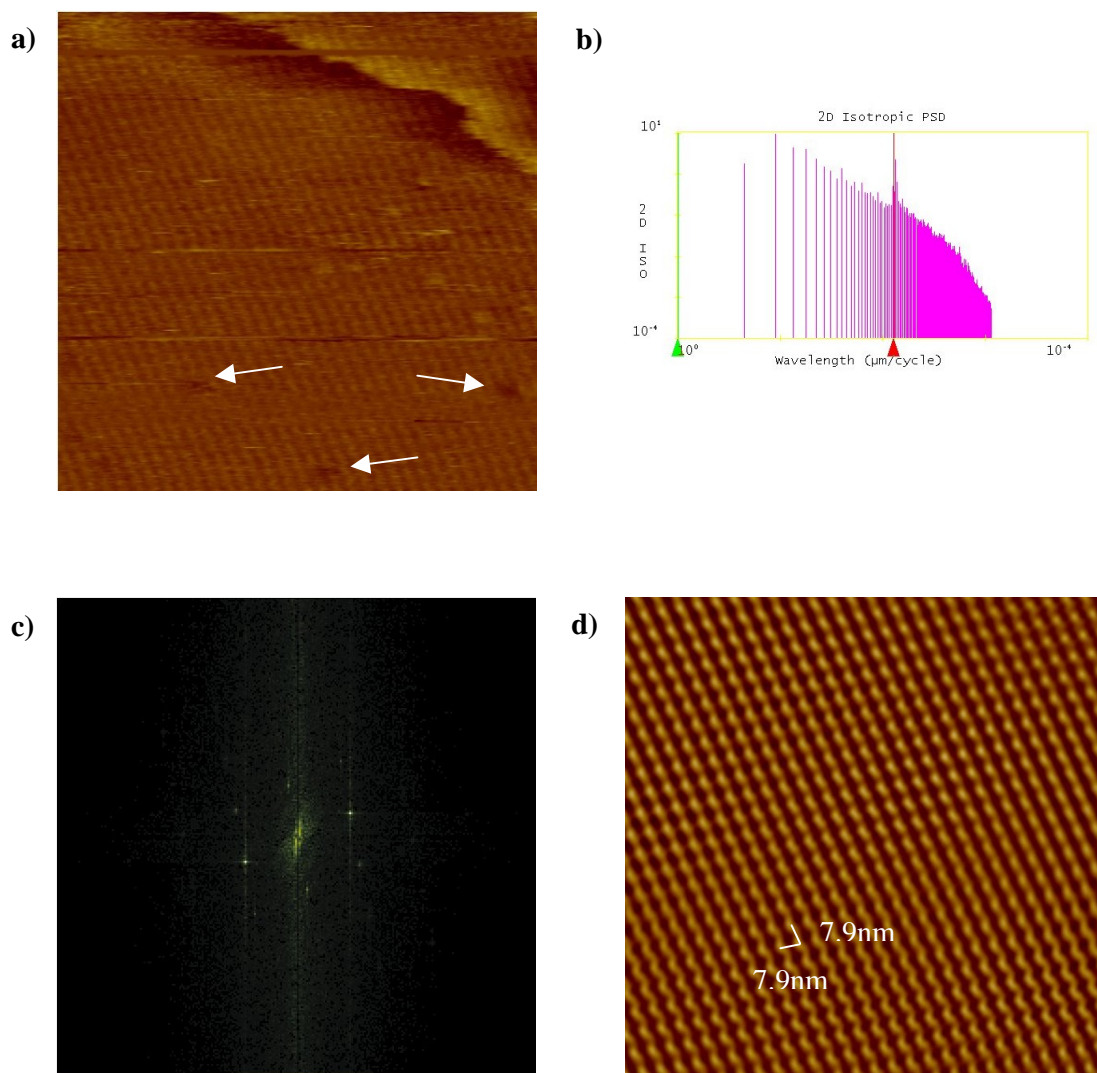


**Figure 3.14.** (a) A 250 nm x 250 nm scan of the (101) face. Surface periodicity and single defects are evident, even in this unfiltered image. (b) The power spectral density plot of this image, showing a clear set of spikes around the 8 nm region. (c) The fourier transform of the raw image, and (d) a 200 nm x 200 nm section of the filtered image clearly displaying periodicities of 7.9 nm x 7.9 nm. The z-ranges in (a) & (d) are 10 nm and 1 nm respectively.

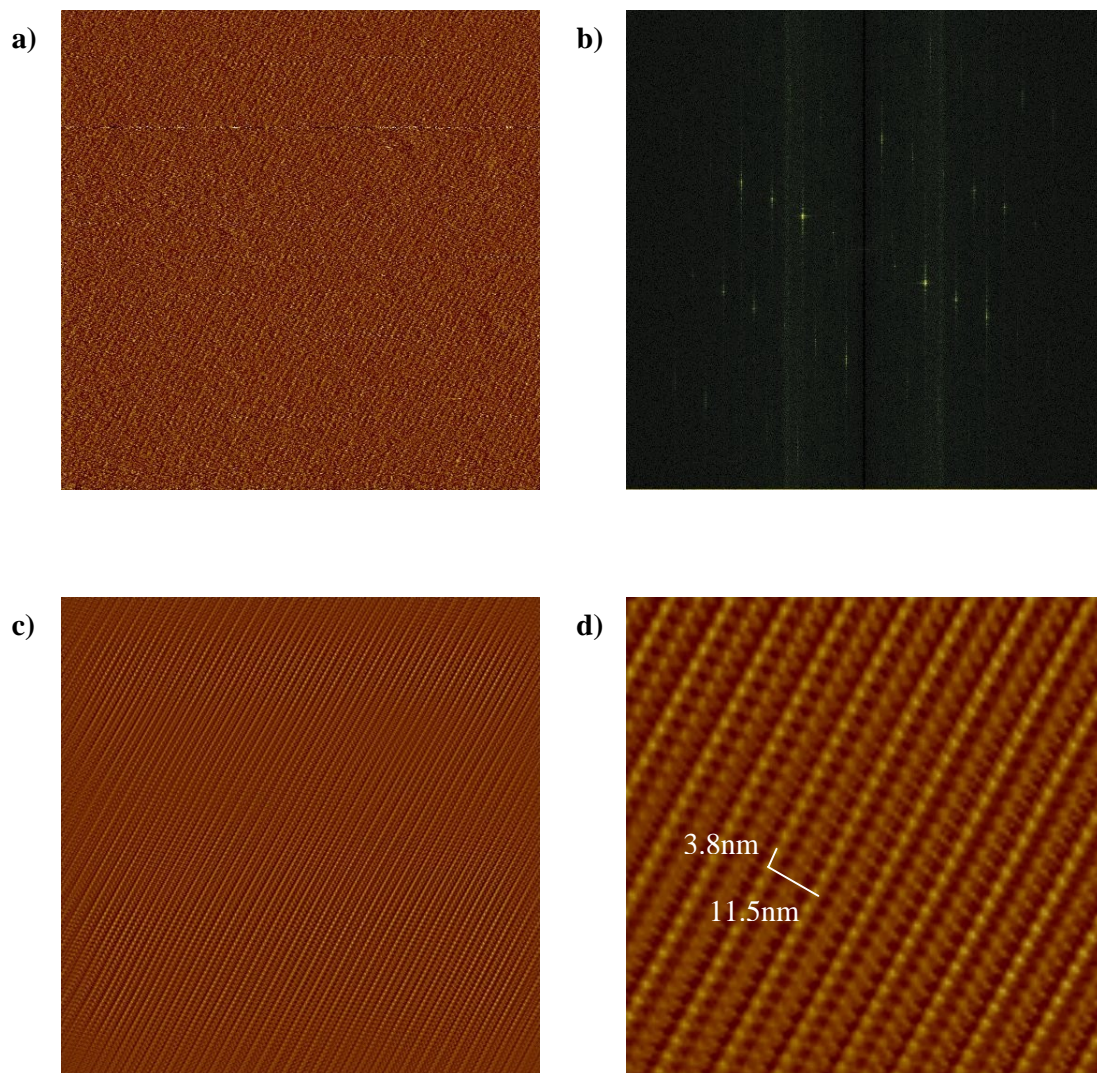


**Figure 3.15.** (a) A 420 nm x 420 nm deflection image of the (110) face. (b) The Fourier transform of the raw image, and (c) the corresponding filtered image. (d) contains a 100 nm x 100 nm section of the filtered image, clearly displaying periodicities of approximately 11.5 nm & 3.8 nm.

frequencies, the image is reconstructed, yielding a significantly improved version as illustrated in figure 3.14(d). The same process was performed for molecular resolution images captured on the (110) face, and the original and fourier filtered images are shown in figure 3.15.

The filtered images in figures 3.14 and 3.15 display an accurate representation of the respective surfaces of the tetragonal lysozyme crystal. The periodicity observed on the (110) face conforms precisely to the 2D unit cell dimensions displayed by this face (11.5 nm x 3.8 nm). Additionally, the 2D unit cell dimensions on the (101) face of 7.9 nm x 7.9 nm are reproduced in the AFM scans, which to the author's knowledge are the most detailed and accurate AFM images reported for this surface.

The images obtained at molecular resolution also tie in well to the molecular mechanisms modeled in figure 3.12. It is clear that if the models are accurate, then the (101) face will be significantly rougher than the (110). This appeared to be the case, as the periodic features observable on the topographic images recorded of the (110) surface were barely visible prior to filtering, even at a z-range as little as 2 nm (data not shown). However, the periodic features on the (101) face were clearly evident, even at a z-range of 10 nm (see figure 3.14(a)).

### 3.4 Conclusions

With the overall aim of developing the experimental protocols necessary to carry out AFM investigations of fragile macromolecular crystals, the model protein crystal lysozyme has been grown and studied using *in situ* AFM.

Initially, a series of optimization experiments were carried out to identify the most reliable methods for the growth and immobilization of lysozyme seed crystals for use in AFM experiments. Batch crystallization was identified as being the most robust and repeatable method for the growth of the crystals, whilst the preferred method for the immobilization of crystals onto a substrate material was by direct nucleation onto electron microscopy grids.

Using these experimental protocols, the (110) and (101) faces of the tetragonal lysozyme crystal seeds were investigated at both a microscopic and nanoscopic level using *in situ* AFM. Initially, the (110) surface was imaged at a range of supersaturations: high ( $\sigma > 1.0$ ), medium ( $0.99 > \sigma > 0.8$ ) and low ( $\sigma < 0.79$ ). As expected, lowering the value of supersaturation progressively lowered both the quantity and tangential growth velocity of the steps in the  $\langle 001 \rangle$  direction from  $11.0 \text{ nms}^{-1} \pm 1.6 \text{ nms}^{-1}$  at  $\sigma = 1.6$ , to  $3.3 \text{ nms}^{-1} \pm 1.2 \text{ nms}^{-1}$  at  $\sigma = 0.67$ . Contrary to a number of recent reports, the generation of the step edges on the (110) surface was apparently a consequence of three distinct growth mechanisms, which were occasionally observed operating concurrently – 3D nucleation, 2D nucleation and screw dislocation. During one experiment, multilayered stacks were clearly being promoted by the edges of a microcrystal that has been adsorbed to the surface of the larger seed crystal, a mechanistic observation never previously reported for any crystal system.

A number of molecular resolution features were also obtained using AFM data. The step edge heights for both the (110) and (101) surfaces were measured to be  $5.3 \text{ nm} \pm 0.5 \text{ nm}$  and  $3.6 \text{ nm} \pm 0.5 \text{ nm}$  respectively, indicating the growth units for both faces are dimeric in height, rather than monomeric, an observation in keeping with the generally accepted growth model for the tetragonal lysozyme crystal.

With careful control of the AFM imaging conditions, it was also possible to obtain molecular resolution data for both faces of the crystal. After performing 2D Fast Fourier Transformations to remove electrical and mechanical noise inherent to high

resolution scans, the periodic features on the (110) face were clearly shown to be 11.5 nm and 3.8 nm, with the (101) face displaying periodicities of 7.9 nm and 7.9 nm. These data conform precisely to the known 2D unit cell measurements for the respective crystallographic faces.

## Chapter

## 4

**Polymorphism in lysozyme crystallization –  
An AFM study**

---

The existence of numerous polymorphs of the protein crystal lysozyme is well documented, with the tetragonal and orthorhombic forms having been studied in some depth with numerous techniques. However, the remaining crystalline forms are not so well understood. One such crystal is the monoclinic polymorph, which has received comparatively little attention. Using *in situ* AFM, we have investigated the  $(10\bar{1})$  face of this crystal on both a microscopic and nanoscopic level.

Imaging of the  $(10\bar{1})$  surface at high protein and precipitant concentrations revealed densely packed step edges, the majority of which seemed to have been generated through the presence of numerous simple and complex screw dislocations. Indeed, 2D nucleation was never observed on this surface, echoing previous reports. We believe this is a consequence of both the particularly tightly packed crystal lattice displayed by the monoclinic polymorph, and relatively small interplanar distance of the  $(10\bar{1})$  surface ( $d_{10\bar{1}} = 2.5$  nm). Upon lowering the protein and precipitant concentrations, we were able to observe characteristic roughening of steps in the  $\langle 010 \rangle$  direction and achieve molecular resolution images of the surface. Such images highlighted periodicities of 6.6 nm and 3.7 nm, which correspond well to the 2D unit cell dimensions of this face of the crystal.

Comparing these data with those collected from the tetragonal form has allowed us to unambiguously distinguish between crystalline polymorphs of the same protein molecule.

---

## 4.1 Introduction

### 4.1.1 Polymorphism

As discussed in chapter 3 of this thesis, the contacts formed between macromolecules within biological crystals can be tenuous as a consequence of both the large molecular weights generally exhibited by macromolecules and the comparatively small quantity of contacts that exist between them (McPherson, 1999). Inevitably, this means that the alteration of the chemical or physical environment surrounding such molecules can dramatically affect how they pack together within a crystal, thus resulting in many biological macromolecules exhibiting significant levels of polymorphism.

Polymorphism, as briefly discussed in the introduction to this thesis, occurs when the solute of interest is able to adopt more than one internal crystal structure. This is a particularly important consideration with materials utilized in drug formulations, as vital pharmacological factors such as bioavailability and dissolution rates can be heavily dependent on the form exhibited by the crystalline solute molecules.

Factors important in crystalline pharmaceutical materials such as dissolution rate generally hold little importance when considering crystals built of biological macromolecules. However, the quantity and quality of structural information available from these can be polymorph-dependent. An excellent example of this is illustrated by the crystallization of satellite tobacco mosaic virus (STMV). STMV produces three major crystal forms from very similar conditions – orthorhombic, monoclinic and cubic. However, these forms all exhibit a vast range of diffraction properties, with the cubic form diffracting to a relatively low resolution of approximately 6 Å, whilst the orthorhombic form diffracts X-rays to a resolution of almost 1.7 Å (McPherson, 1999).

### 4.1.2 Lysozyme polymorphs

As mentioned above, practically all macromolecular crystals exhibit polymorphism to a certain degree. Lysozyme is one such macromolecule, and it has

been reported to exhibit six crystalline modifications or polymorphs – these polymorphs are tetragonal (the form studied in chapter 3 of this thesis), orthorhombic, monoclinic, trigonal, triclinic and hexagonal (Yaminsky *et al.*, 2002).

However, the most remarkable aspect of lysozyme polymorphism is the huge range of conditions under which lysozyme crystals will grow. Lysozyme crystals have been shown to form from (i) an unusually large range of temperatures (ranging from 4 °C to ~50 °C) (Jolles and Berthou, 1972; Berthou and Jolles, 1978; Forsythe *et al.*, 1999b), (ii) from a vast range of buffers at different pHs (Forsythe *et al.*, 1999b), and (iii) from a series of monovalent anions (Ries-Kautt and Ducruix, 1989; Vaney *et al.*, 2001) to name but a few. Additionally, the crystals grown from these exhaustive experiments almost always diffracted to a high resolution.

The tetragonal, orthorhombic and monoclinic polymorphs are undoubtedly the most common forms of the lysozyme crystal. As discussed at length in chapter 3, the tetragonal form has received most attention and, from a biological crystal growth point of view, is generally seen as the ‘model’ protein crystal. The orthorhombic form has also been studied in some detail, with a number of AFM-based studies having been reported (Rashkovich *et al.*, 1998; Chernov *et al.*, 1999; Rashkovich *et al.*, 2001; Matsuzuki *et al.*, 2002; Yaminsky *et al.*, 2002). The monoclinic form has not, however, received such attention, with only two dedicated crystal growth related studies having been reported (Hondoh *et al.*, 2001; Rashkovich *et al.*, 2002). As such, the monoclinic form of the lysozyme crystal is the main subject of this chapter.

#### 4.1.3 Monoclinic lysozyme

To the author’s knowledge, lysozyme crystals grown in the monoclinic form were first reported in the 1950s by Francis Crick (Crick, 1953). Preliminary X-ray studies revealed the unit cell dimensions as being  $a = 28.0$ ,  $b = 62.5$ ,  $c = 60.9$  Å, with two molecules in the asymmetric unit and four molecules in the unit cell. These data were subsequently proved accurate by a handful of atomic resolution X-ray studies performed on the monoclinic form (Hogle *et al.*, 1981; Artymiuk *et al.*, 1982; Rao *et al.*,

1983; Rao and Sundaralingam, 1996; Vaney *et al.*, 2001). A model of the asymmetric unit present in the monoclinic form of the lysozyme crystal is presented in figure 4.1.

A schematic detailing the morphology of the crystal itself is displayed in figure 4.2. The developed faces present on the monoclinic polymorph have been identified as the  $(10\bar{1})$ ,  $(101)$ ,  $(001)$  and  $(010)$  (Hondoh *et al.*, 2001). Crystals displaying this morphology have most commonly been grown from similar conditions to the tetragonal form, with the only difference being the use of sodium nitrate or sodium iodide as the precipitating agent (Steinrauf, 1959; Berthou and Jolles, 1978). Other reports have indicated that potassium thiocyanate (Ries-Kautt and Ducruix, 1989) and ammonium sulphate (Forsythe *et al.*, 1999b) are also suitable for the growth of the monoclinic form of the crystal.

#### 4.1.4 Chapter Aims

In this short experimental study we aim to take advantage of the unique properties of the AFM to investigate a rarely studied polymorph of the lysozyme crystal, and subsequently compare these observations with the work presented in chapter 3 of this thesis concerning the tetragonal form of crystalline lysozyme.

To enable comparison of the images obtained from the two crystal forms we will first optimize the conditions implemented in the growth of the monoclinic crystals to make them as similar as possible to the conditions used in the growth of the tetragonal samples. The major surface of these crystals (the  $(10\bar{1})$  face) will then be examined using AFM on a microscopic scale in an attempt to uncover any differences in the actual growth processes of the crystal. Nanoscale imaging will also be performed with a view to investigating the molecular packing on the  $(10\bar{1})$  face of the monoclinic crystal.

Achieving these aims will add valuable data to a rarely-studied crystal system, and, if successful, will allow two crystalline polymorphs of the same biological molecule to be distinguished from one another on a molecular level using *in situ* AFM.

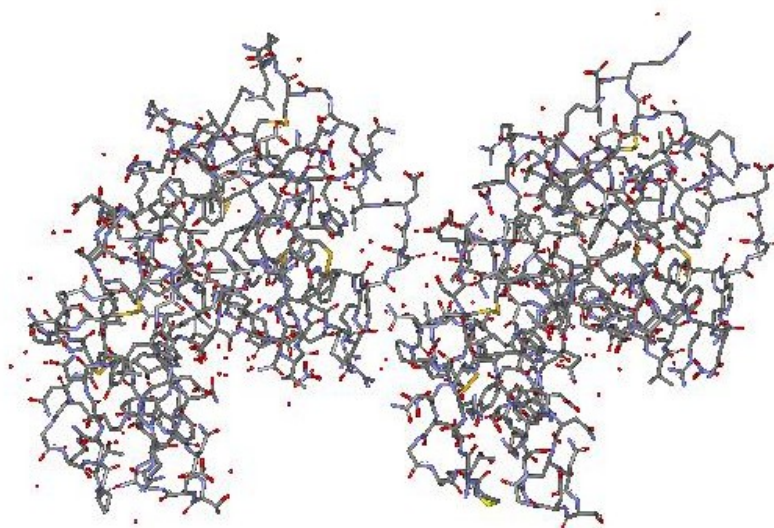


**Figure 4.1.** The asymmetric unit present in the monoclinic polymorph of the lysozyme crystal (PDB ID – 5LYM).

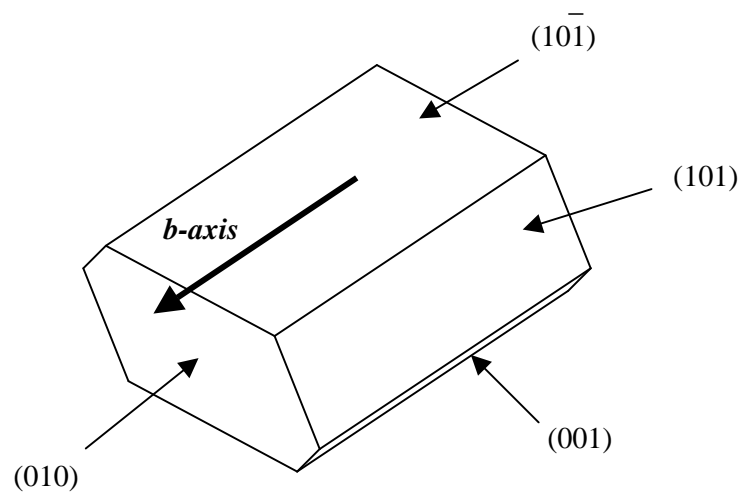


**Figure 4.2.** The habit of lysozyme crystallized in the monoclinic form. The four major faces of the crystal are the  $(10\bar{1})$ ,  $(101)$ ,  $(001)$  and  $(010)$ . Adapted from Hondoh *et al.*, 2001.

## 4.2 Materials & Methods

### 4.2.1 Seed crystal growth & immobilization

As one of our primary aims was to keep the protocol as similar to that described for the growth of tetragonal lysozyme crystals, the buffer and temperature of the crystallizing solutions were kept the same as described in chapter 3, whilst altering the precipitant. Previous work had highlighted the growth of the monoclinic form of lysozyme crystal from solutions containing sodium nitrate (Steinrauf, 1959; Berthou and Jolles, 1978) or sodium iodide (Steinrauf, 1959). As such, a series of screening experiments were performed using NaI and NaNO<sub>3</sub> to identify the most reliable and repeatable method for the growth of the monoclinic polymorph.

NaNO<sub>3</sub> was found to be a superior precipitant for the growth of the monoclinic form, and the following conditions were implemented in the production of seed crystals for AFM studies. Three-fold lyophilized HEWL (Fluka, Dorset, UK) at a concentration of 20-30mg/ml and 20-40mg/ml sodium nitrate (Sigma-Aldrich, Dorset, UK) were both dissolved in a 0.1 M NaOAc/AcOH buffer at pH 4.5 by vortexing and low-speed centrifugation. As in the preparation of the tetragonal seed crystals, the solution was filtered and six 4-6 $\mu$ L drops of the crystallizing solution were placed on previously unused EM grid/glass substrate, which had been attached to a magnetic AFM sample stub. The stubs were then all sealed in separate sitting-drop crystallization wells (Hampton Research Corporation, Laguna Niguel, CA), and left overnight at a temperature of approximately 20 °C. Because the drop size was small, nucleation generally occurred within 8 – 12 hours and seed crystals of 50  $\mu$ m x 50  $\mu$ m or larger had grown within 16 hours.

### 4.2.2 Preparation of imaging solutions

To the author's knowledge, the only solubility data available for lysozyme in the presence of sodium nitrate is available in the publication of Hondoh *et al.* (Hondoh *et*

*al.*, 2001). However, as this data is limited to a narrow range of conditions not directly comparable to ours, this data cannot be used to produce accurate values of supersaturation for the experiments presented below. As such, the concentrations of lysozyme & sodium nitrate present within the imaging solution are quoted throughout, rather than a supersaturation value.

#### 4.2.3 AFM analysis

Prior to imaging, all samples were observed by *ex situ* optical microscopy to assess the optical quality of the crystals. The most promising (usually those samples that contained well faceted, crack-free crystals) were removed from the crystallization plate, the mother liquor wicked away and rapidly replaced with a drop of solution prepared for imaging. The sample was then inserted into the AFM together with the liquid cell, which was equipped with a plastic O-ring to minimize solvent evaporation. The cell was subsequently flooded with imaging solution and, using the optical microscope integrated into the AFM system, the cantilever was positioned above a crystal that displayed a face of interest parallel to the substrate. The sample was then left for ~1 hour to equilibrate before imaging began.

All images were recorded using a DI Multimode atomic force microscope equipped with a Nanoscope IIIa controller and E-type scanner with maximum scan dimensions of 13  $\mu\text{m}$  x 13  $\mu\text{m}$  x 2  $\mu\text{m}$  (Veeco, Santa Barbara, CA). Silicon nitride NP-S cantilevers with a nominal spring constant of 0.1  $\text{Nm}^{-1}$  were used throughout (Veeco).

As with the tetragonal form of the crystal, the monoclinic polymorph was relatively robust and was imaged in contact mode throughout. However, care was taken to minimize the force applied to the sample by continually monitoring and adjusting the setpoint voltage to avoid damaging the crystal surface, particularly during the molecular resolution scans. Images were collected at 512 x 512 pixel resolution, at a scan rate in the range of 3-7 Hz. As with AFM data presented in previous chapters, the images presented throughout this study are in the form of either topography or deflection data. Topography data is used preferentially where possible, however deflection data often highlights rapid changes in topography in greater detail, such as is seen at step edges, so are used for that purpose throughout this chapter.

### 4.3 Results & Discussion

As expected, preliminary AFM investigations revealed that the (101) face of monoclinic lysozyme crystals were much like the surfaces presented earlier in this thesis, in that they appeared to be constructed of steps that developed tangentially across the crystal surface as new growth units from solution became incorporated into kink sites present at the step edges. However, it was immediately noticeable that there were often vast quantities of step edges, which were moving rapidly over the crystal surface. This is illustrated by the AFM images presented in figure 4.3(a) & (b), which were captured with imaging conditions of 8mg/ml lysozyme & 40 mg/ml NaNO<sub>3</sub> and 10 mg/ml lysozyme & 30mg/ml NaNO<sub>3</sub> respectively.

This observation can be explained by a comparison of the limited solubility data available for the monoclinic form with that available for the tetragonal form. According to the report of Hondoh *et al.* (Hondoh *et al.*, 2001) lysozyme is relatively poorly soluble when in a crystallizing solution containing sodium nitrate – this indicates that even at low protein & precipitant concentrations, the supersaturation of a lysozyme crystallizing solution containing sodium nitrate will be relatively high. Effectively, although the quantities of protein and precipitant are almost identical in the tetragonal and monoclinic crystallizing system, the supersaturations produced are vastly different, leading to the high quantity of step edges and extremely rapid growth in the monoclinic system as seen in figure 4.3.

In addition to the large quantity of step edges and rapid growth, the surface also clearly displayed other features. In practically every image recorded there were numerous simple screw dislocation points, as indicated in figure 4.3. Stacking faults were also observed regularly which was possibly a consequence of the crystal lattice relieving the stress caused by impurities and misaligned lysozyme molecules incorporated during the rapid advancement of the step edges.

Figure 4.4 illustrates some other features occasionally captured during AFM imaging. Complex screw dislocations formations were sometimes recorded, along with microcrystal formation at higher concentrations of protein and precipitant. The microcrystal in figure 4.4(b) is clearly misaligned with respect to the underlying lattice (as illustrated in the figure), and was dislodged by the AFM at the point highlighted by the white arrow.

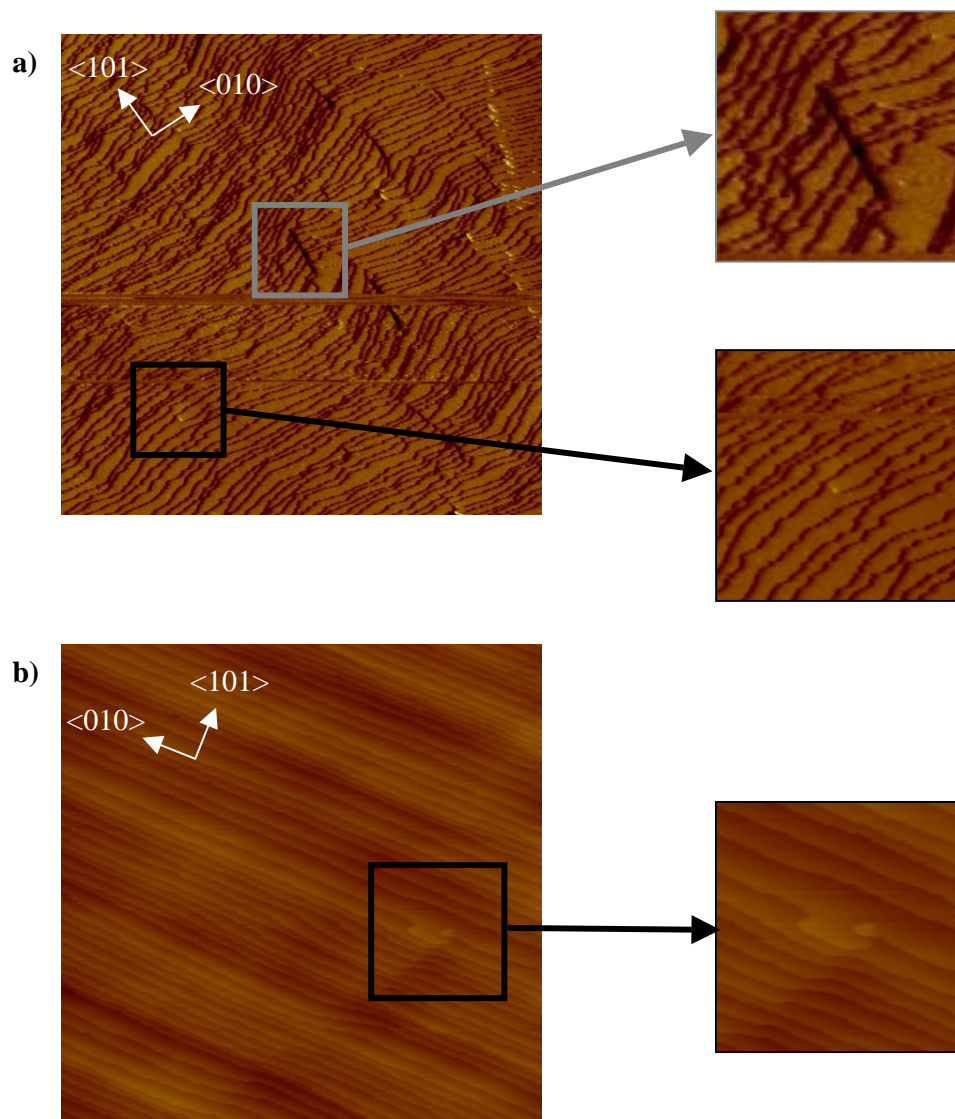


**Figure 4.3.** Arbitrary images of the  $(101)$  faces of monoclinic lysozyme crystals. Imaging conditions: **(a)** 8mg/ml lysozyme & 40 mg/ml  $\text{NaNO}_3$ . **(b)** 10mg/ml lysozyme & 30 mg/ml  $\text{NaNO}_3$ . Image **(a)** is a deflection image of  $7.5 \mu\text{m} \times 7.5 \mu\text{m}$ , with zoomed areas of  $2 \mu\text{m} \times 2 \mu\text{m}$  highlighting a stacking fault and screw dislocation respectively. Image **(b)** is a topography image of  $10 \mu\text{m} \times 10 \mu\text{m}$ , z-range 40 nm, with a zoomed area of  $3 \mu\text{m} \times 3 \mu\text{m}$  highlighting a screw dislocation.

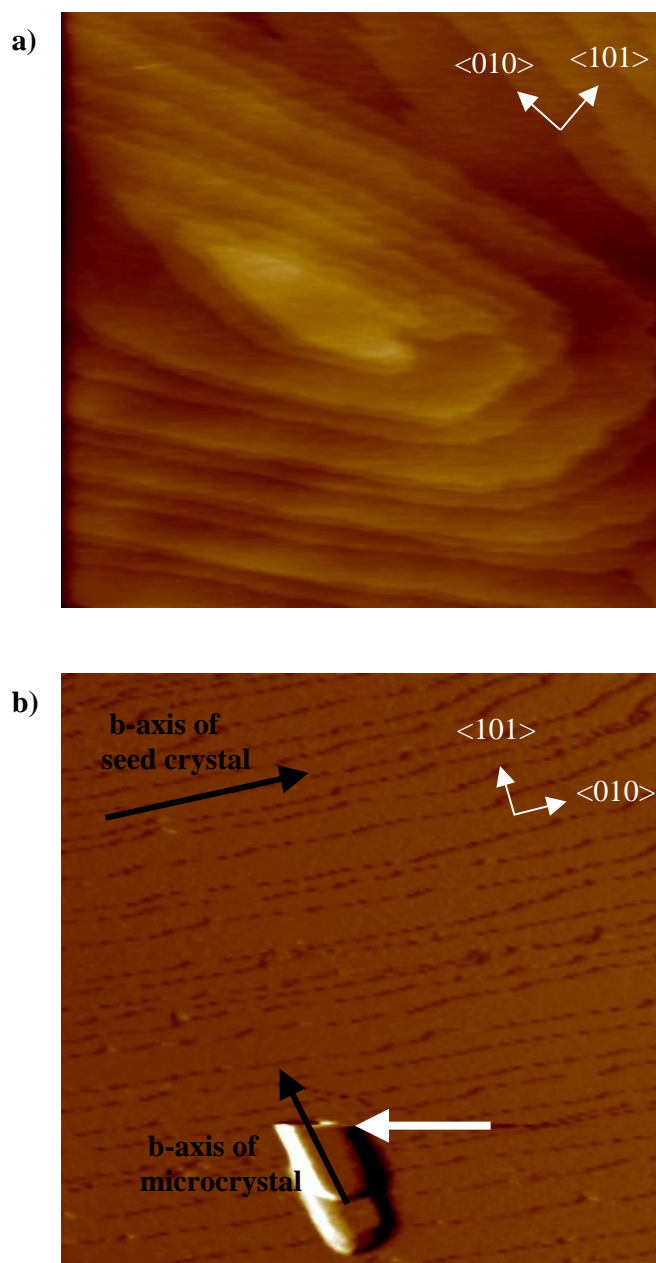


**Figure 4.4.** A complex screw dislocation on the  $(101)$  face of a seed crystal is presented in (a), with a weakly-adsorbed microcrystal clearly displaying the monoclinic morphology in the deflection image presented in (b). The microcrystal was dislodged from the seed crystal during scanning (at the point indicated by the white arrow). This was probably a consequence of microcrystal not being correctly aligned with the underlying lattice (as indicated by the black arrows). Scan sizes, (a)  $5\ \mu\text{m} \times 5\ \mu\text{m}$ , (b)  $2\ \mu\text{m} \times 2\ \mu\text{m}$ , with the z-range in (a) being 40 nm.

Another point of note was the apparent lack of 2D nucleation islands during imaging, at all protein and precipitant concentrations. Inevitably, the lack of such growth islands suggests that screw dislocations are the dominant source of steps on the monoclinic polymorph, a theory echoed by the two previous AFM reports on the subject (Hondoh *et al.*, 2001; Rashkovich *et al.*, 2002).

We believe that there are two possible reasons for this observation. The first concerns the packing of the monoclinic polymorph of the crystal. The X-ray crystallography study carried out by Hogle *et al.* (Hogle *et al.*, 1981) indicated that the monoclinic form is unusually tightly packed – approximately 10 % tighter than the tetragonal form (which, itself, is well-packed compared with the average figure). Such tight packing will undoubtedly pre-dispose the monoclinic crystal to particularly high levels of lattice stress and strain during growth, which is generally relieved by the formation of defects such as screw dislocations and stacking faults as suggested by the results presented here and elsewhere.

The second possible reason concerns the height exhibited by the step edge on the  $(101)$  face of the monoclinic crystal. To measure this accurately, a crystal was imaged in a solution containing relatively small quantities of protein and precipitant to minimize the amount of steps on the surface. Figure 4.5 contains an image captured at a protein/precipitant concentration of 7.5 mg/ml and 20 mg/ml respectively. The step heights were consistently measured to be in the region of 2.5 nm, a figure that both corresponds to the interplanar spacing of the  $(101)$  plane and is in agreement with previous reports.

The figure of 2.5 nm indicates the monoclinic growth unit is monomeric in height, rather than the dimeric species observed in the tetragonal crystal (see chapter 3). As the energy required to create a screw dislocation is directly proportional to the square of the Burger's vector (which, in this case, is represented by the step height) (Chernov, 1984), it is clear that the creation of screw dislocations on this face may be somewhat more likely than the creation of such defects on the tetragonal crystal.

By minimizing the protein and precipitant concentrations as described above, we were also able to record a small number of *in situ* growth images. A selection of such images is presented in figure 4.6. Figure 4.6(a)-(c) contains consecutive images of growth on the  $(101)$  in both the  $\langle 010 \rangle$  and  $\langle 101 \rangle$  directions, with (d) containing a zoomed area of the image contained in 4.6(b).

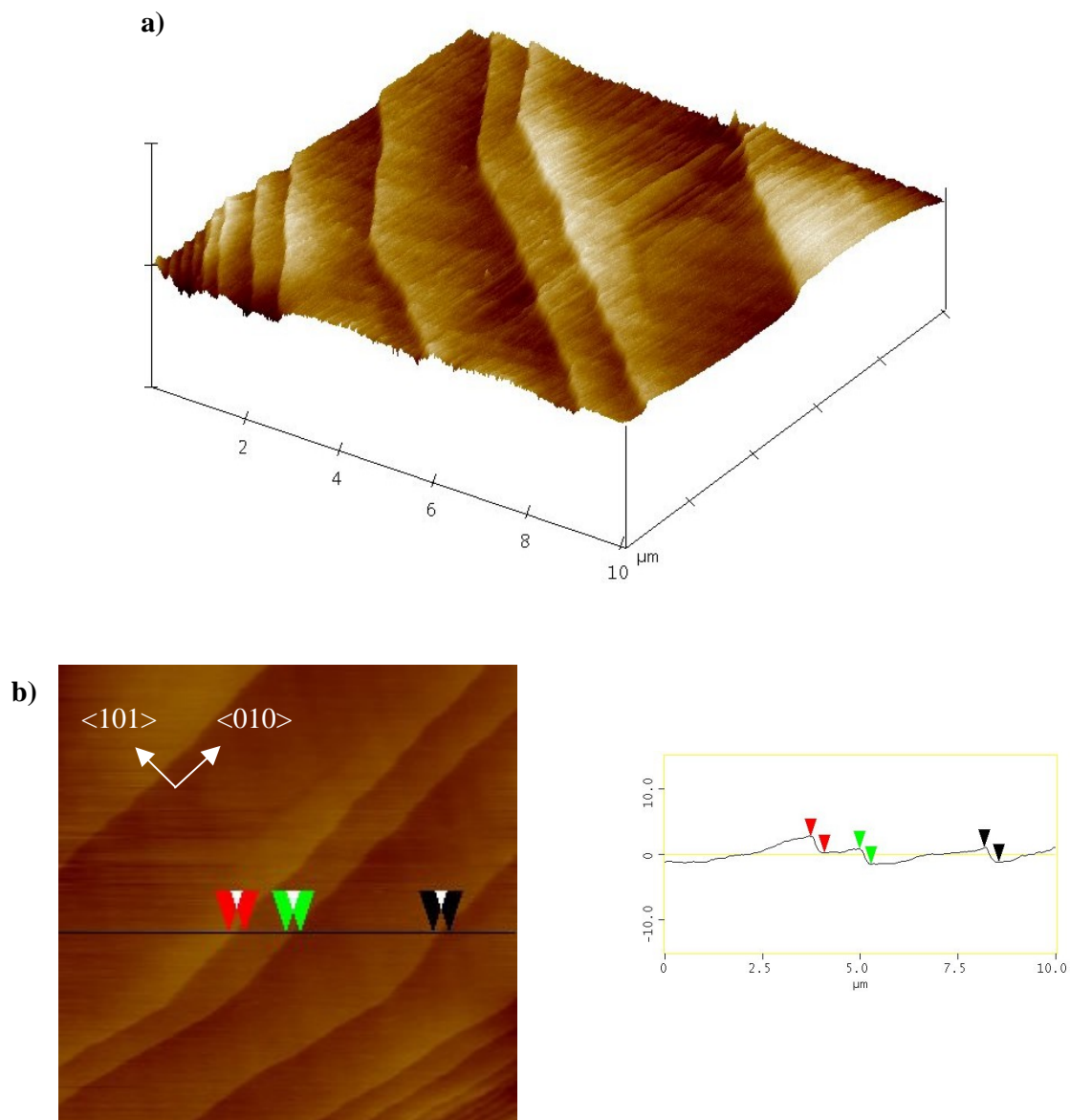


**Figure 4.5.** A  $10\mu\text{m} \times 10\mu\text{m}$  image of the  $(101)$  face of the monoclinic form of lysozyme captured at low protein and precipitant concentrations. The single step edges are clearly visible in the 3D representation of the image in (a), and are measured to be approximately 2.5 nm in height in (b).

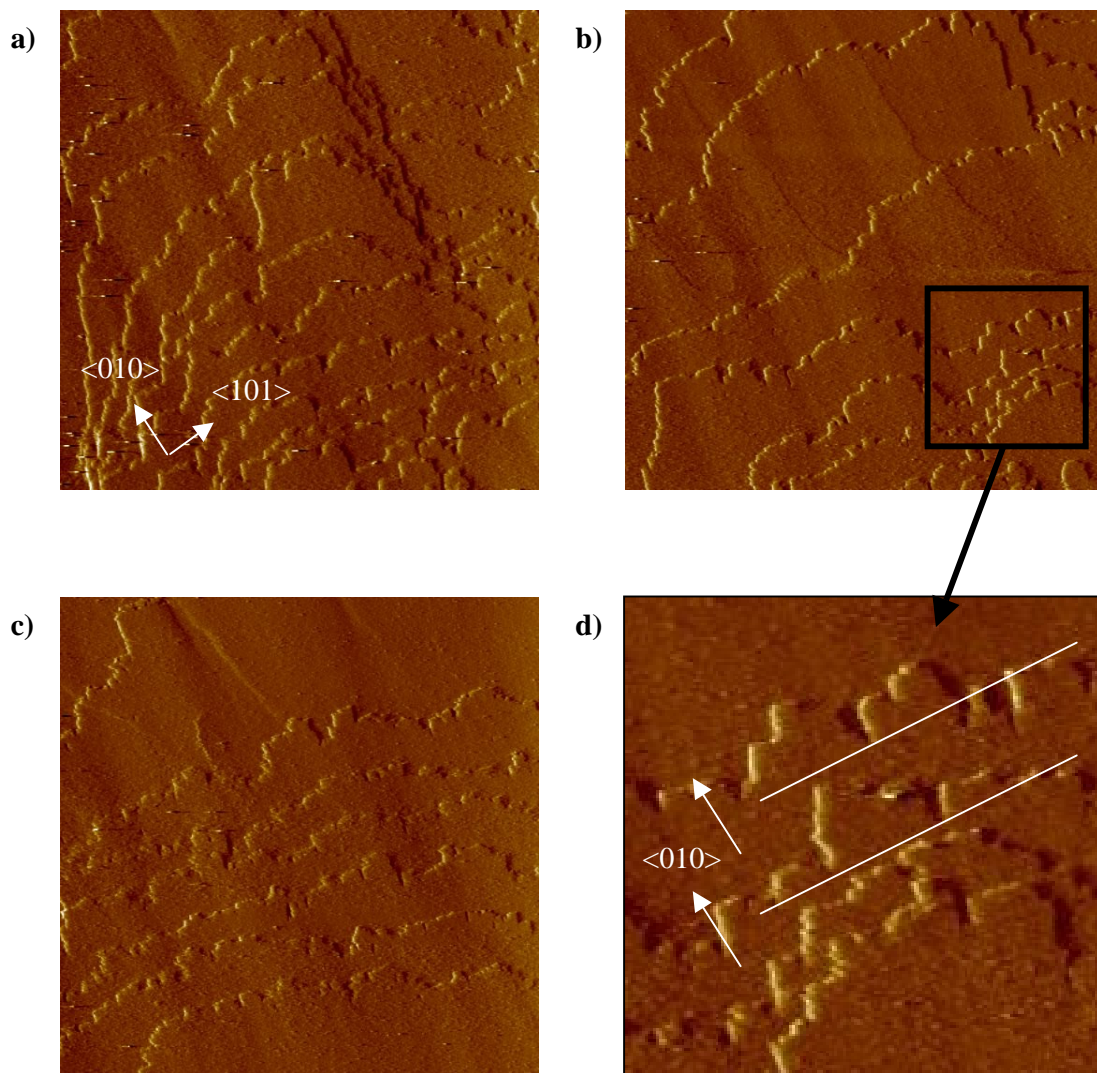


**Figure 4.6.** (a)-(c) consecutive 7.5 μm x 7.5 μm deflection images captured at a protein/precipitant concentration of 7.5 mg/ml and 20 mg/ml respectively. The image presented in (d) is a 2.5 μm x 2.5 μm zoomed area from (b) illustrating the severe roughness present on the steps proceeding in the <math>\langle 010 \rangle</math> direction.

The step fronts progressing in the  $\langle 010 \rangle$  direction clearly exhibit severe roughness, particularly when compared to the steps progressing in the  $\langle 101 \rangle$  direction (for example see the step edges in 4.3(b) & 4.5(b)). This characteristic feature was also observed in the AFM study carried out by Hondoh *et al.* (Hondoh *et al.*, 2001). The reason behind this roughening effect is not completely understood, but it is likely to be a consequence of molecular anisotropy exposing different portions of the lysozyme molecule to the crystallizing solution. It is possible that the portion of the lysozyme molecule exposed when adding to the  $(10\bar{1})$  face in the  $\langle 010 \rangle$  direction is increasingly likely to incorporate misorientated molecules or impurities that subsequently pin the growth step, causing the observed roughening effect.

We were also able to capture higher resolution images displaying the crystal lattice of this face of the monoclinic form. One such image is displayed in figure 4.7(a), with a filtered section of this image presented in 4.7(b). Figure 4.7(a) also contains two step edges, one of which appears to have a number of kink sites at its edge (illustrated with the white arrows). The periodicities displayed in figure 4.7(b) are approximately 6.6 nm and 3.7 nm, both of which correspond well to the 2D unit cell dimensions on this face (Rashkovich *et al.*, 2002).

These data, in addition to the interplanar spacing data of 2.5 nm, have permitted two crystalline polymorphs of the same protein molecule to be unambiguously distinguished from one on a molecular level another utilizing *in situ* AFM.

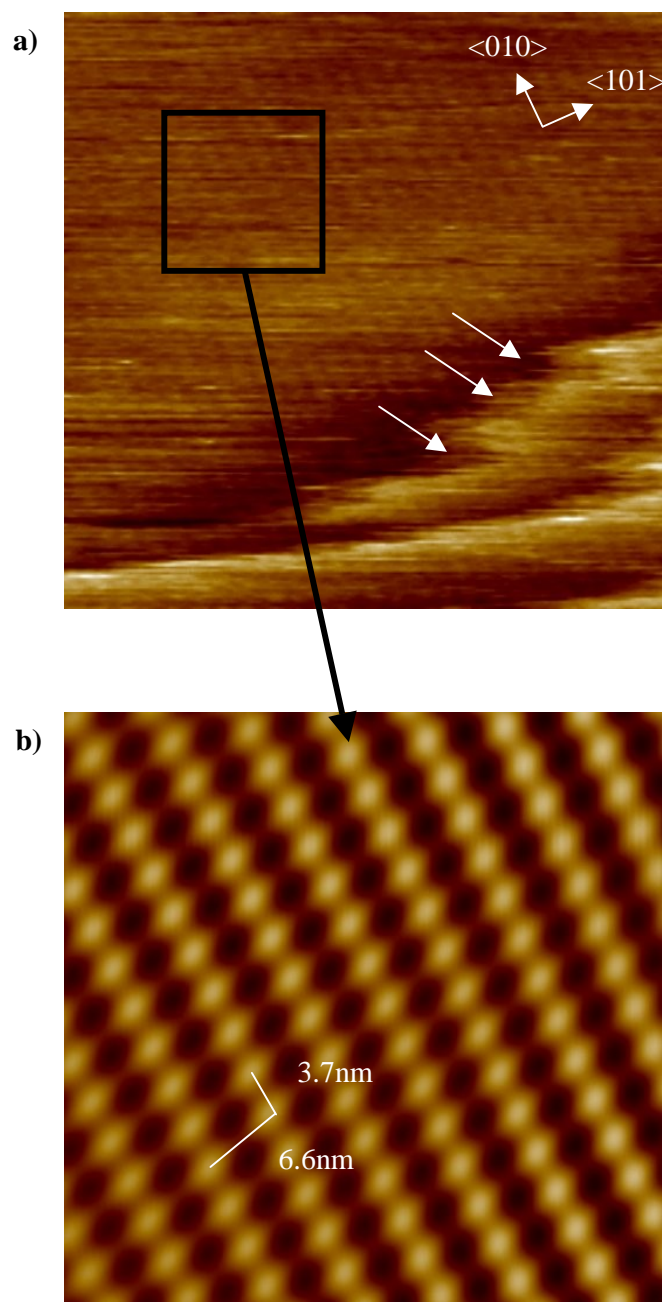


**Figure 4.7.** (a) A 175 nm x 175 nm section of the  $(10\bar{1})$  face of the monoclinic lysozyme crystal showing the surface lattice. Kink sites are also visible at the step edges, as illustrated by the arrows. Image (b) contains a 50 nm x 50 nm section of the image in (a), which has been filtered using the procedure discussed in section 3.3.3.2. This image displays periodic features of approximately 6.6 nm and 3.7 nm.

#### 4.4 Conclusions

In this study the  $(10\bar{1})$  face of the monoclinic form of lysozyme crystal has been investigated using *in situ* AFM and the images discussed with reference to the results obtained for the tetragonal form of the crystal, which were presented in chapter 3 of this thesis.

We were able to grow monoclinic seed crystals for use in the AFM experiments by changing the precipitant from sodium chloride (used to produce the tetragonal form of the crystal) to sodium nitrate, whilst keeping all other variables constant. This subtle alteration to the crystallizing environment severely affects the way in which the lysozyme molecules pack together. This has previously been investigated crystallographically (for example see Hogle *et al.*, 1981), but there have been few studies investigating how the crystal itself is altered when compared with the tetragonal polymorph.

At higher levels of protein and precipitant concentration, the  $(10\bar{1})$  face was always covered with vast quantities of step edges. In agreement with the two previous AFM studies on the monoclinic form (Hondoh *et al.*, 2001; Rashkovich *et al.*, 2002), no 2D nucleation islands were ever observed, suggesting that screw dislocations were the dominant sources of step formation. Indeed, simple screw dislocations, complex screw dislocations and stacking faults were all regularly observed on the crystal surface. We believe such observations are a consequence of both the tightly packed crystal lattice, and the relatively small interplanar spacing of this face (2.5 nm).

When the concentration of protein and precipitant were lowered we were able to record consecutive *in situ* growth images of the surface, which highlighted extreme roughness of the step fronts in the  $\langle 010 \rangle$  direction. This feature was also previously reported, and is believed to be a consequence of the anisotropic nature of the lysozyme molecules in the monoclinic form. Molecular resolution images were also recorded, allowing us to unambiguously distinguish between crystalline polymorphs of the same protein molecule. These images highlighted periodicities of 6.6 nm and 3.7 nm, which correspond well to the 2D unit cell dimensions of this face of the crystal (Rashkovich *et al.*, 2002).

## Chapter

## 5

**An AFM analysis of a poorly diffracting  
protein crystal - Response Regulator 02  
receiver domain (RR02rec)**

---

In an attempt to broaden the understanding of disorder in macromolecular crystals, we have studied poorly diffracting crystals constructed from a protein found in *Streptococcus pneumoniae*, Response Regulator 02 receiver domain (RR02rec). Here we describe the optimization and growth of seed crystals, and their subsequent analysis by *in situ* AFM.

Preliminary imaging showed the RR02rec crystals had extremely poor mechanical properties and a marked lack of linear and planar defects such as stacking faults and screw dislocations. Molecular resolution imaging also revealed unusually large periodic features (22 nm and 10 nm, with an interplanar spacing of 11 nm), which are inconsistent with small protein molecules such as RR02rec. This suggests the protein molecules may associate in solution prior to, or during crystallization – indeed, dynamic light scattering (DLS) studies previously performed on the pure protein solution showed that as the concentration of protein was increased oligomers of varying sizes were formed. Inevitably the presence of dynamic, concentration dependant oligomeric species will add significant levels of disorder to the crystal, particularly as vapour diffusion methods act to further concentrate the protein-containing drop prior to nucleation. If these oligomers do not pack together well (as suggested by the AFM studies) it seems feasible the diffraction resolution will suffer, as indicated by the initial poor resolution data obtained of these crystals.

---

## 5.1 Introduction

As briefly discussed in chapters 1 & 3 of this thesis, biological crystals are generally grown with a view to obtaining structural information regarding the biomolecules that make up that crystal through X-ray diffraction experimentation. Crystals formed of so-called ‘model’ proteins such as lysozyme (see chapters 3 & 4 of this thesis) are extremely rare, in that they offer such information with ease. This is because they form large (>0.1 mm in all dimensions), relatively robust, well-ordered crystals that diffract X-rays with high efficiency.

Whilst it is fair to say that the majority of soluble biological macromolecules of interest will form crystals from carefully optimized and controlled conditions, many of these crystals are of poor diffraction quality – hence they offer limited structural data to the crystallographer. This is undoubtedly the most serious obstacle in the structural determination process.

### 5.1.1 X-ray diffraction

Before discussing macromolecular crystal quality in any detail it is necessary to give a brief overview of the principles of X-ray diffraction as applied to macromolecular crystals. For more detailed information, the reader is directed to the following publications (Blundell and Johnson, 1976; Drenth, 1994; Blow, 2002).

The use of electromagnetic radiation to visualize objects requires the radiation to exhibit a wavelength comparable to the smallest features which are to be resolved. When considering structure on an atomic scale, distances are in the order of single angstroms (internuclear bond distances are typically in the range of 1 – 3 Å). As such, X-rays are generally employed to be sensitive to atomic structure, as their wavelengths are in the region of 1 Å.

When a beam of X-rays is directed into any kind of matter, the separate photons that make up that beam will be absorbed by some of the electrons present in the matter, which acts to set those electrons vibrating at the X-ray frequency. If a single electron absorbs a single photon, the electron will subsequently emit an X-ray photon in a

random direction, of the original energy and wavelength – this process is called coherent scattering, or diffraction (Blow, 2002).

The most important property of X-rays (when considering structural analysis and diffraction) is that they can be thought of as waves. Waves, when they are in the same region of space, are able to interfere with one another. Thus, when a repetitive object such as a crystal lattice diffracts X-rays, each unit of the lattice scatters, but an intensely diffracted beam only arises if the scattered rays from each unit are in phase – that is, they *constructively interfere* with one another. When the scattered X-rays *destructively interfere* with each other, they give a reduced amplitude and, thus, a smaller intensity.

Waves scatter in phase when they have exactly the same pathlength, or when their pathlengths differ by a multiple of the wavelength. These two situations are illustrated schematically in figures 5.1 & 5.2 respectively, and form the basis of the well-known Bragg's law for the diffraction of X-rays by a crystalline material.

In a crystal, any plane of lattice points can be thought of as acting as a 'mirror' that is able to reflect X-rays. Providing the angle of incidence is equal to the angle of reflectance, as illustrated in figure 5.1, the rays must travel exactly the same distance to form a wavefront, no matter at what point on that plane they are scattered. However, when considering multiple planes (as exist in crystalline structures) the situation is slightly more complicated, because the X-rays will not always exhibit the same pathlengths. This situation is displayed schematically in figure 5.2.

The conditions for multiple planes to scatter in phase depends on three quantities – (i) the wavelength of the X-rays ( $\lambda$ ), (ii) the interplanar spacing ( $d$ ) and (iii) the glancing angle of the incidence beam ( $\theta$ ). From figure 5.2 it is clear that the two planes will scatter in phase if the pathlength difference ( $AB+BC$ ) is a whole number of wavelengths, say  $n$ . This simple relationship is known as Bragg's law, which states:

$$n\lambda = 2d \sin \theta \quad \text{equation 5.1}$$

Experimentally, Bragg's law is implemented by directing a monochromatic beam of X-rays into a crystal, and rotating that crystal (ie, varying  $\theta$ ) until an intense reflection is detected. Here, Bragg's law has been satisfied, and the interplanar spacing can be calculated for that glancing angle. Inevitably, there are many different planes in a crystal, and a complete data set consists of the list of angles at which reflections are observed, and their intensities (Atkins, 1998).

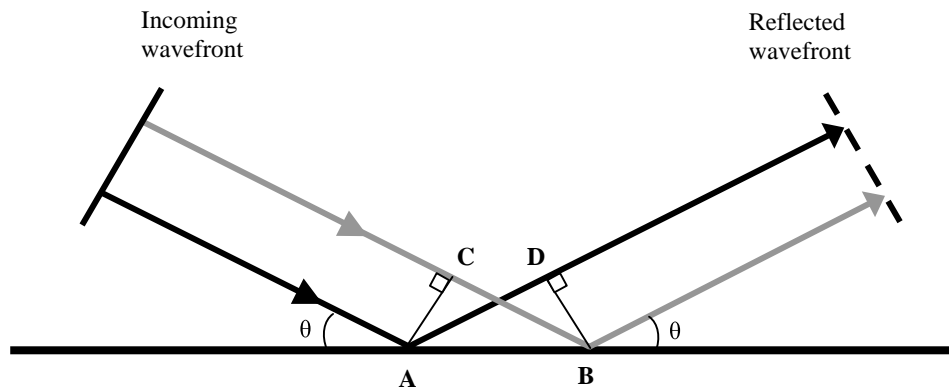


**Figure 5.1.** A schematic depicting scattering from different points along the same plane. Constructive interference occurs when the angle of incidence equals the angle of reflectance. When this is fulfilled,  $AD = CB$  and the waves exhibit identical pathlengths.

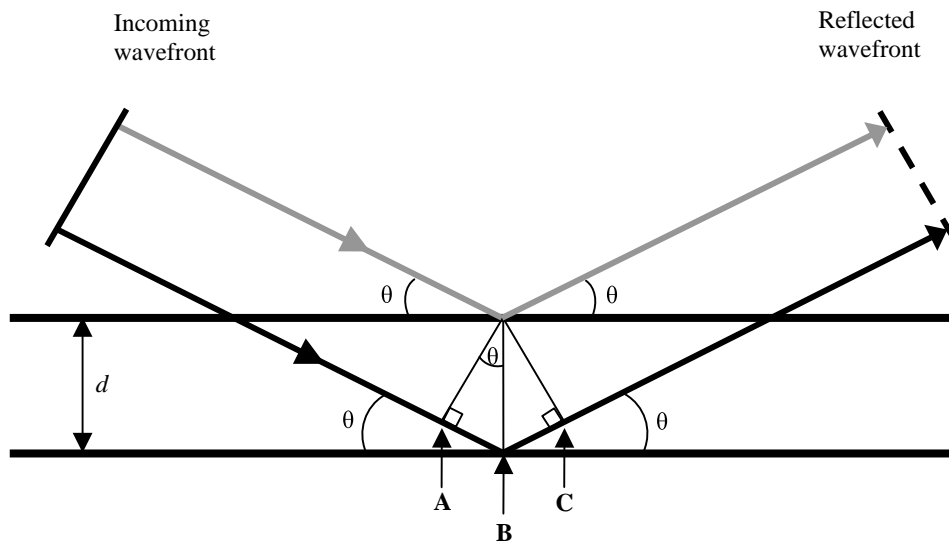


**Figure 5.2.** A schematic depicting multi-plane scattering. When crystalline structures scatter X-rays, constructive interference occurs when  $AB + BC$  is equal to an integer number of wavelengths. Achieving constructive interference is thus dependant on the interplanar spacing ( $d$ ), the glancing angle ( $\theta$ ) and the wavelength of the X-rays ( $\lambda$ ). Bragg's law relates these variables.

It is inevitable therefore that the quality of the information contained in any diffraction pattern produced by a single crystal rotated in a monochromatic beam of X-rays is in dependent, in part, on the degree of order displayed by that crystal. Indeed, there are two specific features of a diffraction pattern that tend to reflect the inherent order of any macromolecular crystal lattice: the diffraction limit (or resolution), and the mosaicity.

#### *5.1.1.1 Diffraction limit (resolution)*

It is clear that the smaller the value of the interplanar spacing,  $d$ , the more finely the family of planes samples the contents of the crystal. To satisfy Bragg's law the scattering angle,  $\theta$ , must increase as the value of the interplanar spacing falls. Experimentally, this means the smaller the value of  $d$ , the farther from the primary X-ray beam the reflection falls in the diffraction pattern (McPherson, 1999). Indeed, the diffraction limit (or resolution) is defined by the smallest interplanar spacing that gives measurable diffraction intensities. The better the resolution, the higher the precision of the structural model derived from that analysis. A high-resolution data set is generally considered to be  $\sim 2$  Å or less, whilst crystals displaying a resolution of 4 Å and above provide scant structural data at an atomic scale (Wiencek, 1999). Generally, low-resolution diffraction indicates the crystal exhibits poor long-range order, and new crystallization conditions must be identified that will pack the molecules more precisely into the crystal lattice.

#### *5.1.1.2 Mosaicity*

The mosaicity of any one crystal is defined by the width, or spread, or the reflection intensities. This measurement effectively represents the width of the Bragg glancing angle over which a particular family of planes in a macromolecular crystal will constructively scatter X-rays (McPherson, 1999).

Mosaicity is a consequence of defects in crystals promoting the formation of 'subdomains' in the crystal lattice – such subdomains are often individually perfect, but may be slightly misaligned with respect to one another. As such, constructive interference may occur at a range of Bragg angles, rather than just one. This situation is

undesirable as a large mosaicity can cause the diffraction spots to overlap, thus making determination of the spot intensities problematic.

### 5.1.2 Variables affecting macromolecular crystal quality

Naturally, the ultimate analysis of macromolecular crystal quality comes from the successful structural determination of the molecule of interest – if the crystal both diffracts to a high resolution and displays limited mosaicity, its constituent macromolecules must be homogenous, and form numerous, strong, geometrically well defined bonds in three-dimensions.

Unfortunately however, the vast majority of macromolecules of interest do not immediately form such ‘diffraction friendly’ crystals – indeed, some never do. This factor, as discussed throughout this thesis, represents the most persistent and frustrating obstacle to the structural determination process. Consequently, numerous macromolecular crystal growth studies have set out to identify, understand and ultimately reduce the disorder that has a deleterious effect on diffraction resolution.

It has long been recognized that minimizing crystal growth rates encourages the growth of larger, more impurity-free crystals. Fast growth is likely to result in molecules becoming trapped in high energy (non-stable) configurations in the lattice, which inevitably has an adverse effect on the diffraction properties of that crystal. This effect has been elegantly demonstrated in lysozyme (Yoshizaki *et al.*, 2001; Yoshizaki *et al.*, 2002) and tRNA crystallization (Ng *et al.*, 1997) by combining X-ray crystallography with AFM studies. The authors in both cases were able to show an improved X-ray diffraction limit when decreasing the supersaturation of the growing crystals, which strengthens the case for seeding metastable solutions to achieve higher quality macromolecular crystals (Bergfors, 2003).

Other informative experimental and theoretical data has originated from studies of macromolecular crystals grown in a zero gravity environment (Littke and John, 1984; Kundrot *et al.*, 2001; Vergara *et al.*, 2003). Comparison of space-grown crystals with crystals grown in control experiments on Earth generally display an increase in crystal size and visible quality. Most important, however, is that in approximately 20 % of cases the diffraction limit for the space-grown crystals is measurably improved

(DeLucas *et al.*, 2002). Such improvements are credited to the elimination of deleterious buoyant convective flows experienced by the crystals in microgravity, along with the dominance of slower, more uniform growth rates. Whilst these studies have undoubtedly provided much useful theoretical data, they are, for obviously reasons, extremely impractical and, with only 20 % of samples showing improved diffraction properties, by no means guarantee success with structural determination.

X-ray topography has also been used as a tool to investigate macromolecular crystal quality. A number of studies have investigated the effect of solution changes, impurity incorporation and post-growth crystal treatments on the mosaicity and diffraction limit of protein crystals (Dobrianov *et al.*, 1998; Caylor *et al.*, 1999; Dobrianov *et al.*, 1999). These studies have suggested that the disorder with most influence over the diffraction limit within macromolecular crystals originates from conformational variations of individual macromolecules within the crystal lattice, rather than microscopic disorder such as defect formation. However, AFM studies do not always reflect this suggestion – for example rhombohedral canavalin crystals diffract to little better than  $\sim 3$  Å resolution and have been shown, by AFM, to possess very high densities of defects and dislocations. On the other hand, the surfaces of tetragonal thaumatin crystals are often almost completely devoid of defects. These crystals regularly diffract to beyond 1.5 Å resolution (McPherson, 1999), suggesting the possibility of an important link existing between defect density and diffraction resolution.

It is clear that a significant number of issues surrounding macromolecular crystal quality are presently unresolved. Work presented in this chapter aims to tackle some of these vital points by investigating a poorly diffracting crystal of significant biological importance, using *in situ* AFM.

### 5.1.3 Response regulator proteins in *Streptococcus pneumoniae*

*Streptococcus pneumoniae* is a Gram-positive bacterial pathogen that affects adults and children worldwide, and is one of the leading causes of illness and death in infants, the elderly and immunocompromised patients (AlonsoDeVelasco *et al.*, 1995).

The bacterium is directly responsible for diseases such as otitis media, pneumonia, bacteraemia and meningitis, and is the cause of many thousands of deaths each year. Additionally, numerous strains of *S. pneumoniae* are beginning to exhibit resistance to various antibiotics including vancomycin and erythromycin. As such, new, novel targets for antibacterial agents are presently being sought.

One such area of research into new antibacterial agents is in the field of Two-Component Signal Transduction Systems (TCSTS) which all bacteria use as their main method of communication and sensing. As their name suggests, TCSTS are comprised of two distinct protein compartments – the Histidine Protein Kinase (HPK) and the Response Regulator (RR). The HPK is anchored to the cell membrane and is comprised of a number of domains, one of which acts as an extracellular sensor. The RR is comprised of two distinct domains – a receiver domain, and a DNA-binding domain that controls gene expression. Generally, TCSTS act to by utilizing energy released from ATP hydrolysis in order to transduce a measured response to a variety of external stimuli. A simplified mechanism of action for typical TCSTS is presented in figure 5.3.

Thirteen TCSTS have been identified in *S. pneumoniae* (Lange *et al.*, 1999; Throup *et al.*, 2000) and they are known to perform a range of important functions including penicillin tolerance and phosphate sensing, with a number of them being essential for bacterial cell growth. The RR portion of one of the thirteen TCSTS, named RR02 or MicA, is a 26 kDa protein that has previously been shown to be essential for bacterial growth, thus making it a prime target for new antibacterial agent design (Bent *et al.*, 2004). The receiver domain of this protein, which shall be termed RR02rec throughout, was cloned, expressed, purified and crystallized with a view to determining the structure of the protein by X-ray diffraction methods. However, whilst numerous well faceted crystals were grown from a variety of conditions, the vast majority of them diffracted to a resolution unsuitable for atomic-level structural analysis (~5 Å). Optical photographs of a selection of these crystals and a typical low-resolution diffraction pattern are displayed in figure 5.4.

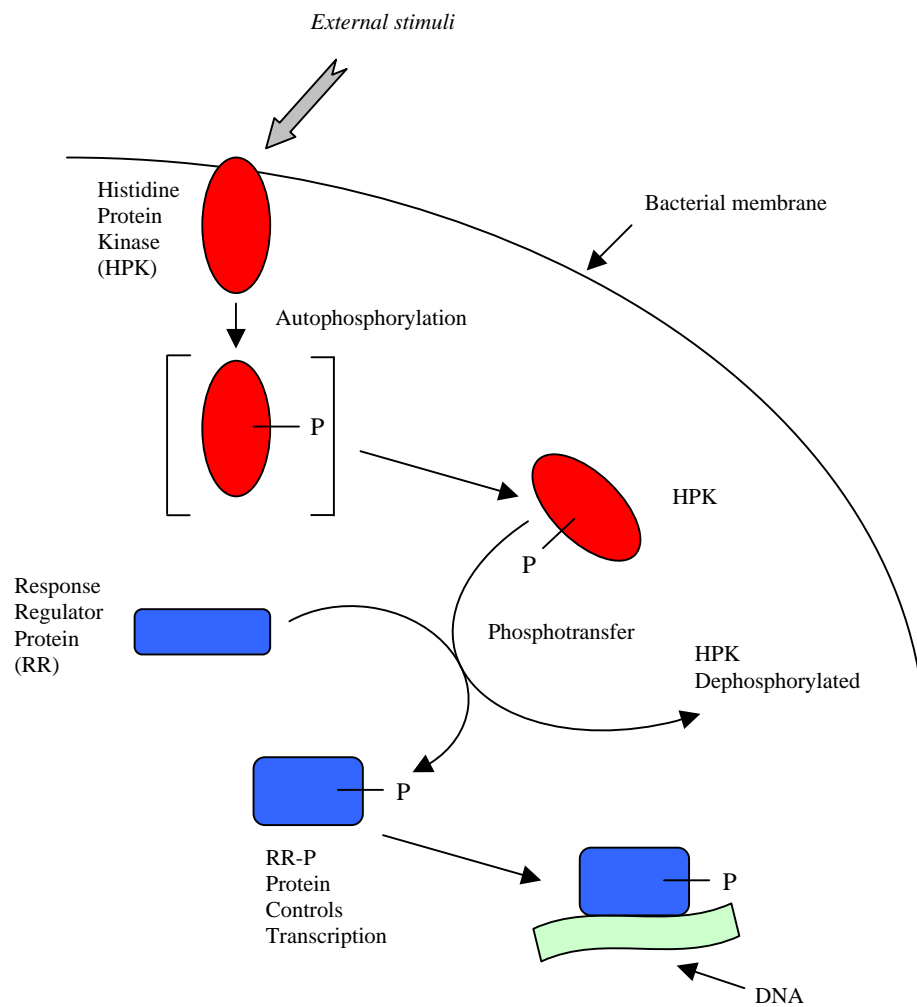


**Figure 5.3.** A schematic representation of two-component signal transduction. The extracellular portion of the HPK senses an environmental stimulus, leading to a separate domain of the HPK being phosphorylated by ATP. This phosphoral group is subsequently transferred to the receiver domain of the RR, which induces a conformational change in the RR protein, essentially freeing the RR output domain to provide a measured response to the initial stimuli. Adapted from Barrett *et al.*, 1998.

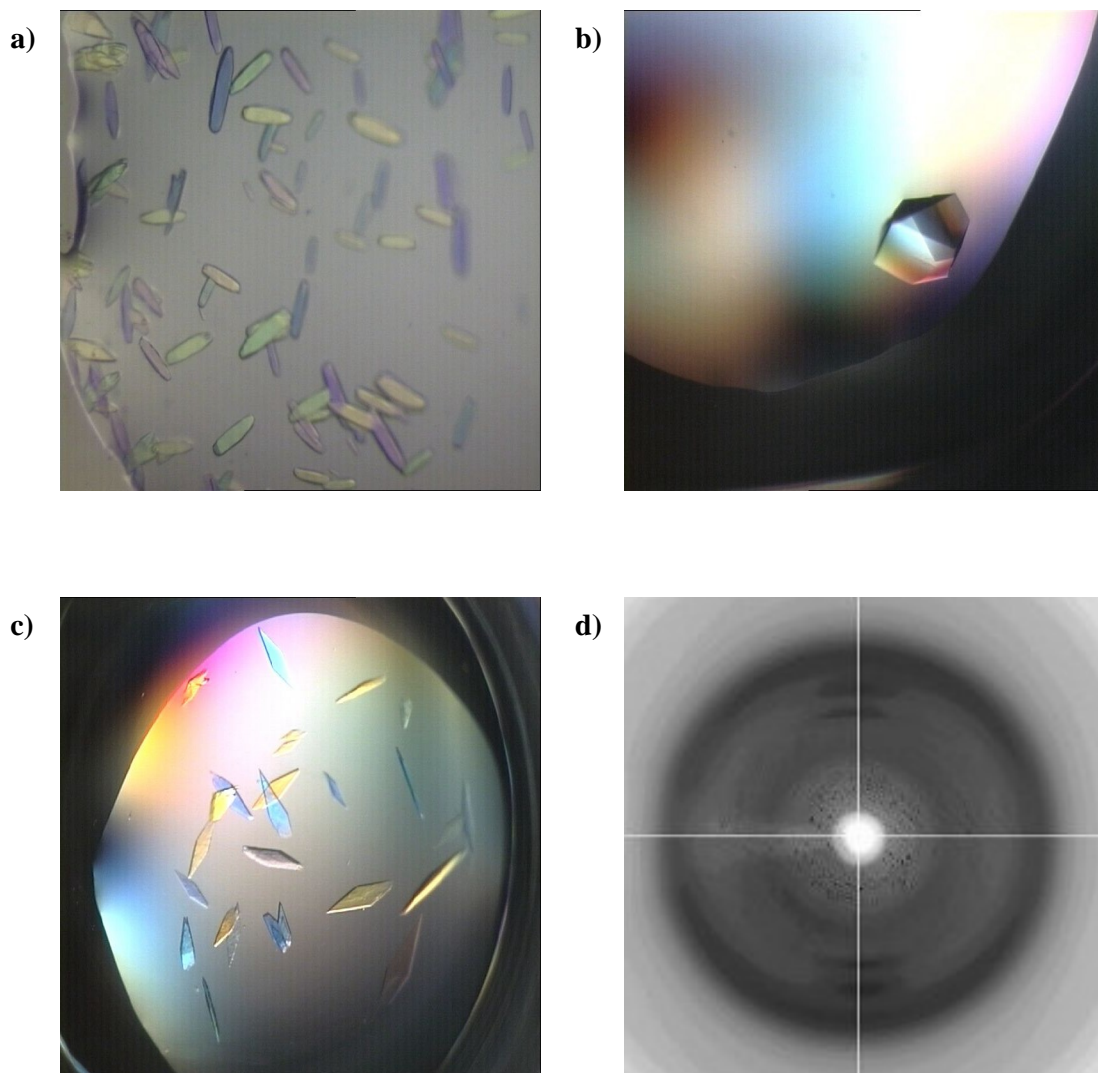


**Figure 5.4.** (a-c) A selection of poorly diffracting crystals of RR02rec grown from optimized conditions, with a typical diffraction pattern obtained in (d).

## 5.1.4 Chapter aims

The growth of high quality macromolecular crystals for use in X-ray diffraction experiments is of paramount importance, and the failure to do so is undoubtedly the most serious impediment to the whole structural determination process. Whilst a variety of studies have taken place with the view to investigating and understanding the problem, many questions still remain concerning the types of disorder present in macromolecular crystals, and which disorder is most deleterious to the diffraction properties of such crystals.

In this chapter, we aim to tackle some of these important issues by carrying out a series of *in situ* AFM studies on a ‘poor quality’ macromolecular crystal built from the *Streptococcus pneumoniae* signal transduction protein, RR02rec. The justification for such studies is clear – AFM permits the observation of the surfaces of macromolecular crystals with exquisite clarity and significant detail, as shown in the previous chapters of this thesis. By investigating a crystal that exhibits poor diffraction properties and subsequently comparing the results with a model protein crystal system of comparable molecular weight whose diffraction properties are unquestionable, it may be possible to draw conclusions as to the microscopic and nanoscopic properties of the crystal lattice that hold an influence on the diffraction quality of the crystal on an atomic scale. Achieving this aim would add significant understanding to the field of macromolecular crystal growth and quality.

## 5.2 Materials & Methods

### 5.2.1 Cloning, over-expression and purification of RR02rec

The majority of the molecular biology and biochemistry techniques used in the production and purification of the RR02 receiver domain are both specialized and complex and, as such, are beyond the scope of this thesis. However for completeness, this section includes a general overview of the methods utilized in the production of purified RR02rec. If more detailed information is required, the reader is referred to the following publications (Bent *et al.*, 2003; Bent *et al.*, 2004).

The section of DNA responsible for encoding the RR02rec protein was amplified over 6 million fold using the Polymerase Chain Reaction (PCR). The products of this reaction were subsequently visualized on an agarose gel, and the required amplified gene isolated from the un-reacted enzymes and primers utilized in the initial PCR reaction. The separated gene was then inserted into plasmid DNA, the result of which forms an ‘expression plasmid’, capable of expressing the RR02rec gene in large quantities.

The plasmid DNA containing the RR02rec gene was then introduced into *E. coli* by heat shocking. This procedure permits the plasmid DNA to enter the *E. coli* through pores that open when the host cells are heated. The *E. coli* was then grown, thus amplifying the plasmid at the same time. When amplification was completed, the pure DNA plasmid was isolated from the redundant *E. coli* components by centrifugation.

This purified DNA plasmid and RR02rec gene was then transferred into an *E. coli* expression host cell, again by heat shock treatment. At this point, isopropylthiogalactoside (IPTG) was added, which acts to catalyze the expression of the RR02rec protein from the DNA plasmid using the *E. coli* machinery in the host cell. After 4 hours of expression, the cells were harvested by centrifugation.

At this stage, the RR02rec protein had been expressed, but was still effectively ‘trapped’ inside the *E. coli* expression cells. It was removed by bursting the cells open using sonication – however, this inevitably releases all of the contents of the *E. coli* cells, not just the RR02rec protein. As such, RR02rec was separated from the unwanted

material using a range of chromatographical techniques, until it was shown to be in excess of 95 % pure by SDS-PAGE analysis. At this point, the protein was deemed to of sufficiently purity to undergo crystallization trials. In preparation for such trials, the protein solution was concentrated to between 7 and 10 mg/ml in a 25 mM Tris buffer at pH 7.5.

## 5.2.2 Crystallization

### 5.2.2.1 Vapour diffusion methods

In chapters 3 & 4 of this thesis, batch crystallization was used to successfully grow lysozyme crystals. To recall, batch methods are implemented when an undersaturated solution containing the biological macromolecule to be crystallized is mixed with a crystallizing agent at a concentration sufficient to immediately bring the combined solution into a supersaturated state, from where spontaneous nucleation may occur. Whilst being the oldest and simplest technique for growing macromolecular crystals, it does not suit all molecules of interest as nucleation is often difficult to control and the resulting crystal growth is rapid, yielding poorly formed crystals.

Because of these problems, the most common technique implemented in the growth of macromolecular crystal is vapour diffusion. Vapour diffusion is an ideal method for screening a broad spectrum of crystallizing conditions on a microlitre scale, thus maximizing the chances of growing high quality crystals even from minute quantities of solute. Indeed, vapour diffusion methods were used to grow all crystals of RR02rec.

The technique itself is extremely straightforward in principle – it relies on evaporation of water from a small droplet containing the protein and precipitating agents to a reservoir solution. The concentration of the protein and precipitants slowly increases as the water in the protein-containing drop equilibrates with the water in the reservoir, eventually causing nucleation and crystal growth. The solubility diagram for this process, and the two main types (sitting drop and hanging drop vapour diffusion) of experimental set-up are presented in figures 5.5 and 5.6 respectively.

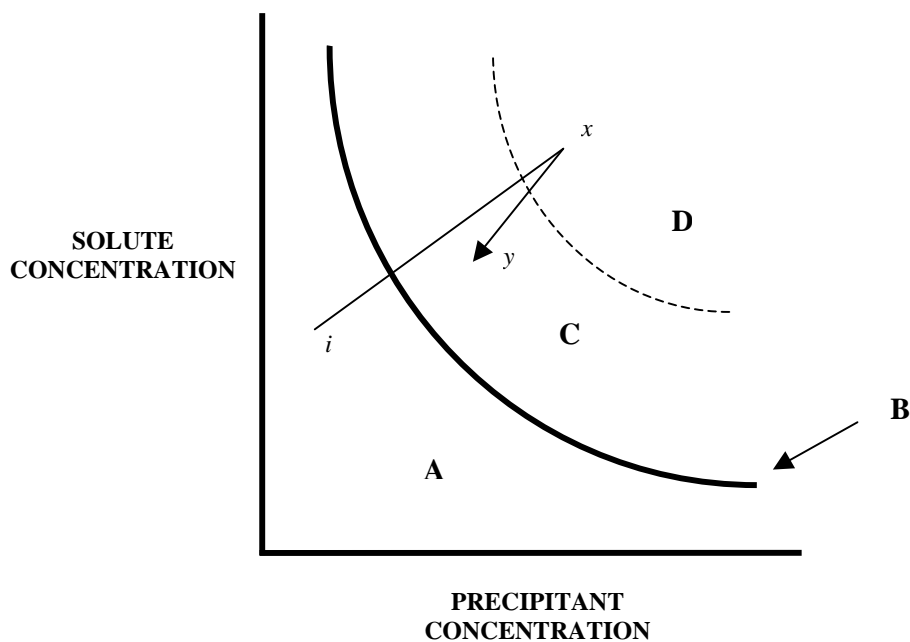


**Figure 5.5.** A typical solubility diagram for the crystallization of a macromolecule, plotting the solute concentration versus the precipitant concentration, where **B** is the limit of solubility, **A** represents the undersaturated region of the system and **C & D** represent the supersaturated region (with **C** being the metastable zone). Vapour diffusion driven crystal growth occurs when an undersaturated solution (point *i*) is brought into a supersaturated state (at point *x*) by means of diffusion of solvent from the protein-containing drop to the reservoir. When the system is sufficiently unstable nucleation can occur which, in turn, lowers the solute concentration, pushing the system towards the metastable zone where further nucleation is minimized (at point *y*).

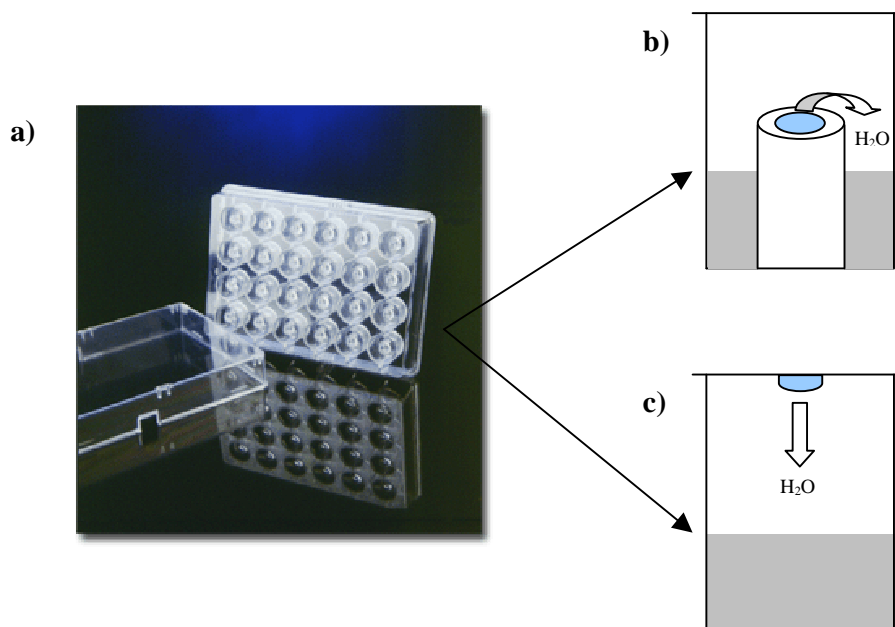


**Figure 5.6.** The schematics in (b) & (c) represent single well experimental set-ups for sitting drop vapour diffusion and hanging drop vapour diffusion respectively, all of which are performed in 24-well Cryschem<sup>TM</sup> plates (a) (Image reproduced with the kind permission of Hampton Research Corporation, Laguna Niguel, CA). Both methods work by ensuring the initial reagent concentration in the droplet (in blue) is less than that in the reservoir (in gray). Over time, the drop will approach supersaturation as the reagents are slowly concentrated via the loss of solvent to the reservoir.

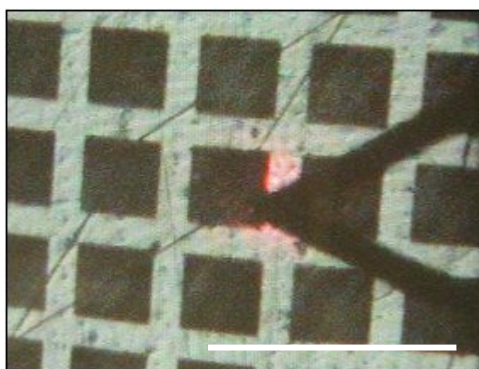


**Figure 5.7.** A typical RR02rec crystal that has been nucleated on an EM grid, and grown using sitting drop vapour diffusion methods. Scale bar, 200  $\mu\text{m}$ .

### 5.2.2.2 Crystallization screens and optimization

Promising crystallization conditions were initially identified using various commercially available sparse matrix screens (Hampton Research & Emerald BioStructures, Bainbridge Island, WA). 1ml of each screen was placed into the reservoir of a 24 well sitting drop plate (Hampton Research). A small drop (2-6  $\mu$ l) of purified protein solution was placed into the support bridge, followed by a small drop (0.5-6  $\mu$ l) of reservoir solution. The two solutions were briefly mixed with the pipette tip, and all wells were covered with CrystalClear sealing tape (Hampton Research) to prevent evaporation, and stored at room temperature.

Conditions displaying promising initial 'hits' were subsequently optimized using conditions prepared in-house, leading to the formation of relatively large, well-faceted crystals (see figure 5.4 for examples). Five conditions gave particularly promising crystals:

- Condition 1.* 200 mM magnesium acetate, 20 % PEG 6000, 100 mM sodium cacodylate (pH 6.6).
- Condition 2.* 20 % PEG 4000, 10 % IPA, 100 mM HEPES (pH 7.5).
- Condition 3.* 40 % PEG 300, 100 mM sodium acetate (pH 4.9).
- Condition 4.* 40 % PEG 300, 50 mM phosphate-citrate (pH 4.3).
- Condition 5.* 40 % PEG 400, 5 % PEG 1000, 100 mM Tris (pH 8.3).

However, all crystals grown from these conditions diffracted to low resolution ( $\sim 5$  Å). These crystals were subsequently investigated as possible candidates for AFM experiments.

### 5.2.3 Seed crystal growth for AFM experiments

As discussed at length in chapter 3 of this thesis, crystals must be adhered firmly to a substrate to undergo the raster scanning action of the AFM tip. To achieve this with RR02rec crystals, a series of optimization experiments were performed using the five

crystallization conditions and the TEM grid substrate utilized in chapters 3 & 4 of this thesis.

It quickly became clear that condition 2 offered the most promising crystals for AFM experimentation. The crystals formed from this condition were generally well faceted, reasonably large (up to ~200  $\mu\text{m}$  in length) and adhered strongly to the substrate, with a face parallel to the substrate surface. The crystals displayed a characteristic diamond shaped morphology, an example of which is displayed in figure 5.7.

The optimized conditions for growing RR02rec crystals on EM grid substrates by sitting drop vapour diffusion methods were as follows:

*Well.* 1.0 ml of 20 % PEG 4000, 10 % IPA, 100 mM HEPES (pH 7.5).

*Drop.* 3.4  $\mu\text{l}$  of protein solution, 0.6  $\mu\text{l}$  well solution.

The plates were kept in a vibration free area at room temperature. Growth of suitably sized seed crystals took approximately 72 hours. All AFM images in this chapter were obtained from crystals grown under the conditions described above.

#### 5.2.4 Imaging conditions

The author was severely restricted by the limited quantity of RR02rec protein solution available throughout (approximately 70 mg for the entire study). Inevitably, this lack of protein prevented the investigation of RR02rec crystals growing *in situ* with AFM. As such, the well crystallization conditions specified above were used as the imaging solution. This is discussed further in the results section below.

#### 5.2.5 AFM analysis

Prior to imaging, all samples were observed by *ex situ* optical microscopy to assess the optical quality of the crystals. The most promising (usually those samples

that contained well faceted, crack-free crystals) were removed from the crystallization plate and inserted into the AFM together with the liquid cell, which was equipped with a plastic o-ring to minimize solvent evaporation. The cell was subsequently flooded with imaging solution and, using the optical microscope integrated into the AFM system, the cantilever was positioned above a crystal that displayed a face of interest parallel to the substrate. Imaging was begun immediately.

All images were recorded using a DI multimode atomic force microscope, which was equipped with a Nanoscope IIIa controller (Veeco, Santa Barbara, CA). Silicon nitride NP-S cantilevers with a nominal spring constant of  $0.1 \text{ Nm}^{-1}$  were used throughout (Veeco). The DI multimode was equipped with an E-type scanner with maximum scan dimensions of  $13 \mu\text{m} \times 13 \mu\text{m} \times 2 \mu\text{m}$ .

Contact mode imaging was not suitable for the collection of images due to the extreme fragility of the RR02rec crystals (see results section below). As such, the NP-S cantilevers were operated in tapping mode at resonant frequency, which is approximately in the region of 8-10 kHz. All images presented throughout this study are in the form of topography data and were collected at  $512 \times 512$  pixel resolution, at a scan rate in the range of 3-5 Hz.

## 5.2 Results

It quickly became clear that the RR02rec crystals were very difficult to image as a consequence of their extremely fragile nature. Using contact mode to investigate the crystals was impossible due to the surface becoming heavily scarred almost immediately after the onset of scanning, with crystals occasionally becoming dislodged from the supporting EM grid substrates even when minimum force was applied to the surface (data not shown). As such, tapping mode imaging was implemented in an attempt to minimize the forces applied to the crystal surface.

Whilst tapping mode undoubtedly alleviated many of the problems, it was still imperative that the absolute minimum force was applied to the crystal surface during imaging by continually monitoring and adjusting the AFM setpoint voltage. Figure 5.8 contains two tapping mode images that exemplify the damage sustained by the crystal when the minimum force was not used during scanning.

When optimum imaging parameters were implemented attaining images of the RR02rec crystals without damaging their surfaces became feasible. Figure 5.9 contains three arbitrary images of RR02rec crystals obtained under the conditions outlined in the materials and methods section above.

As with all of the crystals studied throughout this thesis, the RR02rec crystal surfaces were relatively flat and exhibited step edges. Occasionally, images were of a clarity sufficient to obtain measurements of the step edge dimensions, an example of which is displayed in figure 5.9(a) with the corresponding section analysis data in figure 5.9(b). The steps were consistently measured as being approximately 11 nm in height.

As briefly discussed above the pure protein solution was not used during the imaging experiments, as it was not available in sufficient quantity. As a consequence, supersaturated conditions could not be obtained and evidence of dissolution was observed on a handful of the crystal surfaces during imaging in the form of etch pits, as illustrated in figure 5.9(c) & (d) (and in the undamaged areas of figure 5.8(a)). Similar to the etch pits observed on adipic acid crystals (see section 2.3.3 of this thesis), the pits took on the overall shape and orientation of the seed crystal (in this case a diamond shape, as illustrated in figure 5.7). They ranged from a single layer in depth (as in figure 5.9(d)) up to approximately 10 layers deep.

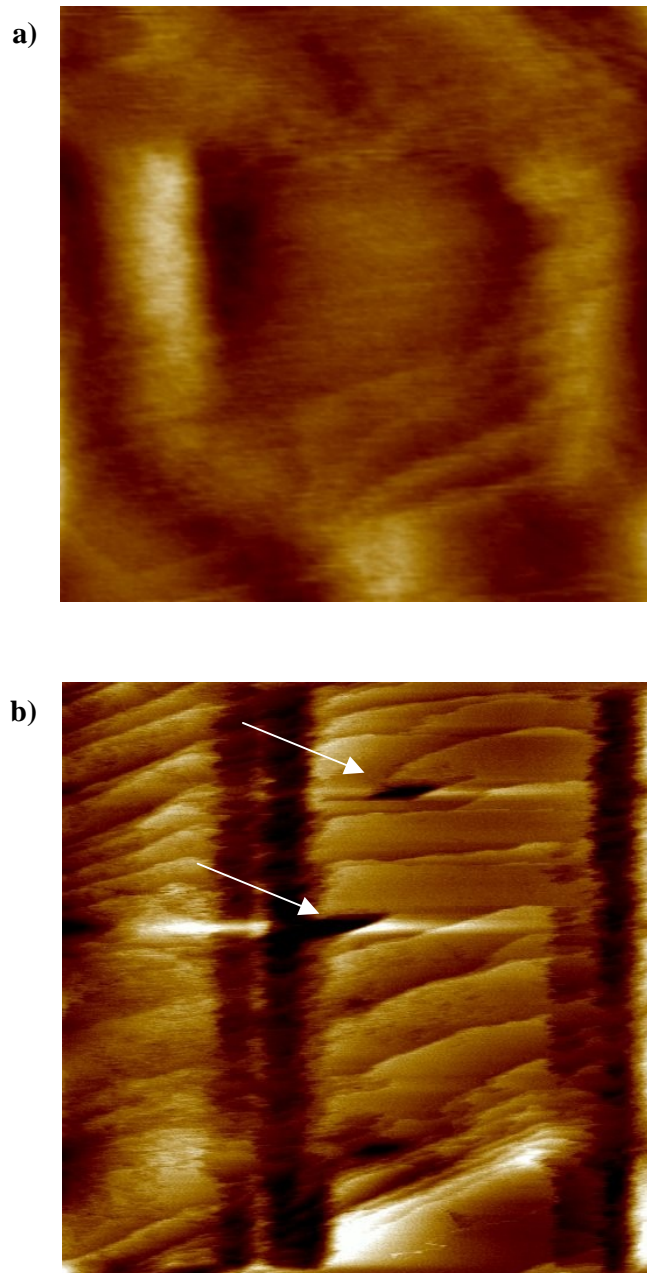


**Figure 5.8.** AFM tip induced scarring on the surfaces of RR02rec crystals. In (b), etch pits are also clearly visible in undamaged areas, examples of which are highlighted with the white arrows. Scan sizes & z-ranges **a)** 2 μm x 2 μm, 25 nm; **b)** 5 μm x 5 μm, 50 nm.

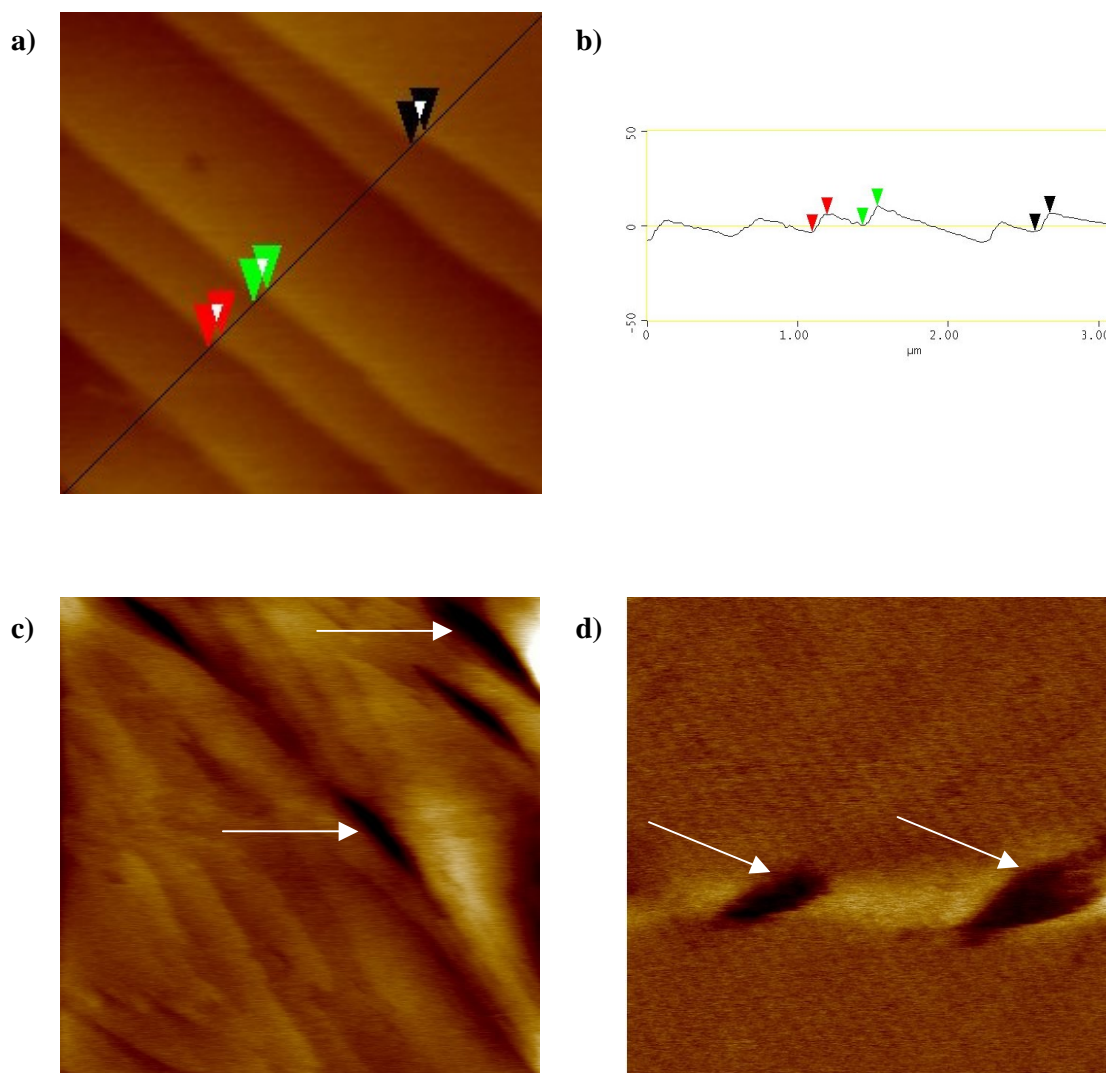


**Figure 5.9.** Arbitrary images of the surface of RR02rec crystals. Step edges were measured to be approximately 11 nm in height as illustrated in (a) & (b). Etch pits were also apparent on some of the crystals investigated, examples of which are presented in (c) & (d). Scan sizes & z-ranges a) 2.5 μm x 2.5 μm, 100 nm; c) 5 μm x 5 μm, 100 nm; d) 600 nm x 600 nm, 10 nm.

Etch pit formation is a common observation on the surface of macromolecular crystals suspended in an undersaturated solution as a consequence of defects in the crystal lattice. At such sites, there is an increased level of lattice strain, which means the chemical potential is higher than in ordered areas – as such, dissolution occurs preferentially at disordered sites. It is thought that pits one layer deep are probably due to point defects in the lattice, whilst deeper pits are a consequence of foreign particle absorption that are believed to cause localized stress in the top few layers of the lattice (Malkin *et al.*, 1999b).

It is clear from the images obtained of the slightly etched crystals that impurities and point defects are present within the RR02rec crystal lattice. However, a more interesting observation derived from the AFM data is the almost complete lack of more ‘serious’ planar defects such as stacking faults and screw dislocations. In fact, throughout the whole series of experiments only one screw dislocation was observed on any crystal surface. This image is presented in figure 5.10.

Similar to the etch pits displayed in figure 5.9, the screw dislocation and resulting step edges clearly exhibit the same morphology as the crystal itself. Indeed, the shape of the crystal and dislocation permit a simple length/width measurement to be taken, which reveals a practically identical ratio existing between the macroscopic photograph ( $L/W = 4.25$ ) and microscopic AFM image ( $L/W = 4.32$ ). This is an excellent illustration of the anisotropic nature of the RR02rec crystals grown from these conditions.

Using the crystallizing solution as the imaging medium in the AFM experiments had advantages and disadvantages. Clearly, the lack of protein meant *in situ* growth experiments could not be performed, which was a severe limitation. However, the crystallizing solution itself did provide a surprisingly stable imaging environment, with a complete lack of uncontrolled dissolution. This allowed the crystals to be imaged at molecular resolution on a number of separate occasions. One such image is displayed in figure 5.11(a), with its corresponding Fourier filtered image in 5.11(b). The observed periodicities were consistently in the region of 22 nm and 10 nm.

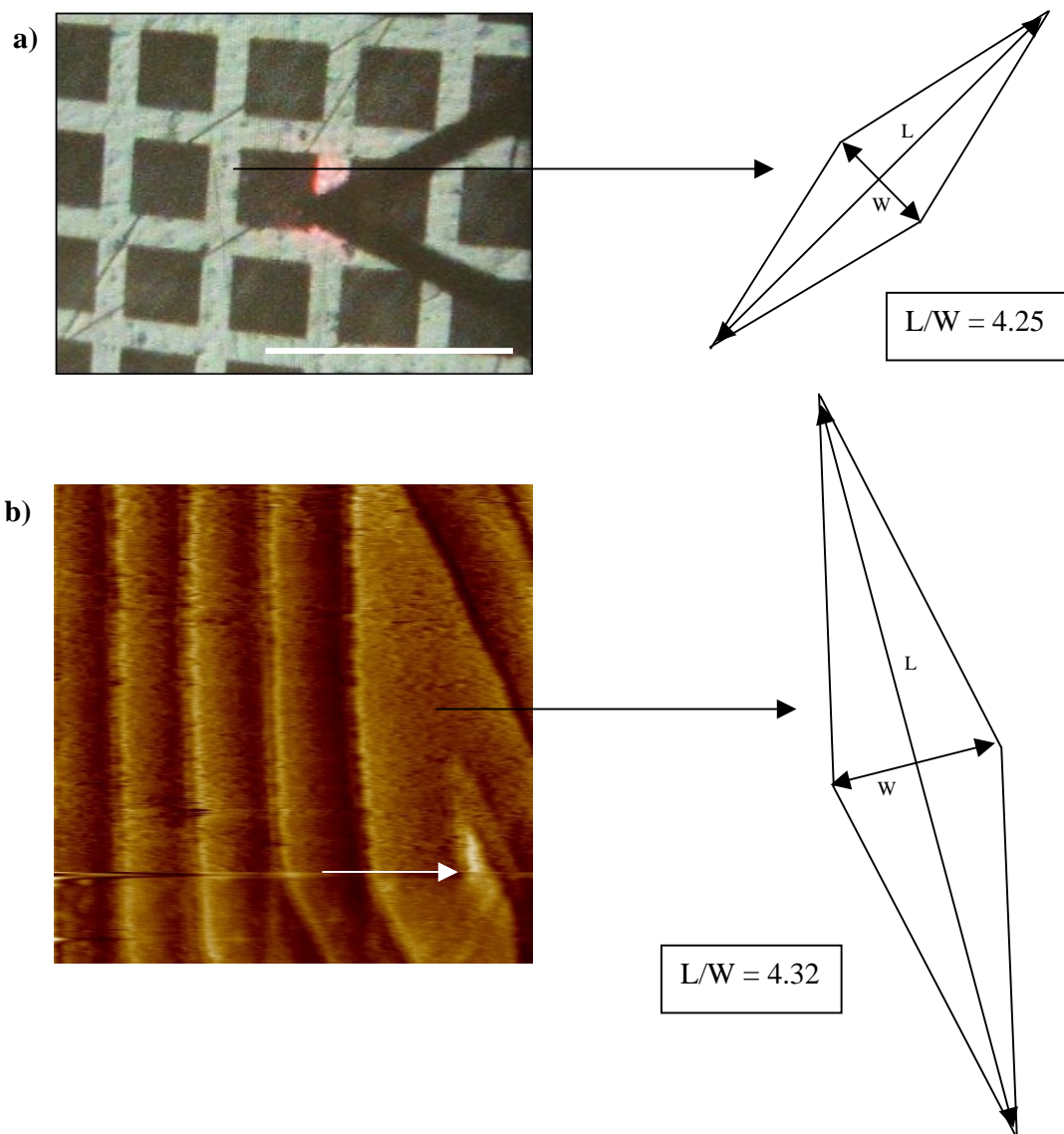


**Figure 5.10.** Anisotropy in RR02rec crystals. In (a), the  $L/W$  ratio derived from the photograph of the crystal is approximately 4.25. This figure compares directly to the  $L/W$  value of 4.32 measured from the screw dislocation clearly observable in the AFM image in (b), the centre of which is highlighted by the white arrow. Scan size & z-range of (b)  $13\ \mu\text{m} \times 13\ \mu\text{m}$ , 40 nm. Scale bar in (a),  $200\ \mu\text{m}$ .

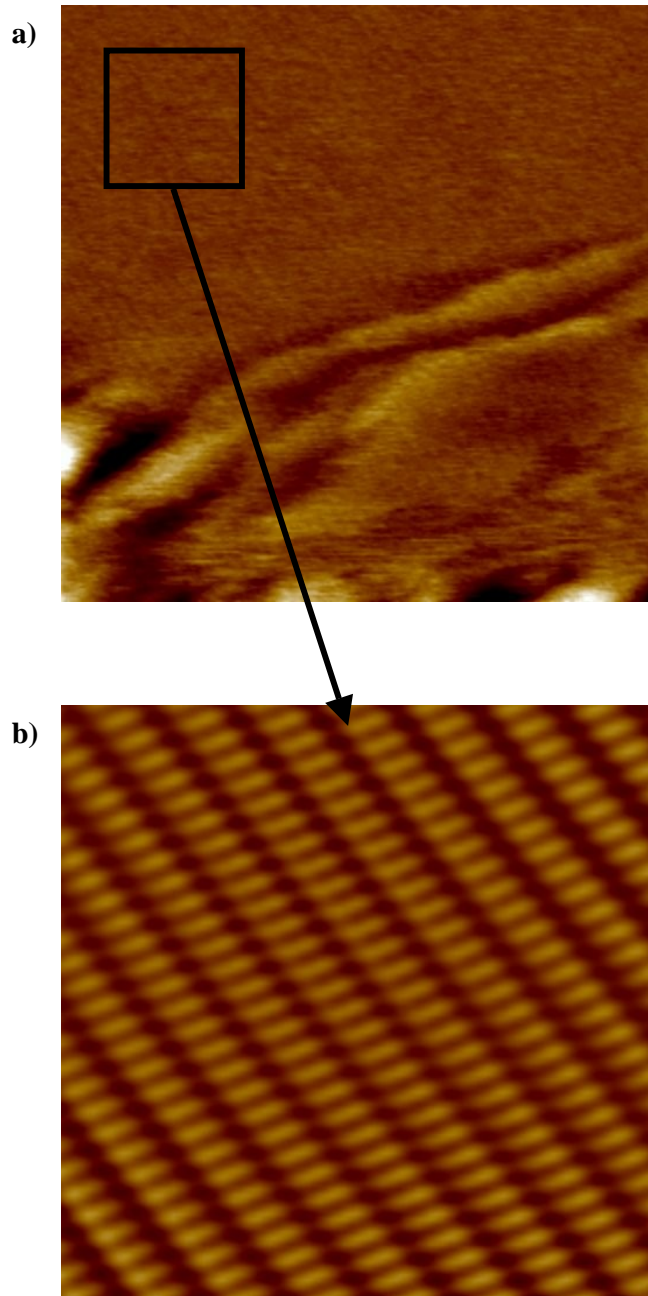


**Figure 5.11.** (a) A  $1\ \mu\text{m} \times 1\ \mu\text{m}$  image of the surface of an RR02rec crystal at lattice resolution. (b) A  $200\ \text{nm} \times 200\ \text{nm}$  portion of this image post-FFT, showing strong periodicities at approximately  $22\ \text{nm}$  and  $10\ \text{nm}$ . Z-ranges, **a)**  $50\ \text{nm}$ , **b)**  $2\ \text{nm}$ .

## 5.4 Discussion

Whilst the studies presented in this chapter were undoubtedly limited by the small quantities of pure protein available, the AFM images obtained may give some indication as to why the RR02rec crystals grown using the conditions outlined above diffracted poorly.

The first interesting observation was the apparent mechanical weakness of the RR02rec crystals, as illustrated in figure 5.8. It must be noted that macromolecular crystals generally are fragile assemblies of molecules, with numerous previous AFM studies having to employ tapping mode in order to avoid scarring the crystal surface (McPherson *et al.*, 2000). However, what is interesting in this case is that RR02rec and lysozyme are both small proteins displaying identical molecular weights, and yet lysozyme was not once damaged during scanning, even when employing contact mode imaging. This suggests, empirically at least, that there may be significant discrepancies between the strength of bonding present in the lysozyme and RR02rec crystal lattices.

The next point of particular note was the almost complete lack of severe linear and planar defects present in the RR02rec crystals. The vast majority of lysozyme images presented throughout this thesis contained at least one screw dislocation or stacking fault – however, stacking faults were never observed in the RR02rec crystals, whilst just one screw dislocation was observed (see figure 5.10).

On first consideration, it seems feasible that the lower the number of severe defects, the better the crystal quality. However, this may not necessarily be the case. A rigorously structured lattice (such as seen with lysozyme crystals) may in fact be more prone to defect formation, as it will be significantly more sensitive to the incorporation of impurities. As impurities are incorporated into the lattice, stress will accumulate and quickly be relieved via the formation of linear and planar defects. In contrast, a less rigorous lattice is likely to be more tolerant to the incorporation of impurities, and suffer significantly less lattice strain. When this is the case, the less rigorous lattice will both display a smaller quantity of severe defects and diminished long-range order (McPherson *et al.*, 2003).

The theory that the RR02rec crystals grown from these specific conditions may not exhibit a particularly rigorous lattice is further borne out by the lattice-resolution imaging carried out on the crystals (see figure 5.11), which display a seemingly well-

ordered crystal lattice exhibiting periodicities in the region of 22 nm and 10 nm. However, when compared with the various molecular resolution images and interplanar spacing of the lysozyme crystal, the periodicities and interplanar spacing exhibited by the RR02rec crystal are unusually large. This is graphically illustrated in figure 5.12, where 100 nm x 100 nm sections of the various macromolecular crystal faces studied throughout this thesis are presented.

The relatively large periodicities observed on the RR02rec crystals indicate the possibility of the formation of large RR02rec oligomeric growth units. Indeed, this possibility has previously been investigated using dynamic light scattering techniques (DLS). Such experiments showed that at low protein concentration (~2 mg/ml) the only species present in solution was the monomeric form of RR02rec. As this concentration was increased to 5 mg/ml, dimers were observed and finally at 10 mg/ml, higher order oligomers were present in solution (Bent and Riboldi-Tunnicliffe, 2004).

This could be a significant factor in the relatively poor diffraction properties of the RR02rec crystals. The crystals were grown by vapour diffusion, so it is quite plausible that the protein solution concentration rises above the 10mg/ml level investigated by DLS. This leads to a situation that may be best viewed as a crystallizing system within a crystallizing system – for the production of high quality crystals, the protein monomers must initially arrange themselves into accurately repeating oligomers, which in turn must form a rigorous crystal lattice suitable for X-ray diffraction studies.

This situation is, of course, far from ideal for the growth of high quality crystals. The first ‘crystallizing system’ (the monomeric ↔ dimeric ↔ oligomeric relationship) is likely to be dynamic, and as the vapour diffusion process alters the concentration of the protein drop, oligomers of various sizes will inevitably become incorporated into the crystal lattice. This will undoubtedly cause significant levels of statistical disorder and variety of packing within the growth units, in turn seriously compromising the X-ray diffraction resolution. Additionally we have shown by AFM that the crystal lattice is mechanically weak and non-rigorous, which suggests the oligomeric growth units themselves do not pack together particularly well – inevitably, this will further compromise the diffraction properties of the crystals grown from these conditions.

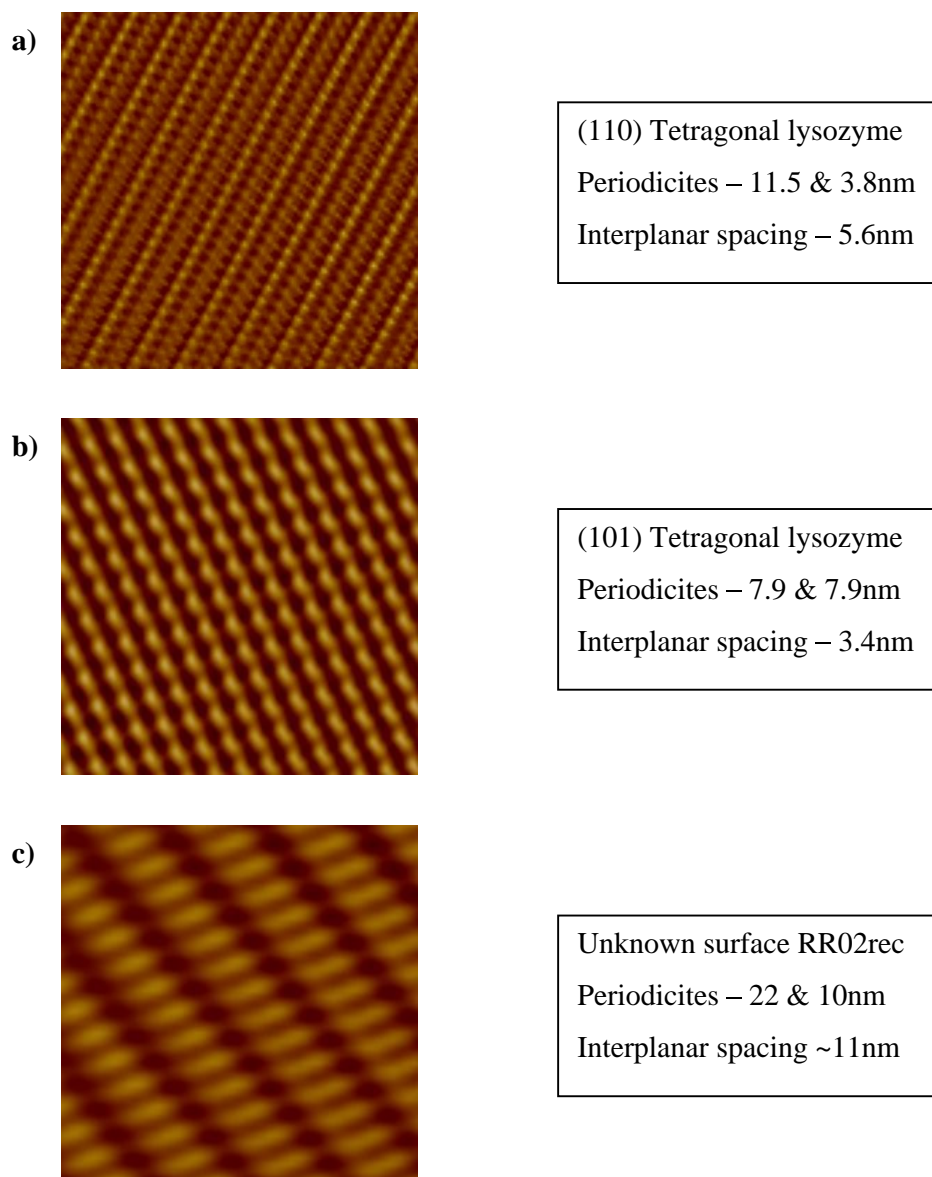


**Figure 5.12.** 100 x 100nm FFT images of the (110) face of tetragonal lysozyme (a), the (101) face of tetragonal lysozyme (b) and RR02rec (c).

During the course of this study, the structure of RR02rec was finally determined at atomic resolution ( $\sim 1.9 \text{ \AA}$ ) using a series of new crystallizing conditions (Bent *et al.*, 2003; Bent *et al.*, 2004). Figure 5.13 contains a darkfield microscopy image of the crystals that provided the data, the crystallization conditions implemented in their growth and an atomic model of RR02rec. Interestingly, the crystallographic data showed the RR02rec molecule does indeed form a symmetrical dimer at a specific monomer-monomer interface. However, how the dimers interact with one another to form the higher order oligomers was not determined.

With the view to further improving the understanding of RR02rec crystallization, high quality crystals of the protein were grown for the purpose of AFM experimentation. Unfortunately however, it ultimately proved impossible to image these crystals because they would not adhere to any substrate material, which is obviously a pre-requisite for meaningful AFM studies. A possible reason for this is that the crystals grew out of a precipitate, as shown in the light microscope image in figure 5.13(a). This precipitate probably coated all surfaces prior to nucleation, thus minimizing the strength of adhesion between crystal and substrate.

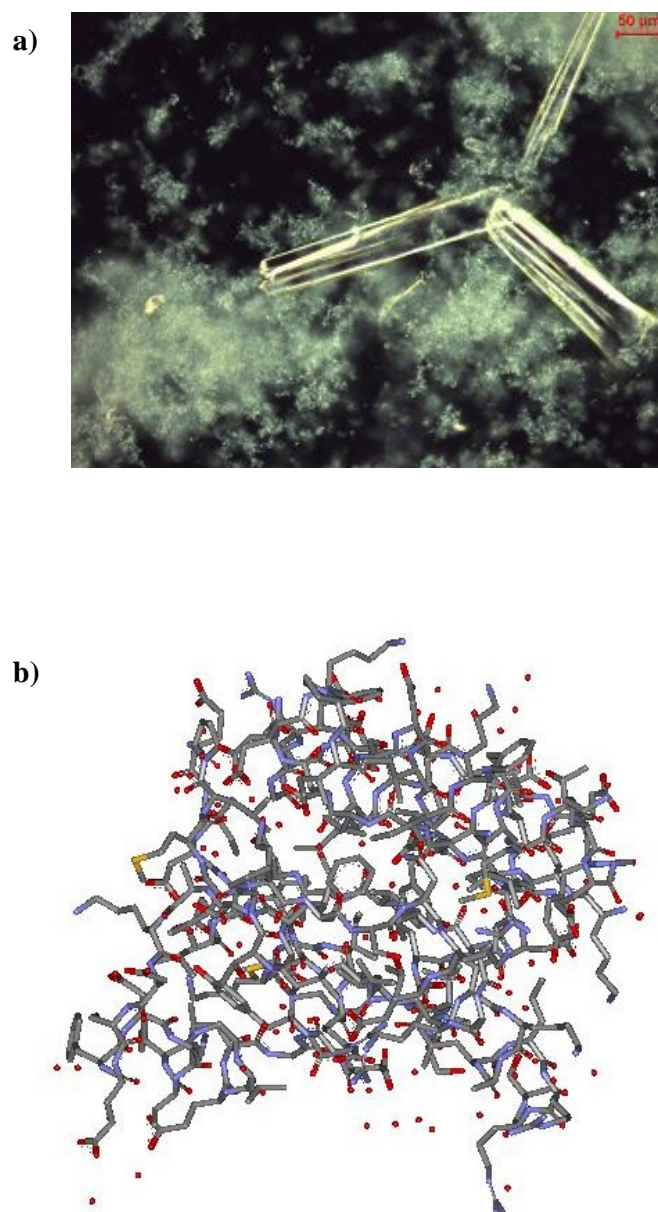


**Figure 5.13.** (a) High quality RR02rec crystals, grown from 40 % PEG 300, 100 mM citrate buffer (pH 5.9). (b) A model of RR02rec attained from atomic resolution diffraction data ( $\sim 1.9 \text{ \AA}$ ) (Bent et al., 2003; Bent et al., 2004).

## 5.5 Conclusions

The determination of biomolecular structure is very much dependent on the growth of highly ordered macromolecular crystals for use in X-ray diffraction experiments. Unfortunately, this is often a difficult task and is generally agreed to represent the most persistent and frustrating obstacle to the structural determination process.

In this study we have attempted to investigate some of the problems associated with macromolecular crystal quality by investigating a poorly-diffracting protein crystal with *in situ* AFM, and comparing the results with those obtained from earlier studies of lysozyme. The protein investigated, RR02rec, is an important response regulator protein found in *Streptococcus pneumoniae*, a Gram-positive bacterial pathogen that is one of the leading causes of illness and death in infants, the elderly and immunocompromised patients worldwide.

RR02rec was crystallized with relative ease in a number of different forms, all of which diffracted to a relatively poor resolution ( $\sim 5$  Å). These crystals were subsequently investigated as possible candidates for AFM experiments, with one condition giving particularly promising crystals after optimization.

Whilst experimental conditions were severely limited by the small quantities of protein available during these studies, AFM imaging was possible on both the microscopic and nanoscopic scale. These studies indicated a number of factors that may have contributed to the relatively poor diffraction properties of the crystal. Firstly, the lattice appeared to be comparatively less rigorous than that of the lysozyme crystals studied in previous chapters. This was indicated by the extremely poor mechanical properties of the crystal, along with the marked lack of linear and planar defects such as stacking faults and screw dislocations. Secondly, the lattice resolution imaging revealed unusually large periodic features that are inconsistent with small protein molecules such as RR02rec (which, like lysozyme, has a RMM of  $\sim 14$  kDa). This suggested the protein molecules might associate in solution prior to, or during crystallization – indeed, DLS studies performed on the pure protein solution showed that as the concentration of protein was increased, the monomers associated first to dimers, and then to higher order oligomers.

Inevitably the presence of dynamic, concentration dependant oligomeric species will add significant levels of disorder to the crystal, particularly as vapour diffusion methods act to further concentrate the protein-containing drop prior to nucleation. Additionally, if these oligomers do not pack together well (as indicated by the AFM studies) it seems feasible the diffraction resolution will suffer, as indicated by the initial poor resolution data obtained of these crystals.

## Chapter

# 6

## General Conclusions

The work presented in this thesis has centred on the application of *in situ* AFM to the study of a number of important aspects of both molecular and macromolecular crystallization. Four crystal systems were studied – adipic acid, tetragonal lysozyme, monoclinic lysozyme and Response Regulator 02 receiver domain – all of which were grown from solution. The fundamental physical chemistry underlying solution-grown crystallization systems is briefly introduced in chapter 1 of this thesis, along with a review of the techniques previously used in crystal growth studies. Literature reviews outlining previous studies of pharmaceutical and macromolecular crystallization using AFM have also been included.

The first experimental study presented in this thesis concerned the crystallization and habit modification of adipic acid, a small organic molecule used as a pharmaceutical excipient in effervescent tablet formulations, and as a tablet lubricant. When crystallized, adipic acid takes the form of a thin plate dominated by the (100) face. This surface is constructed entirely of carboxylic acid groups, making it extremely hydrophilic in nature. It has long been theorized that the chemical nature of this surface plays an important role in many of the interesting characteristics of crystalline adipic acid, but no direct experimental evidence of this has ever been achieved. It was with this overall aim in mind that *ex situ* and *in situ* AFM experiments were performed on the (100) face of adipic acid.

Large, well-faceted seed crystals were initially grown using a temperature lowering method. A series of preliminary *ex situ* studies were then carried out, in which the step heights on the (100) face were measured and compared favourably to the crystallographic interplanar distance. During the course of these *ex situ* studies solute reorganization was observed during scanning both in contact and tapping mode. This is a rarely-reported phenomenon which, using the force-distance capabilities of AFM, was investigated and explained as a possible consequence of the hydrophilic nature of the surface permitting local tip-enhanced dissolution and reorganization of the solute. *In situ* imaging carried out on the seed crystals subsequently revealed the formation of etch pits during dissolution, which was also attributed to the presence of bound water on the (100) face.

The behaviour of the (100) surface in the presence of the structurally-related habit modifier octanoic acid was also investigated. Initially, doped seed crystals were grown and studied using AFM and SEM. These studies showed that although there seemed to be an increased level of stress within the lattice, the development of the (100) face was apparently unaffected by the presence of relatively low levels of the additive, with the (100) surface retaining its morphological dominance. This observation was confirmed by carrying out *in situ* experiments, which showed that the presence of low levels of additive had little effect on the development of the (100) surface, presumably because the strongly adsorbed water layer is able to reject the majority of the more hydrophobic alkanolic acid molecules. However, as the concentration of octanoic acid was progressively increased during these *in situ* experiments, the surface began to exhibit clear changes in step morphology and growth mode. Indeed, at elevated concentrations of octanoic acid, growth on the (100) face was completely inhibited.

It is clear from this study that AFM is well suited to the analysis of crystalline pharmaceutical materials, particularly with respect to their surface-specific interactions with impurities and additives. It is our belief that a relatively straightforward set of experiments can shed a considerable amount of light on the morphological aspects of impurity uptake into crystalline materials, a subject of considerable importance in the pharmaceutical industry.

The production of highly ordered macromolecular crystals for use in X-ray diffraction experiments is one of the most important, yet difficult, parts of the structural determination process. Many of the problems associated with macromolecular crystal

growth stems from the relatively poor fundamental understanding of the technique as a whole.

Until recently, macromolecular crystals were almost impossible to study directly as a consequence of their small size, and extremely fragile nature. However, the advent of instruments such as AFM has dispelled many of these problems, leading to vast improvements in the fundamental understanding of the subject over the past decade.

The results presented in chapter 3 of this thesis concern the crystallization of the model protein molecule lysozyme. Lysozyme was selected for this study as it is generally regarded as a relatively straightforward macromolecule to crystallize in the tetragonal form, and would allow the development of the protocols necessary to produce seed crystals of macromolecules for use in AFM experiments.

After carrying out a series of optimization experiments, we were able to produce seed crystals that were adhered to a substrate firmly enough to undergo the raster scanning motion of the AFM tip. A series of supersaturation-controlled growth experiments were subsequently carried out on the (110) face of the crystal. These studies indicated that, as expected, lowering the value of supersaturation progressively lowered both the quantity and tangential growth velocity of the steps. It also became clear that the step edges were not formed uniformly by a single growth mechanism, but by up to three mechanisms operating concurrently. Additionally, one of the mechanistic observations made during this study (the promotion of multilayered stacks by the edges of adsorbed microcrystals) has not, to the author's knowledge, previously been reported for any crystal system. Measurements taken of the step heights indicated the growth units for both faces were dimeric in height, rather than monomeric, an observation in keeping with the generally accepted growth model for the tetragonal lysozyme crystal.

With careful control of both the crystallization conditions and AFM imaging parameters molecular resolution images of both the (110) and (101) surfaces were obtained. After performing 2D Fast Fourier Transformations (2D FFTs) to remove noise from the images, the periodic features were analysed and shown to conform precisely to the known 2D unit cell measurements for the respective crystallographic faces.

Lysozyme has long been known to crystallize in a number of different forms. Two of these polymorphs – the tetragonal and orthorhombic – have now been studied in

significant detail. However, the other polymorphs have not been investigated in any such detail, and comparatively little is known about them.

In chapter 4 of this thesis, *in situ* AFM has been used to study the  $(10\bar{1})$  face of the monoclinic polymorph of crystalline lysozyme. Seed crystals of the monoclinic form were grown from conditions similar to those used to grow the tetragonal form in chapter 3. Initial experiments performed at high protein and precipitant concentrations revealed a surface covered with densely packed step edges, the majority of which had apparently been formed from the numerous screw dislocations that littered the crystal surface. Screw dislocations were undoubtedly the dominant growth mechanism, possibly as a consequence of the tightly-packed crystal lattice and relatively small interplanar distance on the  $(10\bar{1})$  face. Molecular resolution images were obtained of the surface that highlighted periodicities corresponding to the crystallographic data, allowing the tetragonal and monoclinic forms of crystalline lysozyme to be unambiguously distinguished from one another on a molecular level.

The final study presented in this thesis concerns the growth and AFM analysis of a poorly diffracting crystals constructed from a protein found in *Streptococcus pneumoniae*, Response Regulator 02 receiver domain (RR02rec).

By utilizing the experimental protocols developed throughout previous studies, crystals were grown and adhered to substrates using vapour diffusion methods and subsequently investigated using tapping mode AFM. By comparison with the images obtained of the lysozyme crystals in earlier chapters, a number of factors that may have contributed to the crystals poor diffraction properties were identified and discussed. The crystals were mechanically very weak, and displayed a marked lack of planar and linear dislocations. This indicated the lattice might be markedly non-rigorous, a theory seemingly further borne out by the unusually large lattice periodicities observable during molecular resolution imaging. The apparent oligomerization present in this system was also discussed and related to both the AFM images obtained, and the low-resolution data previously seen during X-ray studies.

The results presented in the last three experimental chapters of this thesis are testament to the considerable strengths exhibited by AFM when applied to the study of macromolecular crystals. In each study we were able to obtain both micro- and nanoscale images of extraordinary clarity and detail. The molecular resolution images

obtained were particularly instructive. We believe that as tip geometries are improved with the implementation of, for example, carbon nanotube technology, AFM will play an increasingly important role in obtaining structural information from biological crystals inadequate for X-ray diffraction studies.

In conclusion, the results presented throughout this thesis have revealed a range of new molecular scale details concerning the structure and growth of four crystal systems important to both pharmaceutical technologists and structural biologists alike. It is clear that *in situ* AFM is a technique well suited to such studies and, in conjunction with continuing developments in AFM technology in areas such as tip dimensions, will begin to play an increasingly vital role in the characterization and understanding of numerous aspects of crystallization from solution.

## References

- Alderton, G. and Fevold, H. L. (1946). Direct crystallization of lysozyme from egg-white and some crystalline salts of lysozyme. *J. Biol. Chem.*, **164**: 1-5.
- Allen, S., Davies, M. C., Roberts, C. J., Tendler, S. J. B. and Williams, P. M. (1997). Atomic force microscopy in analytical biotechnology. *Tibtech.*, **15**: 101-105.
- AlonsoDeVelasco, E., Verheul, A. F. M., Verhoef, J. and Snippe, H. (1995). Streptococcus pneumoniae: virulence factors, pathogenesis and vaccines. *Am. Soc. Microbiol.*, **59**: 591-603.
- Aquilano, D., Veesler, S., Astier, J. P. and Pastero, L. (2003). Polymorphic-polytypic transition induced in crystals by interaction of spirals and 2D growth mechanisms. *J. Crystal Growth*, **247**: 541-550.
- Artymiuk, P. J., Blake, C. C. F., Rice, D. W. and Wilson, K. S. (1982). The structures of the monoclinic and orthorhombic forms of hen egg-white lysozyme at 6Å resolution. *Acta crystallogra.*, **B38**: 778-783.
- Astier, J. P., Bokern, D., Lapena, L. and Veesler, S. (2001).  $\alpha$ -amylase crystal growth investigated by in situ atomic force microscopy. *J. Crystal Growth*, **226**: 294-302.
- Atkins, P. (1998). Physical chemistry, Oxford University Press, Oxford, UK.
- Aulton, M. E., Ed. (1988). Pharmaceuticals - the science of dosage form design. Churchill Livingstone, New York.
- Bent, C. J., Isaacs, N. W., Mitchell, T. J. and Riboldi-Tunncliffe, A. (2003). Cloning, overexpression, purification, crystallization and preliminary diffraction analysis of the receiver domain of MicA. *Acta crystallogra.*, **D59**: 758-760.
- Bent, C. J., Isaacs, N. W., Mitchell, T. J. and Riboldi-Tunncliffe, A. (2004). Crystal structure of the response regulator 02 receiver domain, the essential YycF two-component system of Streptococcus pneumoniae in both complexed and native states. *J. Bacteriol.*, **186**(9): 2872-2879.
- Bent, C. J. and Riboldi-Tunncliffe, A. (2004). Personal communication.
- Bergfors, T. (2003). Seeds to crystals. *J. Struct. Biol.*, **142**: 66-76.
- Berman, H. M., Westbrook, J., Feng, Z., Gilliland, G., Bhat, T. N., Weissig, H., Shindyalov, I. N. and Bourne, P. E. (2000). The protein data bank. *Nucl. Acid. Res.*, **28**: 235-242.
- Bernal, J. D. and Crowfoot, D. (1934). X-ray photographs of crystalline pepsin. *Nature*, **133**: 794-795.

- Berthou, J. and Jolles, P. (1978). Extension of the transition phenomenon in hen egg-white lysozyme crystals : the case of monoclinic crystals. *Biochim.*, **60**: 209-210.
- Best, R. B., Brockwell, D. J., Toca-Herrera, J. L., Blake, A. W., Smith, D. A., Radford, S. E. and Clarke, J. (2003). Force mode atomic force microscopy as a tool for protein folding studies. *Anal. Chim. Acta*, **479**(1): 87-105.
- Binnig, G., Quate, C. F. and Gerber, C. (1986). Atomic force microscope. *Phys. Rev. Lett.*, **56**: 930-933.
- Binnig, G. and Rohrer, H. (1982). Scanning tunneling microscopy. *Helv. Phys. Acta.*, **55**: 726-735.
- Binnig, G., Rohrer, H., Gerber, C. and Weibel, E. (1982). Tunneling through a controllable vacuum gap. *Appl. Phys. Lett.*, **40**: 178-180.
- Blake, C. C., Johnson, L. N., Mair, G. A., North, A. C. T., Phillips, D. C. and Sarma, V. R. (1967). Crystallographic studies of the activity of hen egg-white lysozyme. *Proc. Roy. Soc. B*, **167**: 378-388.
- Blake, C. C., Koenig, D. F., Mair, G. A., North, A. C., Phillips, D. C. and Sarma, V. R. (1965). Structure of hen egg-white lysozyme — a three-dimensional Fourier synthesis at 2 Å resolution. *Nature*, **206**: 757-761.
- Blow, D. M. (2002). Outline of crystallography for biologists. Oxford University Press, Oxford, UK.
- Blundell, T. L. and Johnson, L. N. (1976). Protein crystallography. Academic Press, New York.
- Boerrigter, S. X. M., Cuppen, H. M., Ristic, R. I., Sherwood, J. N., Bennema, P. and Meekes, H. (2002). Explanation for the supersaturation-dependent morphology on monoclinic paracetamol. *Crys. Grow. Des.*, **2**(5): 357-361.
- Braun, N., Tack, J., Fischer, M., Bacher, A., Bachmann, L. and Weinkauff, S. (2000). Electron microscopic observations of protein crystallization: adsorption layers, aggregates and crystal defects. *J. Crystal Growth*, **212**: 270-282.
- Breyton, C., Haase, W., Rapoport, T. A., Kuhlbrandt, W. and Collinson, I. (2002). Three-dimensional structure of the bacterial protein-translocation complex SecYEG. *Nature*, **418**: 662-665.
- Burnham, N. A. and Colton, R. J. (1989). Measuring the nanomechanical properties and surface forces of materials using an atomic force microscope. *J. Vac. Sci. Tech. A*, **7**: 2906-2913.
- Burton, W. K., Cabrera, N. and Frank, F. C. (1951). The growth of crystals and the equilibrium structure of their surfaces. *Phil. Trans. R. Soc. Lond.*, **A243**: 299-358.

- Cabrera, N. and Vermilyea, D. A. (1958). The growth of crystals from solution. Growth and perfection of crystals. R. H. Doremus and D. Turnbull, Wiley, New York: 393-410.
- Cacioppo, E. and Pusey, M. L. (1991). The solubility of the tetragonal form of hen egg white lysozyme from pH 4.0 to 5.4. *J. Crystal Growth*, **114**: 286-292.
- Camesano, T. A., Natan, M. J. and Logan, B. E. (2000). Observation of changes in bacterial cell morphology using tapping mode atomic force microscopy. *Langmuir*, **16**(10): 4563-4572.
- Cappella, B. and Dietler, G. (1999). Force-distance curves by atomic force microscopy. *Surf. Sci. Rep.*, **34**: 1-104.
- Caylor, C., Dobrianov, I., Lemay, S. G., Kimmer, C., Kriminski, S., Finkelstein, K. D., Zipfel, W., Webb, W. W., Thomas, B. R., Chernov, A. A. and Thorne, R. E. (1999). Macromolecular impurities and disorder in protein crystals. *Proteins: Struct. Func. Gen.*, **36**: 270-281.
- Chan, H.-K. and Grant, D. J. W. (1989). Influence of compaction on the intrinsic dissolution rate of modified acetaminophen and adipic acid crystals. *Int. J. Pharm.*, **57**: 117-124.
- Chayen, N. E. (2002). Tackling the bottleneck of protein crystallization in the post-genomic era. *Tibtech.*, **20**(3): 98.
- Chayen, N. E., Radcliffe, J. W. and Blow, D. M. (1993). Control of nucleation in the crystallization of lysozyme. *Protein Sci.*, **2**: 113-118.
- Chayen, N. E. and Saridakis, E. (2001). Is lysozyme really the ideal model protein? *J. Crystal Growth*, **232**: 262-264.
- Chen, X. Y. (2004). Laboratory of Biophysics and Surface Analysis website, accessible at [www.nottingham.ac.uk/lbsa](http://www.nottingham.ac.uk/lbsa).
- Chernov, A. A. (1984). Modern Crystallography, Vol. III, Crystal Growth, Springer-Verlag, Berlin.
- Chernov, A. A. (1997). Crystals built of biological macromolecules. *Phys. Rep.*, **288**: 61-75.
- Chernov, A. A., Rashkovich, L. N., Yaminsky, I. V. and Gvozdev, N. V. (1999). Kink kinetics, exchange fluxes, 1D 'nucleation' and adsorption on the (010) face of orthorhombic lysozyme crystals. *J. Phys.: Condens. Matter*, **11**: 9969-9984.
- Chow, A. H.-L., Chow, P. K. K., Zhongshan, W. and Grant, D. J. W. (1985a). Modification of acetaminophen crystals: influence of growth in aqueous solutions containing p-acetoxyacetanilide on crystal properties. *Int. J. Pharm.*, **24**: 239-258.

- Chow, A. H.-L. and Grant, D. J. W. (1988a). Modification of acetaminophen crystals. II. Influence of stirring rate during solution-phase growth on crystal properties in the presence and absence of p-acetoxyacetanilide. *Int. J. Pharm.*, **41**: 29-39.
- Chow, A. H.-L. and Grant, D. J. W. (1988b). Modification of acetaminophen crystals. III. Influence of initial supersaturation during solution-phase growth on crystal properties in the presence and absence of p-acetoxyacetanilide. *Int. J. Pharm.*, **42**: 123-133.
- Chow, K. Y., Go, J. and Grant, D. J. W. (1986). Influence of fatty acid additives on the dissolution behavior of adipic acid crystals. *Drug Dev. Ind. Pharm.*, **12**(3): 247-264.
- Chow, K. Y., Go, J., Mehdizadeh, M. and Grant, D. J. W. (1984). Modification of adipic acid crystals : influence of growth in the presence of fatty acid additives on crystal properties. *Int. J. Pharm.*, **20**: 3-24.
- Chow, K. Y., Go, J., Zhongshan, W., Mehdizadeh, M. and Grant, D. J. W. (1985b). Modification of adipic acid crystals. II. Influence of growth in the presence of oleic acid on crystal properties. *Int. J. Pharm.*, **25**: 41-55.
- Crick, F. H. C. (1953). The unit cells of four proteins. *Acta crystallogra.*, **6**: 221-222.
- Cullis, A. F., Muirhead, H., Perutz, M. F., Rossmann, M. G. and North, A. C. T. (1962). The structure of haemoglobin IX. A three-dimensional Fourier synthesis at 5.5Å resolution: description of the structure. *Proc. Roy. Soc., A*, **265**: 161-187.
- Danesh, A., Chen, X., Davies, M. C., Roberts, C. J., Sanders, G. H. W., Tendler, S. J. B., Williams, P. M. and Wilkins, M. J. (2000a). Polymorphic discrimination using atomic force microscopy: Distinguishing between two polymorphs of the drug cimetidine. *Langmuir*, **16**: 866-870.
- Danesh, A., Connell, S. D., Davies, M. C., Roberts, C. J., Tendler, S. J. B., Williams, P. M. and Wilkins, M. J. (2001). An *in situ* dissolution study of aspirin crystal planes (100) and (001) by atomic force microscopy. *Pharm. Res.*, **18**: 299-303.
- Danesh, A., Davies, M. C., Hinder, S. J., Roberts, C. J., Tendler, S. J. B., Williams, P. M. and Wilkins, M. J. (2000b). Surface characterization of aspirin crystal planes by dynamic chemical force microscopy. *Anal. Chem.*, **72**: 3419-3422.
- Davey, R. J. (2001). Personal communication.
- Davey, R. J., Black, S. N., Logan, D., Maginn, S. J., Fairbrother, J. E. and Grant, D. J. W. (1992). Structural and kinetic features of crystal growth inhibition : adipic acid growing in the presence of n-alkanoic acids. *J. Chem. Soc. Faraday Trans.*, **88**(23): 3461-3466.
- Davey, R. J. and Garside, J. (2000). From molecules to crystallizers - An introduction to crystallization, Oxford University Press, Oxford, UK.

- Davey, R. J., Mullin, J. W. and Whiting, M. J. L. (1982). Habit modifications of succinic acid crystals grown from different solvents. *J. Crystal Growth*, **58**: 304-312.
- Davies, M. and Griffiths, D. M. L. (1953). Solubilities of di-carboxylic acids in benzene and aqueous solutions. *Trans. Faraday Soc.*, **49**: 1405-1410.
- Davis, A. F. and Hadgraft, J. (1991). Effect of supersaturation on membrane transport: 1. Hydrocortisone acetate. *Int. J. Pharm.*, **76**: 1-8.
- DeLucas, L. J., Moore, K. M., Long, M. M., Rouleau, R., Bray, T., Crysel, W. and Weise, L. (2002). Protein crystal growth in space, past and future. *J. Crystal Growth*, **237-239**: 1646-1650.
- Dobrianov, I., Caylor, C., Lemay, S. G., Finkelstein, K. D. and Thorne, R. E. (1999). X-ray diffraction studies of protein crystal disorder. *J. Crystal Growth*, **196**: 511-523.
- Dobrianov, I., Finkelstein, K. D., Lemay, S. G. and Thorne, R. E. (1998). X-ray topographic studies of protein crystal perfection and growth. *Acta crystallogra.*, **D54**: 922-937.
- Doki, N., Yokota, M., Nakamura, H., Sasaki, S. and Kubota, N. (2003). Seeded batch cooling crystallization of adipic acid from ethanol solution. *J. Chem. Eng. Jap.*, **36**(8): 1001-1004.
- Drenth, J. (1994). Principles of protein X-ray crystallography. Springer-Verlag, New York.
- Ducruix, A. and Giege, R., Eds. (1992). Crystallization of nucleic acids and proteins. IRL Press at OUP, Oxford, UK.
- Durbin, S. D. and Carlson, W. E. (1992). Lysozyme crystal growth studied by atomic force microscopy. *J. Crystal Growth*, **122**: 71-79.
- Durbin, S. D., Carlson, W. E. and Saros, M. T. (1993). *In situ* studies of protein crystallization by atomic force microscopy. *J. Phys. D Appl. Phys.*, **26**: 128-132.
- Durbin, S. D. and Feher, G. (1986). Crystal growth studies of lysozyme as a model for protein crystallization. *J. Crystal Growth*, **76**: 583-592.
- Durbin, S. D. and Feher, G. (1990). Studies of crystal growth mechanisms of proteins by electron microscopy. *J. Mol. Biol.*, **212**: 763-774.
- Durbin, S. D. and Feher, G. (1996). Protein crystallization. *Annu. Rev. Phys. Chem.*, **47**: 171-204.
- Fairbrother, J. E. (1981). Effects of trace additives on the crystal growth rate and habit of a pharmaceutical excipient, adipic acid., Thesis, University of Nottingham.
- Fairbrother, J. E. and Grant, D. J. W. (1978). Crystal engineering studies with an excipient material (adipic acid). *J. Pharm. Pharmacol.*, **31S**: 27P.

- Fairbrother, J. E. and Grant, D. J. W. (1979). The habit modification of a tablet lubricant, adipic acid. *J. Pharm. Pharmacol.*, **30S**: 19P.
- Fermani, S., Falini, G., Minnucci, M. and Ripamonti, A. (2001). Protein crystallization on polymeric film surfaces. *J. Crystal Growth*, **224**: 327-334.
- Florence, A. T. and Attwood, D. (1988). Physicochemical principles of pharmacy, Macmillan Press, Chatham.
- Florence, A. T. and Salole, E. G. (1976). Changes in crystallinity and solubility on comminution of digoxin and observations on spironolactone and oestradiol. *J. Pharm. Pharmacol.*, **28**: 637-642.
- Forsythe, E. L., Nadarajah, A. and Pusey, M. L. (1999a). Growth of (101) faces of tetragonal lysozyme crystals: measured growth-rate trends. *Acta crystallogra.*, **D55**: 1005-1011.
- Forsythe, E. L., Snell, E. H., Malone, C. C. and Pusey, M. L. (1999b). Crystallization of chicken egg white lysozyme from assorted sulfate salts. *J. Crystal Growth*, **196**: 332-343.
- Frank, F. C. (1949). The influence of dislocations on crystal growth. *Faraday Discuss. Che. Soc.*, **5**: 48-54.
- Frank, F. C. (1951). Capillary equilibria of dislocated crystals. *Acta cryst.*, **4**: 497-501.
- Garcia-Ruiz, J. M. (2003). Nucleation of protein crystals. *J. Struct. Biol.*, **142**: 22-31.
- Garnier, S., Petit, S. and Coquerel, G. (2002). Influence of supersaturation and structurally related additives on the crystal growth of alpha-lactose monohydrate. *J. Crystal Growth*, **234**: 201-219.
- Gliko, O., Reviakine, I. and Vekilov, P. G. (2003). Stable equidistant step trains during crystallization of insulin. *Phys. Rev. Lett.*, **90**(22): 1-4.
- Guo, S., Ward, M. D. and Wesson, J. A. (2002). Direct visualization of calcium oxalate monohydrate crystallization and dissolution with atomic force microscopy and the role of polymeric additives. *Langmuir*, **18**: 4284-4291.
- Hafner, J. H., Cheung, C. L., Wooley, A. T. and Mieber, C. M. (2001). Structural and functional imaging with carbon nanotubes. *Prog. Biophys. Mol. Biol.*, **77**: 73-110.
- Haleblian, J. K. (1975). Characterization of habits and crystalline modification of solids and their pharmaceutical applications. *J. Pharm. Sci.*, **64**: 1269-1287.
- Hansma, P. K., Cleveland, J. P., Radmacher, M., Walters, D. A., Hillner, P. E., Bezanilla, M., Fritz, M., Vie, D., Hansma, H. G., Prater, C. B., Massie, J., Fukunage, L., Gurley, J. and Elings, V. (1994). Tapping mode atomic force microscopy in liquids. *Appl. Phys. Lett.*, **64**: 1738-1740.

- Hartman, P. and Perdok, W. G. (1955). On the relationship between structure and morphology of crystals I, II & III. *Acta crystallogra.*, **8**: 49-53, 521-524, 525-529.
- Hendriksen, B. A. and Grant, D. J. W. (1995). The effect of structurally related substances on the nucleation kinetics of paracetamol (acetaminophen). *J. Crystal Growth*, **156**: 252-260.
- Hendriksen, B. A., Grant, D. J. W., Meenan, P. and Green, D. A. (1998). Crystallization of paracetamol (acetaminophen) in the presence of structurally related substances. *J. Crystal Growth*, **183**: 629-640.
- Hobbs, J. K., Humphris, A. D. L. and Miles, M. J. (2001). In-situ atomic force microscopy of polyethylene crystallization. 1. Crystallization from an orientated backbone. *Macromolecules*, **34**: 5508-5519.
- Hogle, J., Rao, S. T., Mallikarjunan, M., Beddell, C., McMullan, R. K. and Sundaralingam, M. (1981). Studies of monoclinic hen egg white lysozyme. 1. Structure solution at 4Å resolution and molecular packing comparisons with tetragonal and triclinic lysozymes. *Acta crystallogra.*, **B37**: 591-597.
- Hondoh, H., Sazaki, G., Miyashita, S., Durbin, S. D., Nakajima, K. and Matsuura, Y. (2001). Macromorphology analysis of the macro- and micromorphology of monoclinic lysozyme crystal. *Crys. Grow. Des.*, **1**(4): 327-332.
- Housty, J. and Hospital, M. (1965). Localisation des atomes d'hydrogène dans l'acide adipique COOH[CH<sub>2</sub>]COOH. *Acta Crystallogra.*, **18**: 693-697.
- Jandt, K. D. (2001). Atomic force microscopy of biomaterial surfaces and interfaces. *Surf. Sci.*, **491**: 303-332.
- Jiang, X. N., Sun, D. L., Xu, D., Yuan, D. R., Lu, M. K., Guo, S. Y. and Fang, Q. (2001). Investigation of growth modes of cadmium mercury thiocyanate crystal by atomic force microscopy. *J. Crystal Growth*, **233**: 196-207.
- Jiang, X. N., Xu, D., Sun, D. L., Yuan, D. R., Lu, M. K., Guo, S. Y. and Zhang, G. H. (2002a). Ex situ atomic force microscopy studies of growth mechanisms of cadmium mercury thiocyanate crystals. *J. Crystal Growth*, **234**: 480-486.
- Jiang, X. N., Xu, D., Yuan, D. R., Sun, D. L., Lu, M. K. and Jiang, M. H. (2002b). Atomic force microscopy studies on phase transitions and surface morphology transformation of CMTC crystals. *Appl. Phys. A*, **75**: 617-620.
- Johnson, L. N. and Phillips, D. C. (1965). Structure of some crystalline lysozyme-inhibitor complexes determined by X-ray analysis at 6 Å resolution. *Nature*, **206**: 761-763.
- Jolles, P. and Berthou, J. (1972). High temperature crystallization of lysozyme: An example of phase transition. *FEBS Lett.*, **23**(1): 21-23.

- Keel, T. R., Thompson, C., Davies, M. C., Tendler, S. J. B. and Roberts, C. J. (2004). AFM studies of the crystallization and habit modification of an excipient material, adipic acid. *Int. J. Pharm.*, **280**, 185-198.
- Kipp, S., Lacmann, R. and Schneeweiss, M. A. (1995). Problems in temperature control performing in situ investigations with the scanning force microscope. *Ultramic.*, **57**: 333-335.
- Ko, T.-P., Kuznetsov, Y. G., Malkin, A. J., Day, J. and McPherson, A. (2001). X-ray diffraction and atomic force microscopy analysis of twinned crystals: rhombohedral canavalin. *Acta Crystallogra.*, **D57**: 829-839.
- Konnert, J. H., D'Antonio, P. and Ward, K. B. (1994). Observation of growth steps, spiral dislocations and molecular packing on the surface of lysozyme crystals with the atomic force microscope. *Acta Crystallogra.*, **D50**: 603-613.
- Kuhlbrandt, W. and Williams, K. A. (1999). Analysis of macromolecular structure and dynamics by electron cryo-microscopy. *Curr. Opin. Struct. Biol.*, **3**: 537-543.
- Kundrot, C. E., Judge, R. A., Pusey, M. L. and Snell, E. H. (2001). Microgravity and macromolecular crystallography. *Crys. Grow. Des.*, **1**(1): 87-99.
- Kuznetsov, Y. G., Konnert, J., Malkin, A. J. and McPherson, A. (1999a). The advancement and structure of growth steps on thaumatin crystals visualized by atomic force microscopy at molecular resolution. *Surf. Sci.*, **440**: 69-80.
- Kuznetsov, Y. G., Malkin, A. J., Glantz, W. and McPherson, A. (1996a). In situ atomic force microscopy studies of protein and virus crystal growth mechanisms. *J. Crystal Growth*, **168**: 63-73.
- Kuznetsov, Y. G., Malkin, A. J., Greenwood, A. and McPherson, A. (1995). Interferometric studies of growth kinetics and surface morphology in macromolecular crystal growth - canavalin, thaumatin and turnip yellow mosaic virus. *J. Struct. Biol.*, **114**: 184-196.
- Kuznetsov, Y. G., Malkin, A. J., Greenwood, A. and McPherson, A. (1996b). Michelson interferometric studies of protein and virus crystal growth. *J. Crystal Growth*, **166**: 913-918.
- Kuznetsov, Y. G., Malkin, A. J., Land, T. A., DeYoreo, J. J., Barba, A. P., Konnert, J. and McPherson, A. (1997). Molecular resolution imaging of macromolecular crystals by atomic force microscopy. *Biophys. J.*, **72**: 2357-2364.
- Kuznetsov, Y. G., Malkin, A. J. and McPherson, A. (1998). Atomic force microscopy studies of phase separations in macromolecular systems. *Phys. Rev. B*, **58**(10): 6097-6103.
- Kuznetsov, Y. G., Malkin, A. J. and McPherson, A. (1999b). AFM studies of the nucleation and growth mechanisms of macromolecular crystals. *J. Crystal Growth*, **196**: 489-502.

- Kuznetsov, Y. G., Malkin, A. J. and McPherson, A. (2001). The influence of precipitant concentration on macromolecular crystal growth mechanisms. *J. Crystal Growth*, **232**: 114-118.
- Lacapere, J. J., Stokes, D. L. and Chatenay, D. (1992). Atomic force microscopy of three-dimensional membrane protein crystals. *Biophys. J.*, **63**: 303-308.
- Land, T. A. and DeYoreo, J. J. (2000). The evolution of growth modes and activity of growth sources on canavalin investigated by in situ atomic force microscopy. *J. Crystal Growth*, **208**: 623-637.
- Land, T. A., DeYoreo, J. J. and Lee, J. D. (1997). An in situ investigation of canavalin crystallization kinetics. *Surf. Sci.*, **384**: 136-155.
- Land, T. A., Malkin, A. J., Kuznetsov, Y. G., McPherson, A. and DeYoreo, J. J. (1995). Mechanisms of protein crystal growth: an atomic force microscopy study of canavalin crystallization. *Phys. Rev. Lett*, **75**: 2774-2777.
- Lange, R., Wagner, C., de Saizieu, A., Flint, N., Monlnos, J., Stieger, M., Caspers, P., Kamber, M., Keck, W. and Amrein, K. E. (1999). Domain organization and molecular characterization of 13 two-component systems identified by genome sequencing of *Streptococcus pneumoniae*. *Gene*, **237**: 223-234.
- Li, H., Nadarajah, A. and Pusey, M. L. (1999a). Determining the molecular-growth mechanisms of protein crystal faces by atomic force microscopy. *Acta Crystallogra.*, **D55**: 1036-1045.
- Li, H., Perozzo, M. A., Konnert, J. H., Nadarajah, A. and Pusey, M. L. (1999b). Determining the molecular-packing arrangements on protein crystal faces by atomic force microscopy. *Acta Crystallogra.*, **D55**: 1023-1035.
- Li, M., Nadarajah, A. and Pusey, M. L. (1999c). Growth of (101) faces of tetragonal lysozyme crystals: determination of the growth mechanism. *Acta Crystallogra.*, **D55**: 1012-1022.
- Li, T., Morris, K. R. and Park, K. (2000). Influence of solvent and crystalline supramolecular structure on the formation of etching patterns on acetaminophen single crystals: A study with atomic force microscopy and computer simulation. *J. Phys. Chem. B*, **104**: 2019-2032.
- Littke, W. and John, C. (1984). Protein crystal growth under microgravity. *Science*, **225**: 203-205.
- Luthi, R., Meyer, E., Howald, I., Haefke, H., Anselmetti, D., Dreier, M., Ruetsche, M., Bonner, T., Overney, R. M., Fromer, J. and Guntherodt, H. J. (1994). Progress in non-contact dynamic force microscopy. *J. Vac. Sci. Tech. B*, **12**: 1673-1676.
- MacGillavry, C. H. (1941). Title unknown. *Rec. Trav. Chim. Pays-Bas*, **60**: 605-608.

- Malkin, A. J., Kuznetsov, Y. G., Glantz, W. and McPherson, A. (1996a). Atomic force microscopy studies of surface morphology and growth kinetics in thaumatin crystallization. *J. Phys. Chem.*, **100**(28): 11736-11743.
- Malkin, A. J., Kuznetsov, Y. G., Land, T. A., DeYoreo, J. J. and McPherson, A. (1995a). Mechanisms of growth for protein and virus crystals. *Nat. Struct. Biol.*, **2**(11): 956-959.
- Malkin, A. J., Kuznetsov, Y. G., Lucas, R. W. and McPherson, A. (1999a). Surface processes in the crystallization of turnip yellow mosaic virus visualized by atomic force microscopy. *J. Struct. Biol.*, **127**: 35-43.
- Malkin, A. J., Kuznetsov, Y. G. and McPherson, A. (1996b). Defect structure of macromolecular crystals. *J. Struct. Biol.*, **117**: 124-137.
- Malkin, A. J., Kuznetsov, Y. G. and McPherson, A. (1996c). Incorporation of microcrystals by growing protein and virus crystals. *Proteins: Struct. Func. Gen.*, **24**: 247-252.
- Malkin, A. J., Kuznetsov, Y. G. and McPherson, A. (1997). An in situ AFM investigation of catalase crystallization. *Surf. Sci.*, **393**: 95-107.
- Malkin, A. J., Kuznetsov, Y. G. and McPherson, A. (1999b). In situ atomic force microscopy studies of surface morphology, growth kinetics, defect structure and dissolution in macromolecular crystallization. *J. Crystal Growth*, **196**: 471-488.
- Malkin, A. J., Land, T. A., Kuznetsov, Y. G., McPherson, A. and DeYoreo, J. J. (1995b). Investigation of virus crystal growth mechanisms by in situ atomic force microscopy. *Phys. Rev. Lett.*, **75**(14): 2778-2781.
- Malkin, A. J. and McPherson, A. (2002). Novel mechanisms for defect formation and surface molecular processes in virus crystallization. *J. Phys. Chem. B*, **106**: 6718-6722.
- Marshall, P. V. and York, P. (1991). The compaction properties of nitrofurantoin samples crystallized from different solvents. *Int. J. Pharm.*, **67**: 59-65.
- Martin, Y., Williams, C. C. and Wickramasinghe, J. (1987). Atomic force microscope force mapping and profiling on a sub 100-Å scale. *J. Appl. Phys.*, **61**(10): 4723-4729.
- Matsuzuki, Y., Kubota, T., Liu, X. Y., Ataka, M. and Takano, K. J. (2002). AFM observation of the surface morphology and impurity effects on orthorhombic hen egg-white lysozyme crystals. *J. Crystal Growth*, **242**: 199-208.
- Mauri, A. and Moret, M. (2000). Growth of potassium sulfate crystals in the presence of organic dyes: in situ characterization by atomic force microscopy. *J. Crystal Growth*, **208**: 599-614.
- McPherson, A. (1985). Crystallization of macromolecules: General principles. *Meth. Enzymology*, **114**: 112-120.

- McPherson, A. (1991). A brief history of protein crystal growth. *J. Crystal Growth*, **110**: 1-11.
- McPherson, A. (1999). Crystallization of biological macromolecules, Cold Spring Harbour Laboratory Press, New York.
- McPherson, A., Kuznetsov, Y. G., Malkin, A. J. and Plomp, M. (2003). Macromolecular crystal growth as revealed by atomic force microscopy. *J. Struct. Biol.*, **142**: 32-46.
- McPherson, A., Malkin, A. J. and Kuznetsov, Y. G. (2000). Atomic force microscopy in the study of macromolecular crystal growth. *Annu. Rev. Biophys. Biomol. Struct.*, **29**(1): 361-410.
- McPherson, A., Malkin, A. J., Kuznetsov, Y. G. and Koszelak, S. (1996). Incorporation of impurities into macromolecular crystals. *J. Crystal Growth*, **168**: 74-92.
- McPherson, A., Malkin, A. J., Kuznetsov, Y. G. and Plomp, M. (2001). Atomic force microscopy applications in macromolecular crystallography. *Acta Crystallogr.*, **D57**: 1053-1060.
- Mehta, S. C., Bernardo, P. D., Higuchi, W. I. and Simonelli, A. P. (1970). Rate of crystal growth of sulfathiazole and methylprednisole. *J. Pharm. Sci.*, **59**: 638-644.
- Michaels, A. S. and Colville, A. R. (1960). The effect of surface active agents on crystal growth rate and crystal habit. *J. Phys. Chem.*, **63**: 13-19.
- Michaels, A. S. and Tausch, F. W. (1961). Modification of growth rate and habit of adipic acid crystals with surfactants. *J. Phys. Chem.*, **64**: 1730-1737.
- Michinomae, M., Mochizuki, M. and Ataka, M. (1999). Electron microscopic studies on the initial process of lysozyme crystal growth. *J. Crystal Growth*, **197**: 257-262.
- Mohan, K. S., Das, S., Chockalingam, C., Shanthi, V. and Sekar, K. (2004). LySDB - Lysozyme Structural DataBase. *Acta crystallogr.*, **D60**: 597-600.
- Mollica, V., Borassi, A., Relini, A., Cavalleri, O., Bolognesi, M., Rolandi, R. and Gliozzi, A. (2001). An atomic force microscopy investigation of protein crystal surface topography. *Eur. Biophys. J.*, **30**: 313-318.
- Monaco, L. A. and Rosenberger, F. (1993). Growth and etching kinetics of tetragonal lysozyme. *J. Crystal Growth*, **129**: 465-484.
- Morris, V. J., Kirby, A. R. and Gunning, A. P. (1999). Atomic force microscopy for biologists, Imperial College Press, London, UK.
- Muhlig, P., Klupsch, T., Schell, U. and Hilgenfeld, R. (2001). Observation of the early stage of insulin crystallization by confocal laser scanning microscopy. *J. Crystal Growth*, **232**: 93-101.

- Muller, D. J., Fotiadis, D., Scheuring, S., Muller, S. A. and Engel, A. (1999). Electrostatically balanced subnanometer imaging of biological specimens by atomic force microscopy. *Biophys. J.*, **76**: 1101-1111.
- Mullin, J. W. (2001). Crystallization, Butterworth-Heinemann, Oxford.
- Myerson, A. S. and Jang, S. M. (1995). A comparison of binding energy and metastable zone width for adipic acid with various additives. *J. Crystal Growth*, **156**: 459-466.
- Nadarajah, A., Li, M. and Pusey, M. L. (1997). Growth mechanism of the (110) face of tetragonal lysozyme crystals. *Acta crystallogra.*, **D53**: 524-534.
- Nadarajah, A. and Pusey, M. L. (1996). Growth mechanism and morphology of tetragonal crystals. *Acta Crystallogra.*, **D52**: 983-996.
- Nakada, T., Sazaki, G., Miyashita, S., Durbin, S. D. and Komatsu, H. (1999). Direct AFM observations of impurity effects on a lysozyme crystal. *J. Crystal Growth*, **196**: 503-510.
- Nanev, C. N. and Tsekova, D. (2000). Heterogeneous nucleation of hen-egg-white lysozyme - Molecular approach. *Crys. Res. Tech.*, **35**(2): 189-195.
- Ng, J. D., Kuznetsov, Y. G., Malkin, A. J., Keith, G., Giege, R. and McPherson, A. (1997). Visualization of nucleic acid crystal growth by atomic force microscopy. *Nucl. Acid. Res.*, **25**(13): 2582-2588.
- Petsev, D. N., Thomas, B. R., Yau, S.-T. and Vekilov, P. G. (2000). Interactions and aggregation of apoferritin molecules in solution: effects of added electrolytes. *Biophys. J.*, **78**: 2060-2069.
- Pfefer, G. and Boistelle, R. (2000). Theoretical morphology of adipic acid crystals. *J. Crystal Growth*, **208**: 615-622.
- Plomp, M. (1999). Crystal growth studied on a micrometer scale, Thesis, University of Nijmegen, NL.
- Plomp, M., McPherson, A., Larson, S. B. and Malkin, A. J. (2001). Growth mechanisms and kinetics of trypsin crystallization. *J. Phys. Chem. B*, **105**: 542-551.
- Plomp, M., McPherson, A. and Malkin, A. J. (2002). Crystal growth of macromolecular crystals: correlation between crystal symmetry and growth mechanisms. *J. Crystal Growth*, **237-239**: 306-311.
- Plomp, M., McPherson, A. and Malkin, A. J. (2003). Repair of impurity-poisoned protein crystal surfaces. *Proteins: Struct. Func. Gen.*, **50**: 486-495.
- Pusey, M. L. and Nadarajah, A. (2002). A model for tetragonal lysozyme crystal nucleation and growth. *Crys. Grow. Des.*, **2**(6): 475-483.

- Radmacher, M., Fritz, M. and Hansma, P. K. (1995). Imaging soft samples with the atomic force microscope - gelatin in water and propanol. *Biophys. J.*, **69**(1): 264-270.
- Raghavan, S. L., Trividic, A., Davis, A. F. and Hadgraft, J. (2000). Effect of cellulose polymers on supersaturation and in vitro membrane transport of hydrocortisone acetate. *Int. J. Pharm.*, **193**: 231-237.
- Raghavan, S. L., Trividic, A., Davis, A. F. and Hadgraft, J. (2001). Crystallization of hydrocortisone acetate: influence of polymers. *Int. J. Pharm.*, **212**: 213-221.
- Rao, S. T., Hogle, J. and Sundaralingam, M. (1983). Studies of monoclinic hen egg white lysozyme. 2. The refinement at 2.5Å resolution conformational variability between the two independent molecules. *Acta crystallogra.*, **C39**: 237-240.
- Rao, S. T. and Sundaralingam, M. (1996). Studies of monoclinic hen egg-white lysozyme. IV. X-ray Refinement at 1.8Å resolution and a comparison of the variable regions in the polymorphic forms. *Acta Crystallogra.*, **D52**: 170-175.
- Rashkovich, L. N., Chernevich, T. G., Gvozdev, N. V., Shustin, O. A. and Yaminsky, I. V. (2001). Steps wandering on the lysozyme and KDP crystals during growth in solution. *Surf. Sci.*, **492**: L717-L722.
- Rashkovich, L. N., Gvozdev, N. V., Sil'nikova, M. I. and Chernov, A. A. (2002). Fluctuations on the step velocity and the generation of a dislocation spiral on the (101) face of monoclinic lysozyme crystals. *Cryst. Rep.*, **47**(5): 859-866.
- Rashkovich, L. N., Gvozdev, N. V. and Yaminsky, I. V. (1998). The mechanism of step motion in growth of lysozyme crystals. *Cryst. Rep.*, **43**(4): 696-700.
- Ries-Kautt, M. and Ducruix, A. (1989). Relative effectiveness of various ions on the solubility and crystal growth of lysozyme. *J. Biol. Chem.*, **264**: 745-748.
- Ristic, R. I., Finnie, S. and Sheen, D. B. (2001). Macro- and micromorphology of monoclinic paracetamol grown from pure aqueous solution. *J. Phys. Chem. B*, **105**: 9057-9066.
- Rodriguez-Hornedo, N. and Murphy, D. (1999). Significance of controlling crystallization mechanisms and kinetics in pharmaceutical systems. *J. Pharm. Sci.*, **88**(7): 651-660.
- Rong, L., Komatsu, H. and Yoda, S. (2002). Control of heterogeneous nucleation of lysozyme crystals by using Poly-L-Lysine modified substrate. *J. Crystal Growth*, **235**: 489-493.
- Rong, L., Yamane, T. and Niimura, N. (2000). Measurement and control of the crystal growth rate of tetragonal hen egg-white lysozyme imaged with an atomic force microscope. *J. Crystal Growth*, **217**: 161-169.
- Rosenberger, F. (1996). Protein crystallization. *J. Crystal Growth*, **166**: 40-54.

- Rossell, J. P., Allen, S., Davies, M. C., Roberts, C. J., Tendler, S. J. B. and Williams, P. M. (2003). Electrostatic interactions observed when imaging proteins with the atomic force microscope. *Ultramic.*, **96**: 37-46.
- Sauter, C., Otalora, F., Gavira, J. A., Vidal, O., Giege, R. and Garcia-Ruiz, J. M. (2001). Structure of tetragonal hen egg-white lysozyme at 0.94 angstrom from crystals grown by the counter-diffusion method. *Acta crystallogra.*, **57**: 1119-1126.
- Sazaki, G., Matsui, T., Tsukamoto, K., Usami, N., Ujihara, T., Fujiwara, K. and Nakajima, K. (2004). In situ observation of elementary growth steps on the surface of protein crystals by laser confocal microscopy. *J. Crystal Growth*, **262**: 536-542.
- Schaper, A., Georgalis, Y., Umbach, P., Raptis, J. and Saenger, W. (1997). Precrystallization structures in supersaturated lysozyme solutions studied by dynamic light scattering and scanning force microscopy. *J. Phys. Chem.*, **106**(20): 8587-8594.
- Scheuring, S., Fotiadis, D., Moller, C., Muller, S. A., Engel, A. and Muller, D. J. (2001). Single proteins observed by atomic force microscopy. *Single Mol.*, **2**: 59-67.
- Shekunov, B. Y. and Grant, D. J. W. (1997). In situ optical interferometric studies of the growth and dissolution behaviour of paracetamol (acetaminophen). 1. Growth kinetics. *J. Phys. Chem. B*, **101**: 3973-3979.
- Shekunov, B. Y., Grant, D. J. W., Latham, R. J. and Sherwood, J. N. (1997). In situ optical interferometric studies of the growth and dissolution behaviour of paracetamol (acetaminophen) crystals. 3. Influence of growth in the presence of p-acetoxyacetanilide. *J. Phys. Chem. B*, **101**: 9107-9112.
- Shekunov, B. Y. and York, P. (2000). Crystallization processes in pharmaceutical technology and drug delivery design. *J. Crystal Growth*, **211**: 122-136.
- Shimon, L. J. W., Lahav, M. and Leiserowitz, L. (1985). Design of stereoselective etchants for organic crystals. Application for the sorting of enantiomorphs and direct assignment of absolute configuration of chiral molecules. *J. Am. Chem. Soc.*, **107**: 3375-3377.
- Simonelli, A. P., Mehta, S. C. and Higuchi, W. I. (1970). Inhibition of sulfathiazole crystal growth by polyvinylpyrrolidone. *J. Pharm. Sci.*, **59**: 633-638.
- Slyter, E. M. and Slyter, H. S. (1992). Light and electron microscopy, Cambridge University Press, Cambridge, UK.
- Srinivasan, K., Sankaranarayanan, K., Thangavelu, S. and Ramasamy, P. (2000). Influence of organic solvents on the habit of NMBA (4-nitro-4'-methylbenzylidene aniline) crystals. *J. Crystal Growth*, **212**: 246-254.
- Steinrauf, L. K. (1959). Preliminary X-ray data for some new crystalline forms of b-lactoglobulin and hen egg white lysozyme. *Acta crystallogra.*, **12**: 77-79.

- Strom, C. S. and Bennema, P. (1997a). Combinatorial compatibility as habit-controlling factor in lysozyme crystallization .1. Monomeric and tetrameric F faces derived graph-theoretically. *J. Crystal Growth*, **173**: 150-158.
- Strom, C. S. and Bennema, P. (1997b). Combinatorial compatibility as habit-controlling factor in lysozyme crystallization .2. Morphological evidence for tetrameric growth units. *J. Crystal Growth*, **173**: 159-166.
- Thompson, C. (2003). Investigating the fundamentals of drug crystal growth using atomic force microscopy, Thesis, University of Nottingham.
- Thompson, C., Allen, S., Davies, M. C., Roberts, C. J., Tendler, S. J. B., Wilkins, M. J. and Williams, P. M. (2004). The effects of additives on the growth and morphology of paracetamol crystals. *Int. J. Pharm.*, **In Press**.
- Thompson, N. H., Fritz, M., Radmacher, M., Cleveland, J. P., Schmidt, C. F. and Hansma, P. K. (1996). Protein tracking and detection of protein motion using atomic force microscopy. *Biophys. J.*, **70**(5): 2421-2431.
- Throup, J. P., Koretke, K. K., Bryant, A. P., Ingraham, K. A., Chalker, A. F., Ge, Y., Marra, A., Wallis, N. G., Brown, J. R., Holmes, D. J., Rosenberg, M. and Burnham, K. R. (2000). A genomic analysis of two-component signal transduction in *Streptococcus pneumoniae*. *Mol. Microbiol.*, **35**(3): 566-576.
- Tsekova, D., Dimitrova, S. and Nanev, C. N. (1999). Heterogeneous nucleation (and adhesion) of lysozyme crystals. *J. Crystal Growth*, **196**: 226-233.
- Vaney, M. C., Broutin, I., Retailleau, P., Douangamath, A., Lafont, S., Hamiaux, C., Prange, T., Ducruix, A. and Ries-Kautt, M. (2001). Structural effects of monovalent anions on polymorphic lysozyme crystals. *Acta Crystallogra.*, **D57**: 929-940.
- Vekilov, P. G. and Alexander, J. I. D. (2000). Dynamics of layer growth in protein crystallization. *Chem. Rev.*, **100**: 2061-2089.
- Vekilov, P. G., Ataka, M. and Katsura, T. (1993). Laser Michelson interferometry investigation of protein crystal growth. *J. Crystal Growth*, **130**: 317-320.
- Vekilov, P. G., Lin, H. and Rosenberger, F. (1997). Unsteady crystal growth due to step-bunch cascading. *Phys. Rev. E*, **55**: 3202-3214.
- Vekilov, P. G. and Rosenberger, F. (1996). Dependence of lysozyme growth on step sources and impurities. *J. Crystal Growth*, **158**: 540-551.
- Vergara, A., Lorber, B., Zagari, A. and Giege, R. (2003). Physical aspects of protein crystal growth investigated with the Advanced Protein Crystallization Facility in reduced-gravity environments. *Acta Crystallogra.*, **D59**: 2-15.
- Weissbuch, I., Popovitz-Biro, R., Lahav, M. and Leiserowitz, L. (1985). Understanding and control of nucleation, growth, habit, dissolution and structure and two- and three-dimensional crystals using 'tailor-made' auxiliaries. *Acta Crystallogra.*, **B51**: 115-148.

- Werten, P. J. L., Remigy, H.-W., de Groot, B. L., Fotiadis, D., Philippsen, A., Stahlberg, H., Grubmuller, H. and Engel, A. (2002). Progress in the analysis of membrane protein structure and function. *FEBS Lett.*, **529**: 65-72.
- Wiechmann, M. (2002). Personal communication.
- Wiechmann, M., Enders, O., Zeilinger, C. and Kolb, H.-A. (2001). Analysis of protein crystal growth at molecular resolution by atomic force microscopy. *Ultramic.*, **86**: 159-166.
- Wienczek, J. M. (1999). New strategies for protein crystal growth. *Annu. Rev. Biomed. Eng.*, **1**: 505-534.
- Wilkins, S. J., Coles, B. A., Compton, R. G. and Cowley, A. (2002). Mechanism and kinetics of salicylic acid dissolution in aqueous solution under defined hydrodynamic conditions via atomic force microscopy: the effects of the ionic additives NaCl, LiCl and MgCl<sub>2</sub>, the organic additives 1-propanol, 2-propanol, and the surfactant sodium dodecyl sulphate. *J. Phys. Chem. B*, **106**: 4763-4774.
- Wilkins, S. J., Suarez, M. F., Hong, Q., Coles, B. A., Compton, R. G., Tranter, G. E. and Firmin, D. (2000). Atomic force microscopy under defined hydrodynamic conditions: Three-dimensional flow calculations applied to the dissolution of salicylic acid. *J. Phys. Chem. B*, **104**(7): 1539-1545.
- Williams-Seton, L., Davey, R. J., Lieberman, H. F. and Pritchard, R. G. (2000). Disorder and twinning in molecular crystals : impurity induced effects in adipic acid. *J. Pharm. Sci.*, **89**(3): 346-354.
- Wilson, L. J., Adcock, L. D. and Pusey, M. L. (1993). A dialysis technique for determining aggregate concentrations in crystallizing protein solutions. *J. Phys. D Appl. Phys.*, **26**(8B): 113-117.
- Winn, D. and Doherty, M. F. (1998). A new technique for predicting the shape of solution-grown organic crystals. *A.I.Ch.E Journal*, **44**: 2501.
- Winn, D. and Doherty, M. F. (2002). Predicting the shape of organic crystals grown from polar solvents. *Chem. Eng. Sci.*, **57**: 1805-1813.
- Wood, W. M. L. (2001). A bad (crystal) habit - and how it was overcome. *Powder Tech.*, **121**: 53-59.
- Yaminsky, I. V., Gvozdez, N. V., Sil'nikova, M. I. and Rashovich, L. N. (2002). Atomic force microscopy study of lysozyme crystallization. *Cryst. Rep.*, **47**: S149-S158.
- Yau, S.-T., Thomas, B. R. and Vekilov, P. G. (2000). Molecular mechanisms of crystallization and defect formation. *Phys. Rev. Lett.*, **85**(2): 353-356.
- Yau, S.-T. and Vekilov, P. G. (2000). Quasi-planar nucleus structure in apoferritin crystallization. *Nature*, **406**: 494-497.

- Yau, S.-T. and Vekilov, P. G. (2001). Direct observation of nucleus structure and nucleation pathways in apoferritin crystallization. *J. Am. Chem. Soc.*, **123**: 1080-1089.
- Yin, L.-W., Li, M.-S., Xu, B., Song, Y.-J. and Hao, Z.-Y. (2002). Step bunching behavior on (111) surface of diamond single crystal. *Chem. Phys. Lett.*, **357**: 498-504.
- Yip, C. M., Brader, M. L., DePhilippis, M. R. and Ward, M. D. (1998a). Atomic force microscopy of crystalline insulins: the influence of sequence variation on crystallization and interfacial structure. *Biophys. J.*, **74**: 2199-2209.
- Yip, C. M., DePhilippis, M. R., Frank, B. H., Brader, M. L. and Ward, M. D. (1998b). Structural and morphological characterization of ultralente insulin crystals by atomic force microscopy: evidence of hydrophobically driven assembly. *Biophys. J.*, **75**: 1172-1179.
- Yip, C. M. and Ward, M. D. (1996). Atomic force microscopy of insulin single crystals: Direct visualization of molecules and crystal growth. *Biophys. J.*, **71**: 1071-1078.
- York, P. (1992). Crystal engineering and particle design. *Drug Dev. Ind. Pharm.*, **18**: 677-721.
- Yoshizaki, I., Nakamura, H., Sato, T., Igarashi, N., Komatsu, H. and Yoda, S. (2002). Systematic analysis of the effect of supersaturation on protein crystal quality. *J. Crystal Growth*, **237-239**: 295-299.
- Yoshizaki, I., Sato, T., Igarashi, N., Natsuisaka, M., Tanaka, N., Komatsu, H. and Yoda, S. (2001). Systematic analysis of supersaturation and lysozyme crystal quality. *Acta Crystallogr.*, **D57**: 1621-1629.
- Zhang, G. G. Z. and Grant, D. J. W. (1999). Incorporation mechanism of guest molecules in crystals: solid solution or inclusion? *Int. J. Pharm.*, **181**: 61-70.
- Zhong, Q., Innis, K., Kjoller, V. B. and Elings, V. (1993). Fractured polymer silica fibre surface studied by tapping mode atomic force microscopy. *Surf. Sci. Lett.*, **290**: L688-L692.
- Zipp, G. L. and Rodriguez-Hornedo, N. (1993). The mechanism of phenytoin crystal growth. *Int. J. Pharm.*, **98**: 189-201.

## **Acknowledgements**

I wish to begin by thanking all of the academics within the LBSA for their constant support and encouragement throughout this project. Particular thanks go to my main supervisor, Dr Clive Roberts, for both his unerring support for my work and proofreading everything I wrote in connection with this project.

I am also indebted to many other people who have helped me along the way. Chief amongst these is Dr. Jeremy Beauchamp, of Roche Pharmaceuticals in Basel. His practical advice at the beginning of this project was invaluable, and his patience and diligence in answering all of my questions concerning X-ray crystallography will always be appreciated. I also wish to thank my collaborators at Glasgow University, namely Prof. Neil Isaacs, Drs. Colin Bent, Alan Riboldi-Tunnicliffe and Paul Blackburn. Special thanks to Colin and Al for their considerable efforts in expressing and purifying two batches of the RR02rec protein for me, Paul for organizing my visit up to their department, and the whole lab for introducing me to some of the watering holes in their brilliant city.

There are numerous people I wish to acknowledge for making my time in Nottingham so enjoyable. Firstly I thank Dan and Lorna for being the best possible housemates and friends over the three years. In the LBSA, Jackie, James, Chris, Liz, Dan, Perky, Mark G, Sarah and Gibbo all, in their own unique ways, made the bad days in the lab more bearable and the evenings in the pubs very enjoyable. Many thanks to you all.

I also acknowledge Professor Anthony Beezer, formerly of the University of Kent. Without the faith he showed in me during my undergraduate degree, I doubt I would have even completed my degree, let alone move to Nottingham to study for a PhD. Thank you.

Finally, I thank my parents, Ruth and Ian, for their constant support throughout my education and Elke for coming to Nottingham and into my life.

## **Publications**

AFM studies of the crystallization and habit modification of an excipient material, adipic acid. Keel, T. R., Thompson, C., Davies, M. C., Tendler, S. J. B. & Roberts, C. J. (2004), *Int. J. Pharm.*, **280**, 185-198.

## **Conference presentations**

Oral presentation entitled 'The application of *in-situ* Atomic Force Microscopy to the study of protein crystallization' delivered in the biocrystallization session of the 15<sup>th</sup> American Association of Crystal Growth and Epitaxy annual meeting, Keystone, Colorado, 2003.

Three poster presentations delivered at UKSPM 2002, UKSPM 2003 and the 2002 AstraZeneca industry/academia research meeting.

This document was created with Win2PDF available at <http://www.daneprairie.com>.  
The unregistered version of Win2PDF is for evaluation or non-commercial use only.